Unveiling Epidemic Management: Understanding Individual Responses to Interventions through Integrated Modeling and Optimal Control Theory

エム ディー ママン アー ラシード カーン

Unveiling Epidemic Management: Understanding Individual Responses to Interventions through Integrated Modeling and Optimal Control Theory

By

Md. Mamun-Ur-Rashid Khan

A THESIS SUBMITTED IN PARTIAL FULFILMENT OF THE REQUIREMENTS FOR THE DEGREE OF

Doctor of Philosophy (PhD)

in

Interdisciplinary Graduate School of Engineering Sciences

Kyushu University

(Fukuoka, Japan)

九州大学

KYUSHU UNIVERSITY

Supervisor: Professor Dr. Jun Tanimoto

May 2024

Abstract

In the battle against infectious diseases, effective intervention comes through two essential approaches aimed at reducing both human suffering and economic impact. Firstly, non-pharmaceutical measures such as social distancing, mask-wearing, and lockdowns play a pivotal role. While authorities may enforce these measures, their success largely hinges on voluntary adherence from individuals. On the other hand, pharmaceutical interventions like vaccination and treatment offer a direct means of disease control but can face challenges in availability, particularly during the initial stages of a pandemic such as COVID-19. With the scarcity of pharmaceutical options in the early phases, the effectiveness of disease control heavily relies on the widespread adoption of non-pharmaceutical measures. However, accurately gauging the efficacy of these interventions demands a deep understanding of individual behaviors within diverse circumstances. In our research, we delve into epidemic models alongside behavior models to discern how individuals respond to interventions across varying scenarios. Moreover, the successful implementation of interventions by authorities is paramount to their impact. To gauge the societal repercussions of interventions, we introduce the concept of the social efficiency deficit (SED). This entails comparing an individual's payoff factoring in intervention and disease costs to the payoff in an ideal social scenario. By doing so, we pinpoint instances of social dilemmas. Initially, we adopt traditional methodologies to calculate the social optimum, but we later propose an approach rooted in optimal control theory. This enables us to dynamically optimize interventions in response to evolving epidemic dynamics. Through the amalgamation of behavior modeling and optimal control theory, our analysis yields valuable insights into how individuals react to interventions within different epidemic contexts. By comprehending the intricacies of individual decision-making and fine-tuning intervention strategies accordingly, we aim to inform more effective epidemic management practices.

Preface

The thesis delves into various aspects of epidemic modeling, integrating insights from behavior modeling and optimal control theory. Its primary focus is on devising decision-making policies aimed at preventing epidemics across diverse scenarios. Chapters 2-5 have already been published, and Chapter 6, where I serve as the primary author, is currently undergoing peer review in esteemed journals. Each chapter is structured to present a thorough exploration of specific research topics, following a format conducive to publication.

Chapter 2 is published as:

M.M.-U.-R. Khan, M.R. Arefin, J. Tanimoto, Investigating the trade-off between self-quarantine and forced quarantine provisions to control an epidemic: An evolutionary approach, Appl. Math. Comput. 432 (2022) 127365. https://doi.org/10.1016/j.amc.2022.127365 .

Chapter 3 is published as:

M.M.-U.-R. Khan, M.R. Arefin, J. Tanimoto, Time delay of the appearance of a new strain can affect vaccination behavior and disease dynamics: An evolutionary explanation, Infect. Dis. Model. 8 (2023) 656 - 671. https://doi.org/10.1016/j.idm.2023.06.001 .

Chapter 4 is published as:

M.M.-U.-R. Khan, J. Tanimoto, Investigating the social dilemma of an epidemic model with provaccination and antivaccination groups : An evolutionary approach, Alexandria Eng. J. 75 (2023) 341–349. https://doi.org/10.1016/j.aej.2023.05.091.

Chapter 5 is published as:

M.M.-U.-R. Khan, J. Tanimoto, Influence of Waning Immunity on Vaccination Decision-making: A Multi-Strain Epidemic Model with an Evolutionary Approach Analyzing Cost and Efficacy, Infect. Dis. Model. 9 (2024) 657 - 672. https://doi.org/10.1016/j.idm.2024.03.004 .

Table of Contents

Acknowledgments

This thesis comprises several research projects completed during my PhD journey. Professor Jun Tanimoto, my supervisor, encouraged me to publish my work promptly upon completion. Consequently, assembling all my projects for the thesis was not a daunting task. However, writing each manuscript, submitting them to journals, and responding to the comments of reviewers and editors proved to be quite challenging. Engaging in these tasks significantly enhanced my understanding of the entire project process, from inception to publication. Moreover, it equipped me with the skills to undertake future projects independently and effectively supervise students. To conclude this journey, I am grateful to many individuals who directly or indirectly supported me in my PhD endeavors.

First and foremost, all praise goes to the almighty Allah for blessing me with good health and enabling me to complete my PhD study, especially during the COVID-19 pandemic. I am grateful to the Japanese government (Monbukagakusho: MEXT) scholarship for providing financial support for my PhD in Japan. Although I received the scholarship in 2020, due to COVID-19, I was permitted to commence my PhD six months later, and MEXT graciously extended the scholarship until the completion of my PhD studies. The most influential person in my PhD journey is my supervisor, Professor Jun Tanimoto. Without his guidance, I would not have reached this stage in the initial phase of my PhD. He consistently supports my research endeavors, offers valuable suggestions for each project, and ensures my well-being during my time in Japan. I have learned from him the dedication a supervisor demonstrates in guiding their students through every stage of their studies and nurturing them to achieve their best. I am also indebted to two other professors, Prof. Aya Hagishima and Prof. Naoki Ikegaya, who have shown immense kindness and support to all students, especially foreign students, in adapting to the laboratory environment and life in Japan. When I encountered a difficulty with a course-related issue, Hagishima sensei promptly resolved that within a day.

Most of the work in this thesis was conducted by me under the guidance of my supervisor. However, when I embarked on my first project, Dr. Md. Rajib Arefin, a former PhD student in our lab, provided invaluable assistance in understanding the process from inception to publication. He co-authored two projects with me. Following his graduation, I endeavored to complete the remaining projects with the support of my supervisor. Subsequently, I collaborated on two projects with another PhD student, Khadija, which are yet to be published. I must also acknowledge another former PhD student of our lab, Dr. K. M. Ariful Kabir, who provided me with valuable insights into the research conducted in this lab before I arrived in Japan. I hope to engage in collaborative projects with both of them soon upon my return to my home country. I must also mention the names of individuals who have been instrumental in assisting me during my time in this lab: Lab secretary Yoshizuru-san, Dr. Anowar, Tatsukawa-san, Utsumi-san, Ikeo-san, Masaka-san, Okita-san, and Nishimura-san. They have provided invaluable

support with various issues I encountered upon joining this lab. Additionally, I am grateful to Gopal-san, another International PhD student, who has been exceptionally helpful to international students like myself. He provided valuable guidance on navigating living arrangements in Japan, particularly in situations where knowledge of the Japanese language is essential. I am also thankful to the other international and Japanese students for making the lab very cooperative.

On a personal note, I am grateful to all my family members, including my parents, my wife Ankhi, my sister Jhuma, my daughter Manha, and my son Marwan. Despite the distance between us, my parents always keep me in their prayers. My wife joined me in Japan six months after my arrival, bringing our daughter with her, and later our son was born during the final year of my PhD. They have provided unwavering support throughout this journey. Leaving behind a two-month-old baby during the peak of the COVID-19 pandemic in my home country was a difficult decision, but my wife took care of her and later traveled to Japan alone with our eight-month-old baby during another critical phase of the pandemic. Their sacrifices and support have been invaluable. My sister, who is also pursuing a PhD at my university, has been a constant source of assistance and encouragement throughout this journey. Together, they have made my life joyful and fulfilling in Japan. I must also mention Dr. Rajib, along with his wife Dr. Toosty, and their daughter Rayat, for their assistance during the first six months of my stay in Japan. Their presence made me feel welcomed and supported, and I never felt alone because of them.

Chapter 1

Introduction and Thesis Structure

1.1 Background

Mathematical epidemiology, employing mathematical and computational techniques, is pivotal in understanding and managing infectious diseases within populations. Emerging from the imperative to predict and comprehend epidemic dynamics, the field informs public health policies and devises effective disease control strategies. Its roots can be traced back to the 18th century, with mathematicians like Daniel Bernoulli pioneering mathematical models to elucidate disease spread, notably smallpox. However, it wasn't until the 20th century that the field truly burgeoned. A seminal contribution was made by Ronald Ross, a British mathematician and Nobel laureate, who developed mathematical models to probe malaria transmission, laying the groundwork for subsequent epidemiological modeling endeavors. Over the 20th and 21st centuries, mathematical epidemiology has undergone transformative growth, driven by technological advancements and the escalating complexity of infectious disease challenges. In the 20th century, the formalization of compartmental epidemic models, exemplified by the SIR model by Kermack and McKendrick, established a foundational understanding of disease dynamics. With the advent of computers, computational capabilities burgeoned, facilitating the development of stochastic models and the exploration of intricate epidemic scenarios. In the 21st century, the field has surged to prominence amid the emergence of infectious diseases like SARS, H1N1, Ebola, and COVID-19. Integration with data science has revolutionized epidemic modeling, enabling real-time analysis and informed decision-making. Agent-based modeling has furnished insights into the social and spatial dynamics of disease transmission, while decision support tools have assisted policymakers in optimizing intervention strategies. Overall, mathematical epidemiology has played a pivotal role in advancing our comprehension of infectious diseases and augmenting our capacity to control and prevent outbreaks in the contemporary era [1-5].

Interventions and decision-making assume pivotal roles in controlling and mitigating the spread of infectious diseases within epidemic modeling. By simulating various intervention strategies, decision-makers can evaluate their efficacy in reducing disease transmission, minimizing morbidity and mortality, and mitigating socio-economic impacts. These interventions span non-pharmaceutical measures like social distancing and mask-wearing to pharmaceutical interventions such as vaccination campaigns and treatment allocation. Decision-making in epidemic modeling necessitates optimizing resource allocation, prioritizing interventions based on their anticipated impact, and adapting strategies in response to evolving epidemic dynamics and emerging evidence. By amalgamating epidemiological data, population demographics, healthcare capacity, and societal preferences, decision-makers can

devise evidence-based strategies for epidemic control that balance public health objectives with ethical considerations and practical constraints [6-8].

Epidemic modeling often illuminates the presence of social dilemmas, wherein individual actions may diverge from collective epidemic control goals. These dilemmas stem from the inherent tension between individual behaviors and societal well-being. For instance, individuals may prioritize personal freedom over adherence to preventive measures, jeopardizing population-wide health outcomes. Epidemic models quantify the impact of such behaviors on disease transmission dynamics, underscoring the need for collective action and coordination to surmount social dilemmas. By integrating insights from behavioral science and game theory, researchers can identify strategies to incentivize cooperation and promote pro-social behaviors, ultimately bolstering epidemic control efforts and curtailing the societal costs of infectious disease outbreaks [9-10].

Epidemic modeling coupled with optimal control theory furnishes a potent framework for designing and optimizing intervention strategies to curb infectious disease spread within populations. By amalgamating mathematical models of disease transmission with optimization techniques, optimal control theory empowers decision-makers to discern the most effective and efficient intervention strategies. These interventions, spanning vaccination campaigns, quarantine measures, treatment allocation, and social distancing policies, are dynamically adjusted over time in response to changing epidemic conditions, thereby maximizing control efforts and minimizing societal costs. Through the synergistic application of epidemic modeling and optimal control theory, researchers can inform evidence-based decision-making, fortify epidemic preparedness and response, and ultimately mitigate the impact of infectious disease outbreaks on public health and society [5-10].

1.2 SIR Model

The SIR model is a compartmental model used to study the spread of infectious diseases within a population. It divides the population into three compartments: Susceptible (S), Infected (I), and Recovered (R). The model tracks the flow of individuals between these compartments over time using a set of differential equations [11-17].

The basic flow diagram and equations of the SIR model are as follows:

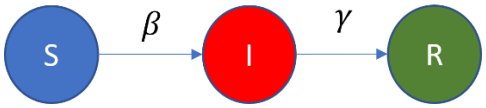

Figure 1.1: Flow diagram of SIR Model

1. Rate of change of Susceptible individuals ($\frac{dS}{dt}$):

$$\frac{dS}{dt} = -\beta\, S\, I$$

Here, S represents the number of susceptible individuals, I represents the number of infected individuals, and β is the transmission rate, which represents the average number of contacts per person per time multiplied by the probability of disease transmission per contact.

2. Rate of change of Infected individuals ($\frac{dI}{dt}$):

$$\frac{dI}{dt} = \beta\, S\, I - \gamma\, I$$

The first term on the right side of the equation represents the rate at which susceptible individuals become infected, while the second term represents the rate at which infected individuals recover or leave the infected compartment. γ is the recovery rate, representing the inverse of the average duration of infectiousness.

3. Rate of change of Recovered individuals ($\frac{dR}{dt}$):

$$\frac{dR}{dt} = \gamma\, I$$

This equation describes the rate at which individuals recover from the infection and move into the recovered compartment. The total population in this model is considered as 1.

In summary, the SIR model describes how the number of susceptible individuals decreases as they become infected, how the number of infected individuals changes over time due to new infections and recoveries, and how the number of recovered individuals increases as infections are resolved. These differential equations provide a mathematical framework for simulating the dynamics of infectious disease spread within a population.

1.3 Behavior Model

Incorporating any interventions such as vaccination dynamics into the SIR model involves modifying the equations to include terms representing the vaccination rate and the proportion of vaccinated individuals [18-19]. The logistic equation can then describe how the vaccination coverage evolves, considering factors such as vaccine availability, hesitancy, cost, and the capacity for vaccine distribution. Here's the logistic equation for behavior change (vaccination) within the SIR model:

Let V represent the proportion of the population that is vaccinated.
The logistic equation for vaccination within the SIR model can be expressed as follows:

$$\frac{dV}{dt} = m\, V\, (1 - V)\, (c\, I - k\, c_v)$$

Where:

- V represents the proportion of the population that is vaccinated.
- t represents time.
- m is the inertial effect of the rate of vaccination.
- c is disease cost.
- c_v is the vaccination cost.
- I represents the number of infected individuals at time t.
- k is the sensitivity constant due to vaccination cost.

The last term in the open bracket on the right side of the equation has two terms both are positive and must have the same unit. If $c\,I > k\,c_v$, vaccination flow will increase, and if $c\,I < k\,c_v$, then the vaccination flow will decrease. The term $V\,(1-V)$ keeps the rate between 0 to 1. By incorporating the logistic equation for vaccination into the SIR model, it is easy to simulate how vaccination coverage evolves in response to the dynamics of the infectious disease outbreak and the vaccination campaign. This allows for the assessment of the impact of vaccination coverage on disease transmission and the effectiveness of vaccination strategies in controlling the spread of the disease within the population.

1.4 Optimal Control Theory (Pontryagin's Maximum Principle)

Let us consider a simple example where Pontryagin's Maximum Principle is applied to an epidemic model with vaccination as the control variable [20-28]. We'll consider the basic SIR (Susceptible-Infectious-Recovered) model mentioned in the previous section and introduce a control variable representing the vaccination rate. The objective is to minimize the total number of infections over a fixed time horizon.

Here are the flow diagram and equations and the setup of the example:

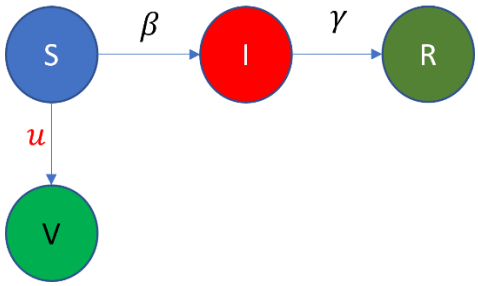

Figure 1.2: Flow diagram of SIR Model with vaccination where vaccination rate needs to be optimized

1. Epidemic Model (SIR Model):

$$\frac{dS}{dt} = -\beta\,S\,I$$

$$\frac{dI}{dt} = \beta\, S\, I - \gamma\, I$$

$$\frac{dR}{dt} = \gamma\, I$$

2. Control Variable (Vaccination Rate):

We introduce a control variable $u(t)$ representing the vaccination rate at time t. The vaccination rate represents the proportion of susceptible individuals that are vaccinated per unit of time.

3. Objective Function:

We define the objective function J as the integral of the number of infections over a fixed time horizon:

$$J = \int_0^T I(t)\, dt$$

4. Constraints:

We consider constraints on the vaccination rate $u(t)$ to ensure that it remains within feasible bounds (e.g., availability of vaccines, vaccination capacity, vaccination cost).

5. Pontryagin's Maximum Principle:

We apply Pontryagin's Maximum Principle to derive the optimal control strategy $u(t)$ that minimizes the objective function while satisfying the dynamics of the epidemic model and the constraints on the control variable.

The optimal control problem can be formulated as follows:

- Objective: Minimize the integral of the number of infections $I(t)$ over a fixed time horizon t.
- Dynamics: Governed by the SIR model equations.
- Control Variable: Vaccination rate $u(t)$.
- Constraints: Constraints on the vaccination rate $u(t)$.
- Optimization: Apply Pontryagin's Maximum Principle to find the optimal vaccination strategy $u(t)$ that minimizes the objective function while satisfying the system dynamics and constraints.

Solving this optimal control problem using Pontryagin's Maximum Principle yields the optimal vaccination strategy that minimizes the total number of infections over the specified time horizon, taking into account the dynamics of the epidemic and the constraints on vaccination.

1.5 Thesis Structure

Each chapter of this thesis delves into distinct yet interconnected topics, with many having already undergone peer review and publication. Within each chapter, readers will find a comprehensive structure comprising a self-contained abstract, introduction, model description, results and discussion, conclusion, and reference list. This delineation underscores the autonomy of each section while also highlighting their interconnectedness. Chapters 2-5 primarily explore epidemic models intertwined with behavior models, while Chapter 6 shifts focus to epidemic models coupled with optimal control theory. Despite these thematic distinctions, the inherent connections among all chapters will be elucidated in the concluding section, offering a cohesive synthesis of the thesis's overarching themes and findings.

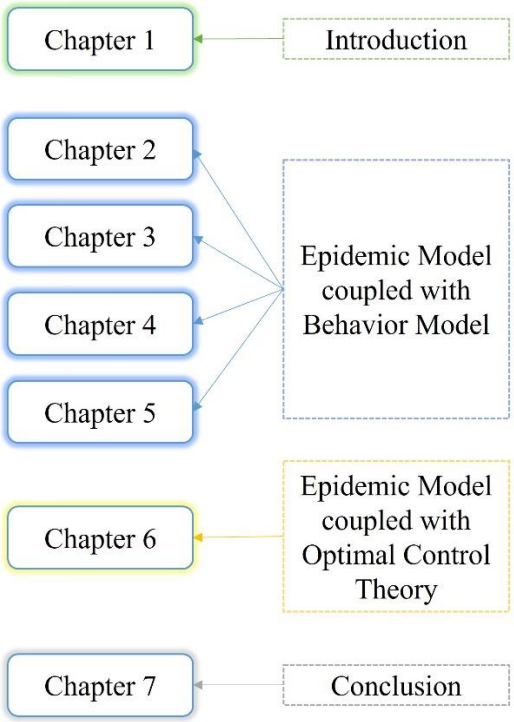

Figure 1.3: Flow chart of the thesis. Chapters 2-5 are concerned with the epidemic model coupled with the behavior model and Chapter 6 is concerned with the inclusion of optimal control theory along with the epidemic model.

Chapter 2 introduces an epidemiological model based on SEIR dynamics, integrating two interventions: self-quarantine and forced quarantine driven by human behavior dynamics. We explore disease spread within a population where individuals can choose self-quarantine by bearing costs for safety, while others behave normally until symptomatic, triggering government-imposed forced quarantine. The government covers forced quarantine costs within a budget limit. Each intervention, derived from the behavior model, is governed by a dynamic equation balancing costs, budget constraints, and infection risk. Our findings underscore the necessity of proactive enforcement to reduce infection peaks.

Additionally, comparative analysis highlights forced quarantine's superior efficacy in reducing disease prevalence and minimizing the social efficiency deficit, measuring the gap between social optimum and equilibrium payoff.

Chapter 3 presents a two-strain epidemic model with a delayed appearance of the new strain. We explore two vaccination strategies—pre-infection and post-infection vaccinations—guided by human behavior dynamics. Individuals can choose vaccination before contracting the first strain or opt for post-recovery vaccination to mitigate the second strain. Both vaccinated and unvaccinated individuals remain susceptible to the second strain. The time delay allows additional vaccination opportunities and protection against the second strain. Our analysis, considering vaccine cost, severity of the new strain, and effectiveness, shows that delaying the second strain reduces the peak size of infections. Moreover, we find a decrease in the social dilemma associated with immunization as the arrival of the second strain is delayed.

Chapter 4 introduces an epidemiological model with provaccination and antivaccination susceptible groups, examining the inherent social dilemma. Amidst pandemics like COVID-19, individuals face the decision between provaccination and antivaccination strategies, influenced by factors like infection rates and associated payoffs. Our model allows individuals to gain immunity through vaccination or natural infection, with waning immunity impacting strategy choices. Using the behavior model, we analyze how individuals choose between strategies based on infection rates. Those already infected weigh the cost of disease versus vaccination. Our findings show that at Nash equilibrium, both groups exhibit similar behavior. Increasing vaccination rates alleviate the social dilemma, while higher waning immunity exacerbates it.

Chapter 5 presents a comprehensive epidemiological model incorporating multiple strains of an infectious disease and two vaccination options. While vaccination remains the most effective preventive measure, the presence of diverse vaccines, each with its costs and effectiveness, complicates individual decision-making. Additionally, waning immunity post-vaccination significantly influences these choices. Employing a behavioral model, we analyze how individuals decide amidst multiple strains and waning immunity. Factors such as the total number of infected individuals and vaccine cost-effectiveness guide vaccination choices. Our findings show that with increasing waning immunity, individuals prioritize vaccines with higher costs and greater efficacy. Furthermore, in the presence of more contagious strains, equilibrium in vaccine adoption is reached more swiftly. Finally, we explore the social dilemma by quantifying the social efficiency deficit (SED) across various parameter combinations.

Chapter 6 introduces a novel methodology utilizing optimal control theory (OCT) to assess the Social Optimum (SO) of a vaccination game, addressing complexities such as cost, availability, and

distribution policies. Using an SIRS/V epidemic model enhanced with a behavior model, we analyze individual vaccination strategies. Our unique optimal control framework, focusing on vaccination costs, differs significantly from previous approaches. Results affirm the efficacy and practicality of this method in managing vaccination strategies. Additionally, we investigate the social dilemma underlying the vaccination game by examining key parameters. By computing the Nash equilibrium (NE) using the behavior model and determining the SO via our method, we quantify the Social Efficiency Deficit (SED), measuring the total cost disparity between the NE and SO. Findings indicate that a higher waning immunity rate exacerbates the social dilemma, although increasing vaccination costs somewhat alleviates it. This research provides valuable insights into optimizing vaccination strategies amidst complex societal dynamics.

References

[1] M. J. Keeling and P. Rohani, Modeling infectious diseases in humans and animals, Princeton University Press, 2011, https://doi: 10.2307/j.ctt7s7v9.

[2] P. Fine, K. Eames, and D. L. Heymann, Herd immunity: A rough guide, Clinical Infectious Diseases, vol. 52, no. 7, pp. 911-916, 2011, https://doi: 10.1093/cid/cir007.

[3] J. Wallinga and M. Lipsitch, How generation intervals shape the relationship between growth rates and reproductive numbers, Proceedings of the Royal Society B: Biological Sciences, vol. 274, no. 1609, pp. 599-604, 2007, https://doi: 10.1098/rspb.2006.3754.

[4] R. M. Anderson and R. M. May, Infectious diseases of humans: dynamics and control, Oxford University Press, 1991.

[5] H. W. Hethcote, The mathematics of infectious diseases, SIAM Review, vol. 42, no. 4, pp. 599-653, 2000, https://doi: 10.1137/s0036144500371907.

[6] M. E. Halloran and C. J. Struchiner, "Study designs for dependent happenings," Epidemiology, vol. 2, no. 5, pp. 331-338, 1991, https://doi: 10.1097/00001648-199109000-00009.

[7] N. M. Ferguson et al., Strategies for mitigating an influenza pandemic, Nature, vol. 442, no. 7101, pp. 448-452, 2006, https://doi: 10.1038/nature04795.

[8] C. T. Bauch, A. P. Galvani, and D. J. D. Earn, "Group interest versus self-interest in smallpox vaccination policy," Proceedings of the National Academy of Sciences, vol. 100, no. 18, pp. 10564-10567, 2003, https://doi: 10.1073/pnas.1831989100.

[9] S. Funk et al., The spread of awareness and its impact on epidemic outbreaks, Proceedings of the National Academy of Sciences, vol. 106, no. 16, pp. 6872-6877, 2009, https://doi: 10.1073/pnas.0810762106.

[10] L. A. Rvachev and I. M. Longini Jr, "A mathematical model for the global spread of influenza," Mathematical biosciences, vol. 75, no. 1, pp. 3-22, 1985, https://doi: 10.1016/0025-5564(85)90064-1.

[11] W. O. Kermack and A. G. McKendrick, A contribution to the mathematical theory of epidemics, Proceedings of the Royal Society of London. vol. 115, no. 772, pp. 700-721, 1927, https://doi.org/10.1098/rspa.1927.0118.

[12] O. Diekmann, J. A. Heesterbeek, and J. A. Metz, On the definition and the computation of the basic reproduction ratio R0 in models for infectious diseases in heterogeneous populations, Journal of Mathematical Biology, vol. 28, no. 4, pp. 365-382, 1990, https://doi.org/10.1007/BF00178324

[13] F. Brauer and C. Castillo-Chávez, Mathematical Models in Population Biology and Epidemiology. Springer Science & Business Media, 2012.

[14] P. Van den Driessche and J. Watmough, Reproduction numbers and sub-threshold endemic equilibria for compartmental models of disease transmission, Mathematical Biosciences, vol. 180, no. 1-2, pp. 29-48, 2002, https://doi.org/10.1016/S0025-5564(02)00108-6.

[15] L. J. Allen, An introduction to stochastic epidemic models in Mathematical Epidemiology. Springer, Berlin, Heidelberg, 2007, pp. 81-130, https://doi.org/10.1007/978-3-540-32964-8_3.

[16] F. Brauer, Compartmental models in epidemiology, Springer, Berlin, Heidelberg, 2008, pp. 19-79, https://doi.org/10.1007/978-3-540-78911-6_2.

[17] R. Pastor-Satorras and A. Vespignani, Epidemic spreading in scale-free networks, Physical Review Letters, vol. 86, no. 14, p. 3200, 2001, https://doi.org/10.1103/PhysRevLett.86.3200.

[18] C. T. Bauch, Dynamics of behavior change in infectious disease models, Interface Focus, vol. 4, no. 5, p. 20140076, 2014, https://doi: 10.1098/rsfs.2014.0076.

[19] C. T. Bauch, Imitation dynamics and vaccination decision making on social networks, Proceedings of the Royal Society B: Biological Sciences, vol. 276, no. 1666, pp. 469-476, 2009, https://doi: 10.1098/rspb.2008.0788.

[20] R. Bellman, On the theory of dynamic programming, Proc. Natl. Acad. Sci. USA, vol. 38, no. 8, pp. 716-719, Aug. 1952, https://doi: 10.1073/pnas.38.8.716.

[21] L. S. Pontryagin, V. G. Boltyanskii, R. V. Gamkrelidze, and E. F. Mishchenko, The Mathematical Theory of Optimal Processes. New York, NY: Wiley, 1962.

[22] A. V. Fiacco and G. P. McCormick, Nonlinear Programming: Sequential Unconstrained Minimization Techniques. New York, NY: SIAM, 1968.

[23] D. P. Bertsekas, Dynamic Programming and Optimal Control, vol. 1. Belmont, MA: Athena Scientific, 2017.

[24] M. H. A. Davis, Optimization Theory and Applications: Problems with Ordinary Differential Equations, vol. 4. New York, NY: Springer, 1982, https://doi: 10.1007/978-3-642-87556-1.

[25] G. Leitmann, Optimal control: An introduction, SIAM Rev., vol. 9, no. 1, pp. 1-52, Jan. 1967, https://doi: 10.1137/1009001.

[26] A. J. Kurdila and M. Zabarankin, Convex Functional Analysis and Applications. Boston, MA: Birkhäuser, 2005, https://doi: 10.1007/b137743.

[27] E. Polak, Optimization: Algorithms and Consistent Approximations. New York, NY: Springer, 1997.

[28] H. Kushner and P. Dupuis, Numerical Methods for Stochastic Control Problems in Continuous Time. New York, NY: Springer, 2001, https://doi: 10.1007/978-1-4613-0007-9.

Chapter 2

Investigating the trade-off between self-quarantine and forced quarantine provisions to control an epidemic: an evolutionary approach

Abstract

During a pandemic event like the present COVID-19, self-quarantine, mask-wearing, hygiene maintenance, isolation, forced quarantine, and social distancing are the most effective nonpharmaceutical measures to control the epidemic when vaccination and proper treatments are absent. In this study, we proposed an epidemiological model based on the SEIR dynamics along with the two interventions defined as self-quarantine and forced quarantine by human behavior dynamics. We consider a disease spreading through a population where some people can choose the self-quarantine option of paying some costs and be safer than the remaining ones. The remaining ones act normally and are sent to forced quarantine by the government if they get infected and symptomatic. The government pays the forced quarantine costs for individuals, and the government has a budget limit to treat the infected ones. Each intervention derived from the so-called behavior model has a dynamical equation that accounts for a proper balance between the costs for each case, the total budget, and the risk of infection. We show that the infection peak cannot be reduced if the authority does not enforce a proactive (quantified by a higher sensitivity parameter) intervention. While comparing the impact of both self- and forced quarantine provisions, our results demonstrate that the latter is more influential in reducing the disease prevalence and the social efficiency deficit (a gap between social optimum payoff and equilibrium payoff).

2.1 Introduction

Quarantine, lockdowns, and other distancing restrictions may be the only way to stop a pandemic from spreading, especially if there are no vaccinations or proper medications available to treat the symptoms of infection [1-15]. Epidemiologists and other professionals usually define these social principles but putting them into practice can be very difficult [9, 16]. Despite evidence of prospective concerns, the current COVID-19 situation reveals how certain people are more prone to self-isolation under voluntary quarantine than others. Individuals who refuse to accept any type of limitation put themselves and their communities at risk. In these situations, knowing how to encourage and maintain prosocial behavior is crucial [9].

In this study, we examine the impact of individual quarantine preferences and government-imposed quarantine on epidemic dynamics. We model an individual's decision to commit to self-quarantine based on the overall scenario, including the number of infected people, self-quarantine cost, and self-quarantine effort, as well as the government's decision to maintain the forced quarantine based on the

forced quarantine cost, total budget, and number of infected peoples, using evolutionary game theory (EGT) [17-19].

Currently, sustaining self-quarantine by individuals and compulsory quarantine by the government are the two most powerful control strategies against the transmission of SARS-CoV2 during this COVID-19 epidemic [20–23]. There are substantial disagreements among people in various locations about maintaining self-quarantine, particularly in low-income countries where everyone cannot pay the cost of self-quarantine because of economic constraints. However, in many nations, the government has funding constraints, space constraints, healthcare personnel, and instrumentation constraints when caring for diseased people. These behavioral treatments have already demonstrated their value in studying the interaction between illnesses and human decision-making in the context of social dilemmas [24–30].

Compartmental models, a common tool in epidemiology and current health management systems, are widely used to investigate a pandemic or epidemic process [1, 6, 7, 9, 11, 15, 18, 26, 29–37]. One of the most widely used epidemiological models is the SIR model [32, 38, 39]. It shows how illness spreads in agents from the susceptible compartment, S, to the infectious compartment, I, and finally to the recovered (or eliminated) compartment R, imparting immunity against re-infection [9]. It has been widely used to retrieve relevant parts of epidemic processes that have the SIR structure despite its simplicity [9, 34, 38–41]. Since its creation by Kermack and McKendrick, the model has been thoroughly explored and expanded to meet a variety of hypotheses and situations [9]. Some epidemics, for example, may demand the addition of additional compartments, such as those harboring exposed, asymptomatic agents, Quarantined agents, and Hospitalized agents (known as SEIR, SEAIR, SEIAQR, SEIAQHR models respectively) [9, 42–45]. Other applications for compartmental models in epidemiology include the investigation of control and mitigation techniques such as vaccination, the modeling of vector-borne diseases, and the effects of birth and death dynamics [9, 39]. Even the propagation of misinformation and corruption has found a natural home in the SIR model [9]. However, most of these models focus solely on illness progression, with agents doing no conscious activities concerning the condition [9]. Meanwhile, many infectious disease control techniques rely on individual decision-making. In this setting, the new discipline of behavioral epidemiology [9, 39, 42, 46, 47], which applies psychology, and game theory approaches to epidemiology, has attracted significant attention. Behavioral epidemiology considers dynamic behavior changes instead of static roles for agents. This is ideal ground for the new field of social dynamics or sociophysics, which combines statistical physics tools with evolutionary game theory (and other approaches) to better understand human behavior [9,17]. For example, Bauch used a unique way to examine vaccination decision dynamics by including a SIR model into an EGT framework [46, 47]. Agents adjust their vaccination strategy dynamically because of based on their perceptions of the vaccine's advantages and costs. This was eventually developed into the framework of "vaccination games" [24, 46, 48–51]. As a result of

this technique, several intriguing observations and predictions in vaccination procedures have been made. Unfortunately, vaccination is not always an option, and social isolation may be the only method to keep the disease from spreading further. This was true during the Spanish flu, the SARS epidemic of 2002–2003, and most recently, the COVID-19 pandemic [9, 52–53].

We modeled the epidemic formulation using the epidemic technique, where the population is initially divided into two divisions: committing self-quarantine and acting normally. From a game-theoretical perspective, individuals can go from the normal active state to the self-quarantine state based on their choices. Similarly, the government can send symptomatic sick people to a forced quarantine condition. EGT provides a framework for describing individual behavior in situations where people's preferred options are committing self-quarantine or not, as well as being sent to coercive quarantine or not. We also used the cost of individuals' self-quarantine, the cost of individuals' forced quarantine, and overall government expenditure in this study. Finally, to get the social dilemma in EGT, the model introduces the concept of social efficiency deficit (SED), which is the difference between Nash equilibrium (NE) and social optimum (SO) [1, 8, 24, 29–30].

2.2 Model Description

2.2.1 Epidemiological model

We propose an epidemiological model based on the SEIR dynamics. We also introduce two behaviors known as self-quarantine by individuals and forced quarantine by the government. Figure 1 shows the schematic of the proposed model, and the formulation is given as follows:

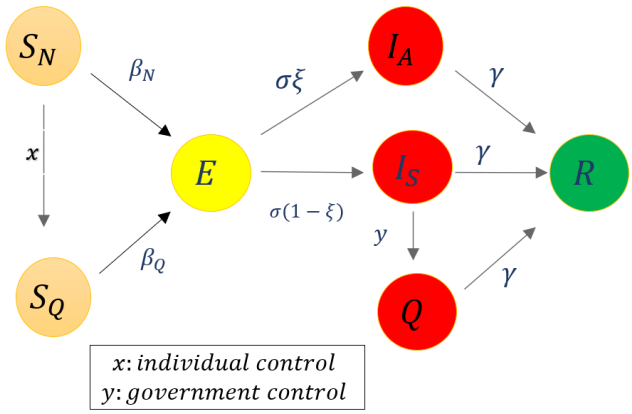

Figure 1: Schematic of the proposed model.

$$\frac{dS_N(t)}{dt} = -S_N \cdot \left(\beta_N \cdot \left(\varepsilon_I \cdot I_A(t) + I_S(t) + \varepsilon_Q \cdot Q(t)\right)\right) - x(t)\,.\,S_N(t) \quad (1.1),$$

$$\frac{dS_Q(t)}{dt} = -S_Q \cdot \left(\beta_Q \cdot \left(\varepsilon_I \cdot I_A(t) + I_S(t) + \varepsilon_Q \cdot Q(t)\right)\right) + x(t)\,.\,S_N(t) \quad (1.2),$$

$$\frac{dE(t)}{dt} = S_N \cdot \left(\beta_N \cdot \left(\varepsilon_I \cdot I_A(t) + I_S(t) + \varepsilon_Q \cdot Q(t)\right)\right) + S_Q \cdot \left(\beta_Q \cdot \left(\varepsilon_I \cdot I_A(t) + I_S(t) + \varepsilon_Q \cdot Q(t)\right)\right) - \sigma \cdot E(t) \quad (1.3),$$

$$\frac{dI_A(t)}{dt} = \xi \cdot \sigma \cdot E(t) - \gamma \cdot I_A(t) \quad (1.4),$$

$$\frac{dI_S(t)}{dt} = (1-\xi) \cdot \sigma \cdot E(t) - \gamma \cdot I_S(t) - y(t) \cdot I_S(t) \quad (1.5),$$

$$\frac{dQ(t)}{dt} = y(t) \cdot I_S(t) - \gamma \cdot Q(t) \quad (1.6),$$

$$\frac{dR(t)}{dt} = \gamma \cdot \big(I_A(t) + I_S(t) + Q(t)\big) \quad (1.7),$$

$$S_N(t) + S_Q(t) + E(t) + I_A(t) + I_S(t) + Q(t) + R(t) = 1 \quad (1.8),$$

where, $S_N, S_Q, E, I_A, I_S, Q,$ and R are the fractions of susceptible acting normal, susceptible self-quarantine, exposed (i.e., infected but not infectious), asymptomatic infected, symptomatic infected, forced quarantine, and recovered individuals, respectively. Susceptible normal people get exposed at a rate of β_N, and susceptible people commit self-quarantine getting exposed at a rate of β_Q. Clearly, $\beta_N > \beta_Q$. At a rate ξ, the exposed people go to the asymptomatic infected state. In our model, we choose the asymptomatic infected people quite low than the symptomatic infected people. γ is the recovered rate for all people. σ is the rate of progression from E to I_A or I_S. ε_I and ε_Q are the contact discount factors for the asymptomatic infected people and forced quarantined people, respectively. Obviously, $\varepsilon_I > \varepsilon_Q \approx 0$, because people get infected by having contact with the asymptomatic people while people are not getting a chance to contact the forced quarantined people due to the quarantine policy. The contact discount factor for the symptomatic infected people is set at 1 because people always get infected by having contact with symptomatic people.

2.2.2 Behavior model

We introduce the concept of behavior model [46, 47, 54] which accounts for the time-varying flux from normal acting susceptible (S_N) to self-quarantine susceptible (S_Q) denoted by x, which we call the individual control, and from the symptomatic infected (I_S) to forced quarantine (Q) denoted by y, which we call the government control. We define the following two dynamical equations:

$$\frac{dx(t)}{dt} = \tau_x \cdot x(t) \cdot \big(1 - x(t)\big) \cdot \big[(I_S + Q) \cdot C_I - w.\ \Delta_Q\big] \quad (1.9),$$

$$\frac{dy(t)}{dt} = \tau_y \cdot y(t) \cdot \big(1 - y(t)\big) \cdot \Big[A_p - \big(\delta_{I_S+Q}\big) \cdot \int_0^t y(\tau)\, d\tau\Big] \quad (1.10),$$

where τ_x and τ_y are the effort rate by individuals and government, respectively. $(I_S + Q)$ is the total number of visible infected people, C_I is the disease cost which is set as 1.0 throughout the study. Parameter w is the relative sensitivity resulting from taking self-quarantine to reduce self-quarantine due to its cost Δ_Q [54]. δ_{I_S+Q} is the cost for an individual to treat the forced quarantine people. A_P is the government total budget for the treatment of the forced quarantine people. All the model parameters and their description are shown in Table 1.

Table 1: List of parameters and their description

Parameters	Description
β_N	Disease Transmission rate from S_N
β_Q	Disease Transmission rate from S_Q
σ	Rate of progression from E to I_A or I_S
ξ	Asymptomatic infection rate
γ	Recovery rate
τ_x	Self-quarantine effort rate
τ_y	Forced quarantine effort rate
Δ_Q	Self-quarantine cost for individual
ε_I	Contact discount factor for asymptomatic people
ε_Q	Contact discount factor for forced quarantine people
A_p	Government total budget (resource)
δ_{I_S+Q}	Forced quarantine cost for individual
w	Relative sensitivity due to individual's self-quarantine cost

We also investigated the possibility of susceptible self-quarantined people returning to their susceptible normal behaving state [31], but the results were similar using both directions with one direction. We only investigated the one-way direction from susceptible normal to susceptible self-quarantine.

2.2.3 Basic Reproduction Number

To obtain the basic reproduction number (R_0), we use the next-generation matrix approach [31, 38, 39, 42, 55, 56]. Using the infected class equations (1.3–1.5), we obtain

$$\mathcal{F} = \begin{pmatrix} (S_N\beta_N\varepsilon_I + S_Q\beta_Q\varepsilon_I)I_A + (S_N\beta_N + S_Q\beta_Q)I_S + (S_N\beta_N\varepsilon_Q + S_Q\beta_Q\varepsilon_Q)Q \\ \xi\sigma E \\ (1-\xi)\sigma E \end{pmatrix}, \quad \nu = \begin{pmatrix} \sigma E \\ \gamma I_A \\ (\gamma + y)I_S \end{pmatrix}.$$

At disease-free equilibrium (DFE), we have

$$F = \begin{pmatrix} 0 & (S_{N_0}\beta_N\varepsilon_I + S_{Q_0}\beta_Q\varepsilon_I) & (S_{N_0}\beta_N + S_{Q_o}\beta_Q) \\ \xi\sigma & 0 & 0 \\ \sigma(1-\xi) & 0 & 0 \end{pmatrix}, \qquad V = \begin{pmatrix} \sigma & 0 & 0 \\ 0 & \gamma & 0 \\ 0 & 0 & \gamma + y \end{pmatrix}.$$

Next-generation matrix, $M = FV^{-1} = \begin{pmatrix} 0 & \frac{(S_{N_0}\beta_N\varepsilon_I + S_{Q_0}\beta_Q\varepsilon_I)}{\gamma} & \frac{(S_{N_0}\beta_N + S_{Q_o}\beta_Q)}{\gamma+y} \\ \xi & 0 & 0 \\ (1-\xi) & 0 & 0 \end{pmatrix}$.

Thus, we obtain the basic reproduction number as follows:

$$R_0 = \sqrt{\frac{S_{N_0}\beta_N + S_{Q_0}\beta_Q}{\gamma+y}(1-\xi) + \xi\frac{S_{N_0}\beta_N\varepsilon_I + S_{Q_0}\beta_Q\varepsilon_I}{\gamma}} \qquad (1.11),$$

at DFE $= (S_{N_0}, S_{Q_0}, 0,0,0,0,0)$.

The basic reproduction number in our model decreases monotonically with an increase in y because it depends on the factors and government control flux y (Figure 2).

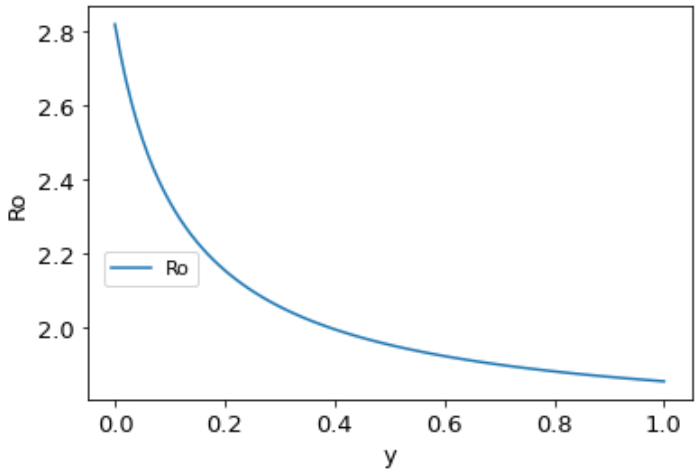

Figure 2: Basic reproduction Number (1.11) in terms of forced quarantine rate y. Here, $S_{N_0} = 0.9887, \beta_N = 1.0, S_{Q_0} = 0.01, \beta_Q = 0.5, \gamma = 0.1, \varepsilon_I = 0.6,\ \xi = 0.1$. With the increasing y from 0 to 1, R_0 reduces to 2.82 to 1.85.

2.2.4 Final Epidemic size, critical point, average social payoff, and social efficiency deficit

In the present model, final epidemic size (FES) [42, 54] is defined as

$$FES = R(\infty) \qquad (1.12),$$

where the argument ∞ denotes a state of equilibrium (let us call it as, NE) at $t = \infty$ [54].

We also define the difference in FES between with and without interventions:

$$\Delta FES = \text{FES(No intervention)} - \text{FES(with both interventions)} \qquad (1.13).$$

ΔFES is mainly controlled by Δ_Q and δ_{I_S+Q}. One interesting exploration is the analysis of critical points $\left(\Delta_Q, \delta_{I_S+Q}\right)$ such that the reduced cost by both interventions, i.e., exactly quantified by ΔFES, is stringently equal to the sum of the total self-quarantine cost and total forced quarantine cost, i.e.,

$$\Delta FES = \text{Total self} - \text{quarantine cost (at t} = \infty) + \text{Total forced quarantine cost (at t} = \infty) \quad (1.14).$$

The average social payoff, ASP^{NE}, in the model, can be defined as follows [54]:

$$ASP^{NE} = \left(-\Delta_Q\right) \cdot \int_0^\infty x(t) \cdot S_N(t)\, dt + \left(-\delta_{I_S+Q}\right) \cdot \int_0^\infty y(t) \cdot I_S(t)\, dt - C_I \cdot R(\infty) \quad (1.15).$$

where the first term on the right-hand side indicates the total cost of committing self-quarantine, the second term indicates the total cost of the implementation of forced quarantine, and the third term indicates the individual's disease cost ($C_I = 1.0$) who should be called as a failed free rider [54].

Since the rates of self- and forced quarantine provisions change over time according to the behavior dynamics (Eq. (1.9-1.10)), the overall social gain estimated at the equilibrium (i.e., ASP^{NE} in Eq. (1.15)) may not reach the expected social optimum (say, ASP^{SO}). In other words, there might be a gap between the overall payoffs at social optimum and equilibrium. Such a gap is formally called social efficiency deficit (SED) [29], which helps us understand the existence of social dilemmas as well as the control parameters to improve the system towards social optimum. SED demonstrates how to improve the system's ASP from an evolutionary final state (NE) to a social ideal situation to achieve the maximum ASP^{SO} that could be realized if both the evolutionary processes for x and y are optimally controlled [54]. SED is mathematically defined as follows:

$$SED = ASP^{SO} - ASP^{NE} \quad (1.16).$$

The social optimal state can be defined as a time-constant vector $(x^{for\,SO}, y^{for\,SO})$, both elements ranging from [0,1]. So,

$$\boldsymbol{SO} = \arg\max\left[ASP(x^{for\,SO}, y^{for\,SO})\right] \quad (1.17).$$

There is no dilemma when NE is consistent with SO, meaning that SED implies zero. However, when a positive nonzero SED occurs, a certain amount of social dilemma exists [54].

2.3 Result and Discussion

2.3.1 Standard (Basic) case: Figure 3 shows the time-series graph using the standard (basic) set of parameters for the proposed model. Table 2 shows the standard values of the parameters.

Table 2: Parameters and their values (Standard case)

Parameter	Value	Parameter	Value
β_N	1.0	τ_y	1.0
β_Q	0.5	Δ_Q, δ_{I_S+Q}	0.01
σ	0.9	ε_I	0.6
ξ	0.1	ε_Q	0.0
γ	0.1	A_p	1.0
τ_x	1.0	w	0.1

Additionally, the initial values for the compartments are considered as: $S_N[0] = 0.9887, S_Q[0] = 0.01, E[0] = 0.0001, I_A[0] = 0.001, I_S[0] = 0.0001, Q[0] = 0.0001, R[0] = 0.0, x[0] = 0.0001, y[0] = 0.0001$.

Figure 3 confirms the present model fairly shows plausible dynamics accounting for all the aspects built into our model.

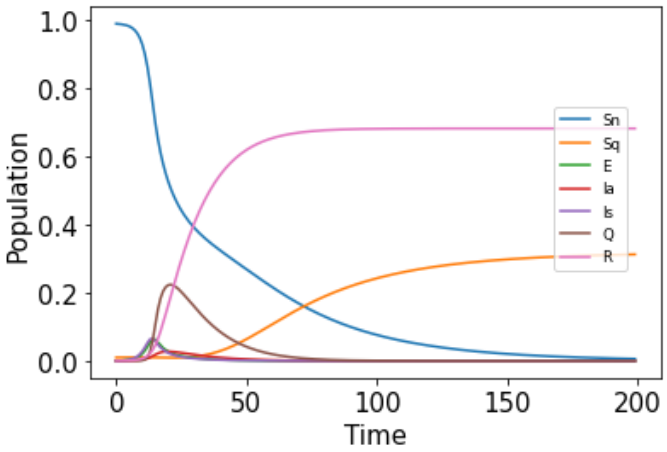

Figure 3: Time series for all compartments. The blue curve depicts susceptible people acting normally; the orange curve depicts susceptible people who have self-quarantined themselves; and the brown curve depicts people who have been infected and forced quarantined by the government at time t. The final epidemic size is determined by the pink curve. The green, red, and violet curves represent the exposed, asymptomatic infected, and symptomatic infected patients, respectively. Here, all the parameters are taken as the standard one from Table 2.

2.3.2 Self- versus forced quarantine

Figure 4 shows the trade-off between self- and forced quarantine in diminishing the epidemic size. We set the self-quarantine effort rate to 1 (100%) in the first column but varied the forced quarantine rate to 30%, 50%, and 70%. The results illustrate that as the forced quarantine effort rate increases, the ultimate epidemic size decreases steadily, and it reduces to its smallest when the effort rate is 100%. The forced quarantine, in contrast to the self-provision, also reduces the peak epidemic size (see the first column in Fig. 4). In the second column, we varied the self-quarantine effort while keeping the maximum forced quarantine rate at 1. It is worth noting that as the self-quarantine effort was increased, more people moved from the S_N stage to the S_Q stage, meaning that people's awareness is growing aiding the epidemic management.

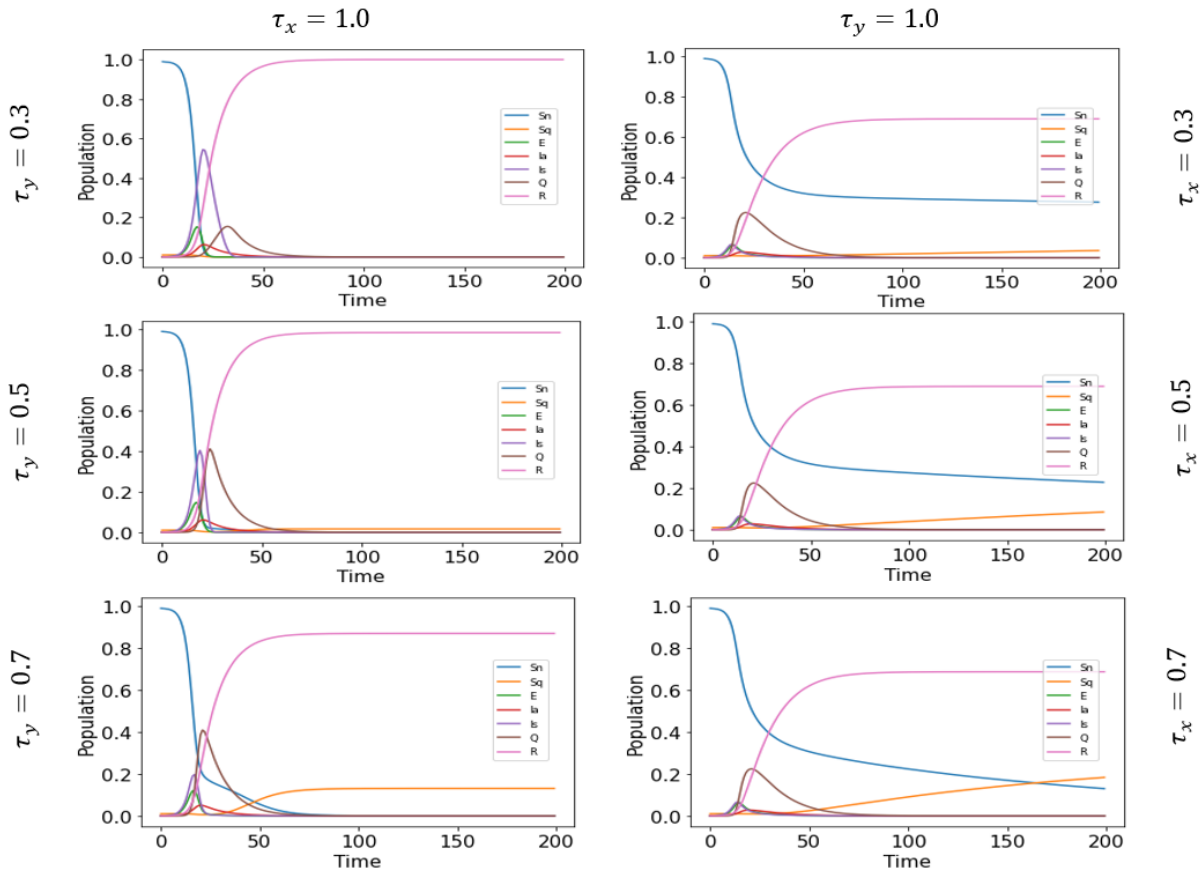

Figure 4: The entire population's time series is depicted in this graph by adjusting the self-quarantine and forced quarantine effort rates. The other parameters and initial values are left at their default settings (Figure 3). In the three graphs of the first column, τ_x is fixed as 1, and $\tau_y$varies with $0.3, 0.5,$ and 0.7, respectively. Similarly, in the second column, τ_y is fixed as 1, but τ_x varies with $0.3, 0.5,$ and 0.7, respectively. In the first column, we can see that increasing the governmental effort can reduce the infection peak, whereas in the second column a proactive intervention by the government ($\tau_y = 1.0$) indirectly influences people to adhere to voluntary self-provision (orange colored line in the second

column). Also, a higher sensitivity (i.e., higher τ_x) increases the proportion of self-quarantined individuals.

2.3.3 Varying the Governmental Total Budget

Figure 5 shows the time evolution of the symptomatic infected, self-quarantined, and forced quarantined individuals. We demonstrate the results by varying the governmental budget. In the first graph, we see that increasing the budget reduces the peak size of symptomatic infected people. If the budget is kept at a minimum level meaning that if there is no governmental intervention, the peak of infected people occurs around 0.6, i.e., 60% of the total population can be infected. Increasing the budget can successively reduce the peak of infected people because the government can provide more facilities. In the second graph, increasing the total budget also increases the number of self-quarantine people as people are motivated by the government to increase themselves for committing self-quarantine. In the third graph, we can see that increasing the budget also increases the number of people in forced quarantine but, as self-quarantine increases there is less necessity to make people forced quarantined because the infected people are reduced due to conforming self-quarantine. Thus, forced quarantine is reduced by increasing the budget to the maximum level.

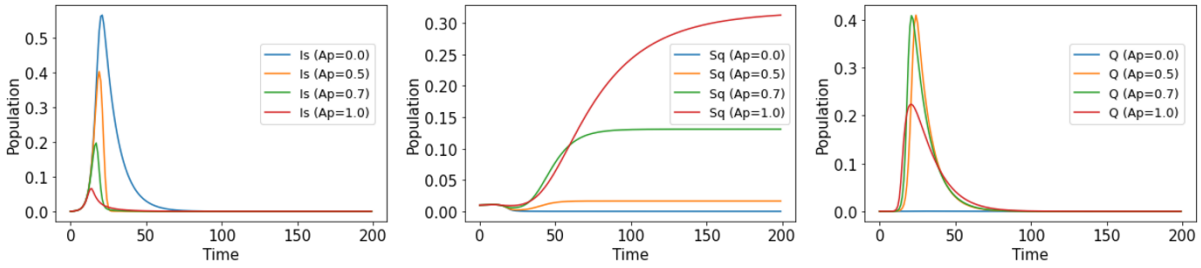

Figure 5: Time series of symptomatic infected people (I_s), self-quarantine people (S_Q) and forced quarantine people (Q) are shown by varying the government's total budget A_p from 0 to 1 where all the remaining parameters are taken as standard cases.

2.3.4 Final epidemic size, time accumulated self-quarantine, time accumulated forced quarantine:

In this section, we show some heatmaps (Figures 6, 7, and 8) of FES, time-integrated self-quarantine, and time-integrated forced quarantine when the parameters that primarily contribute to the basic reproduction number are varied. We also justify our parameter assumptions. We modify two parameters in each graph, while the remaining values are fixed according to our standard assumption.

As shown in Figure 6, row (1), we can see that raising τ_y reduces FES while increasing τ_x does not affect FES. We can also observe that increasing τ_x and τ_y sends more people into self-quarantine conditions. Increasing τ_y also causes more people to be forced into quarantine.

In row (2), the disease transmission rate from normal-acting people, β_N, must be close to 1 to notice any influence on FES, whereas the disease transmission rate from the self-quarantined people, β_Q, can be set anywhere from 0 to 1.

In row (3), the asymptomatic infection rate, ξ, should be lower to keep people in the self-quarantine and forced quarantine states. Increasing ξ makes the FES larger.

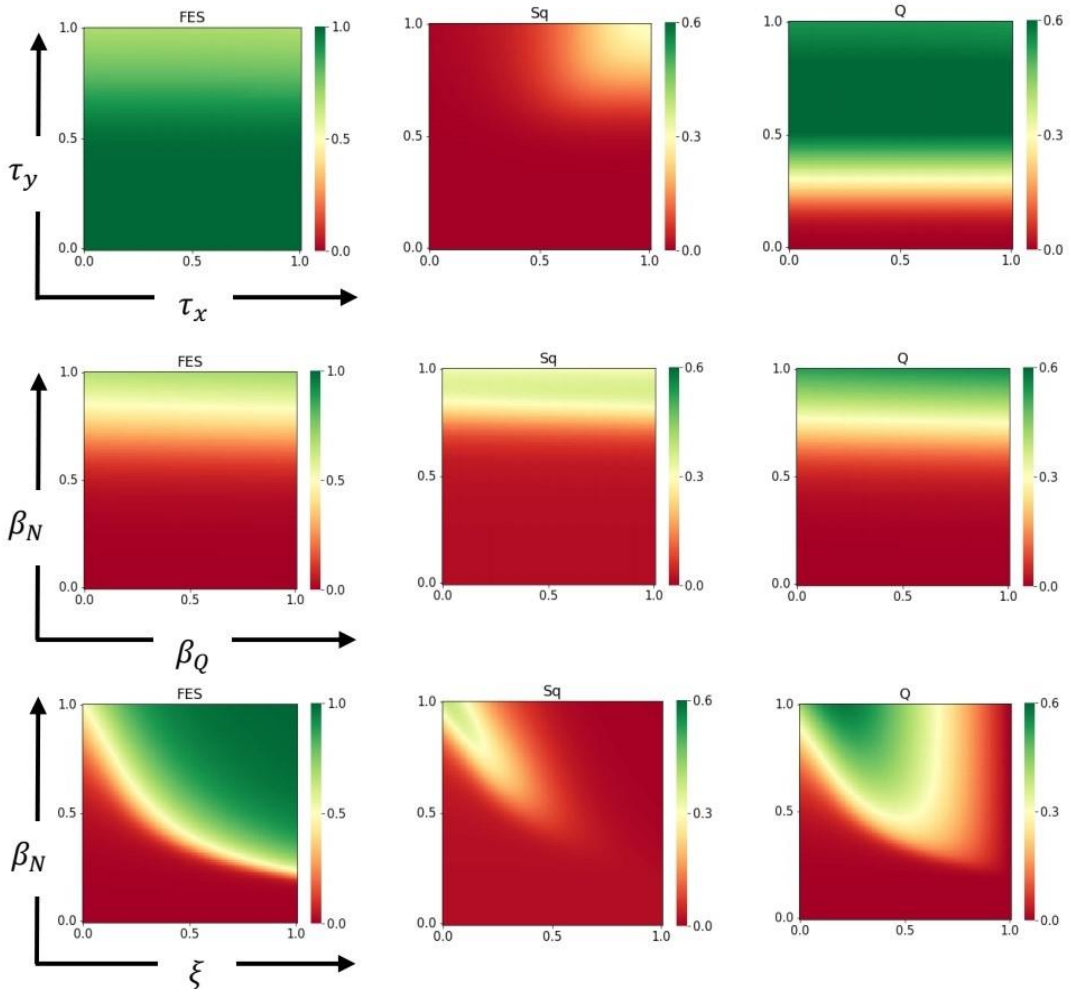

Figure 6: Heatmaps of FES, $\sum S_Q$, $\sum Q$. Three different types of heatmaps are shown in each of the three rows. In the first column, FES is represented by a color bar ranging from 0 to 1. In the second and third columns, time-integrated self-quarantined and time-integrated forced-quarantined people are represented by a color bar ranging from 0 to 0.6. In the first row, the panels are displayed by varying τ_x and τ_y from 0 to 1. The remaining parameters are set fixed with the standard ones. Similarly, in rows 2 and 3, the panels are displayed by varying β_Q and β_N, ξ and β_N from 0 to 1. Apparently, τ_y plays a pivotal role in reducing FES. Also, the fraction of self-conscious individuals (S_q) increases with β_N (second heatmap in the second row) although it does not improve the epidemic scenario as the self-provision is not perfect (first heatmap in the second row).

In rows (1–3) of Figure 7, increasing the contact discount factor for asymptomatic people ε_I increases the FES. Like the previous panels of Figure 5, the setting β_Q from 0 to 1 does not have any significant impact on the FES. Increasing of ξ can increase FES which is also observed in the previous panels of Figure 6.

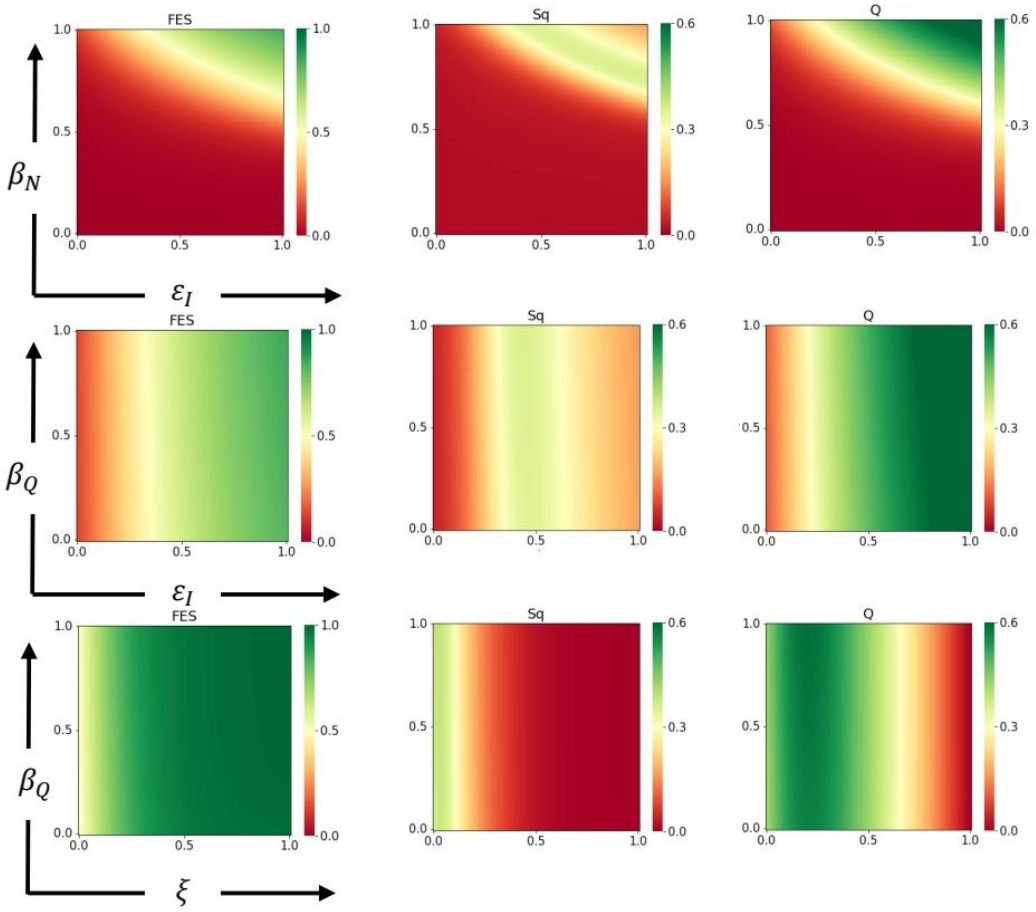

Figure 7: Heatmaps of FES, $\sum S_Q$, $\sum Q$. In each of the three rows, three different kinds of heatmaps are displayed. A color bar ranging from 0 to 1 represents FES in the first column. A color bar ranging from 0 to 0.6 is used in the second and third columns to represent time-integrated self-quarantined and time-integrated forced-quarantined people. In the first row, the panels are displayed by varying ε_I and β_N from 0 to 1. The remaining parameters are set fixed with the standard ones. Similarly, from rows 2 to 3, the panels are displayed by varying ε_I and β_Q, ξ and β_Q, respectively, from 0 to 1.

In row 1 of Figure 8, increasing the self-quarantine cost for an individual from 0 to 0.1 does not have an impact on the reduction of FES but increasing the individual cost for forced quarantine greater than 0.03 significantly increases the value of FES. Additionally, the government's total budget needs to be set greater or equal to 1 (rows 2 and 3) to reduce the FES.

These results, Figs. 6–8 confirm the sensitivities from major model parameters on FES and the total amount of quarantine individuals, which seems quite plausible.

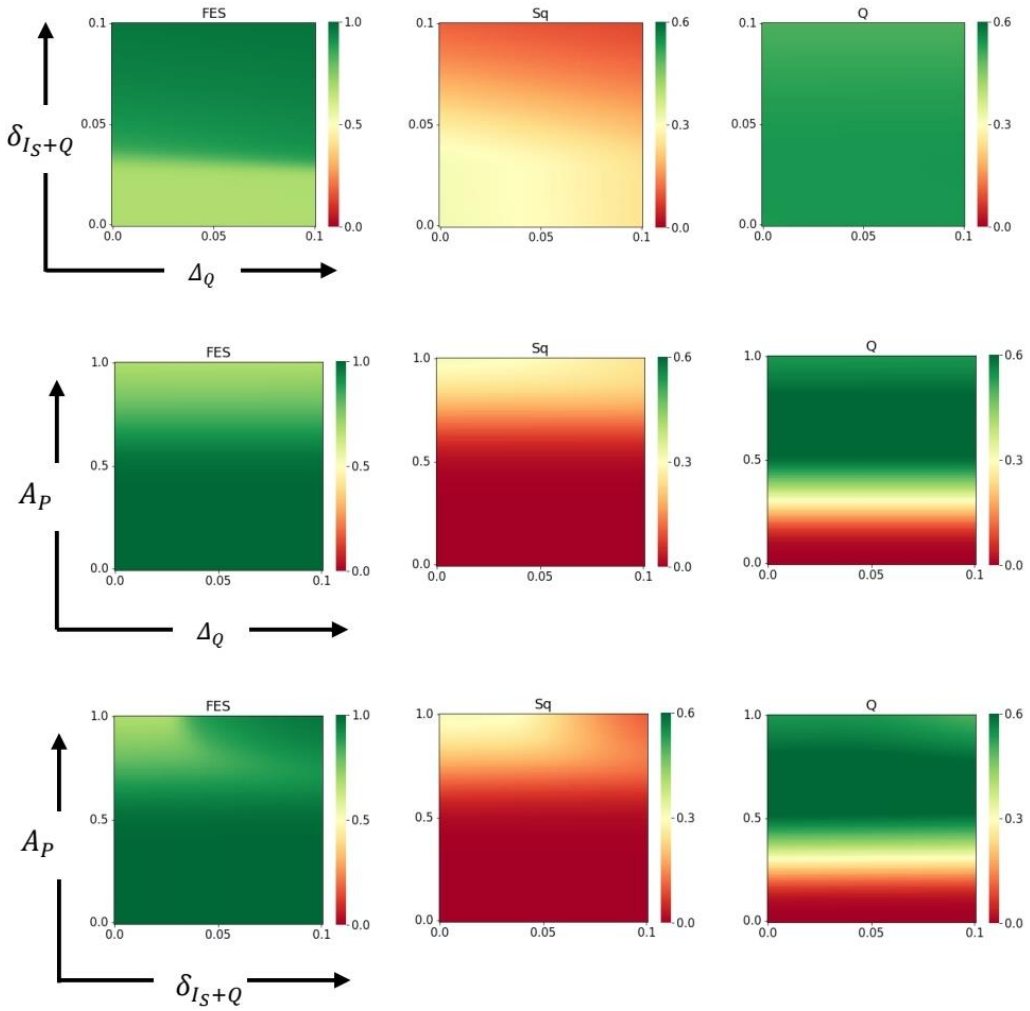

Figure 8: Heatmaps of FES, $\sum S_Q$, $\sum Q$. Each of the three rows contains three different types of heatmaps. A color bar ranging from 0 to 1 represents FES. A color bar ranging from 0 to 0.6 represents time-integrated self-quarantined and time-integrated forced-quarantined people in the second and third columns, respectively. In the first row, the panels are displayed by varying Δ_Q and δ_{I_S+Q} from 0 to 0.1. The remaining parameters are set fixed with the standard ones. Similarly, from rows 2 to 3, the panels are displayed by varying Δ_Q and A_P, δ_{I_S+Q} and A_P where Δ_Q and δ_{I_S+Q} vary from 0 to 0.1 and A_P varies from 0 to 1.

2.3.5 ΔFES and critical points

In this section, we show (Figure 9) the previously defined critical points and their consecutive lines, as well as the ΔFES in terms of the two cost parameters. In the region below the critical line, the total cost for self-quarantine and forced quarantine is less than the reduction of disease cost, indicating a favorable situation for cost-effective epidemic control by the two quarantine policies. When we reduce the self-

quarantine effort (τ_x) by half (second panel of the first row), ΔFES decreases, implying less extent of reduction on FES by both interventions. Needless to say, it is a worse scenario than the standard settings. If we reduce the forced quarantine effort (τ_y) (third panel of the first row), the situation deteriorates even more than in the previous two cases. Increasing (first panel of the second row) and decreasing (second panel of the second row) β_Q results in a worse and better scenario than the standard case that is conceivable. As the rate of asymptomatic infection (ξ) rises (third panel of the second row), the situation worsens.

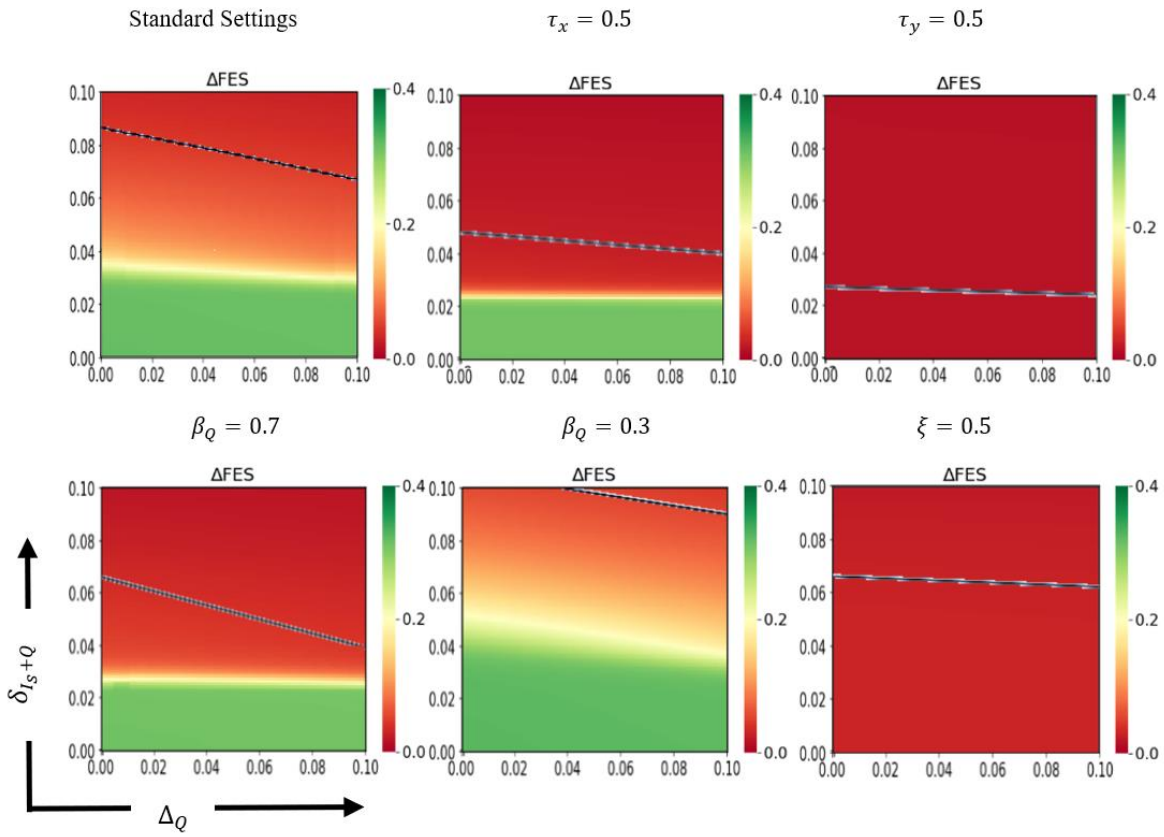

Figure 9: ΔFES and critical lines are presented to observe the reduced cost margin using both interventions. In this figure, all panels represent the difference between FES with no intervention and FES with both interventions with a color bar ranging from 0 to 0.4 in terms of the individual cost parameters Δ_Q *and* δ_{I_S+Q}. All critical points are linked to form a line where the total cost of the epidemic equals the difference of two FES. With the standard set of parameters, ΔFES is represented in the first panel (upper leftmost) by green, yellow, and red zones, with moving from green to red indicating an increase in FES. Keeping the value of δ_{I_S+Q} less than 0.03, is the best option to make the government intervention more successful. The critical line marked the maximum value of cost combining the two total costs that can be used to control the epidemic. It was observed that, for the first panel when the self-quarantine cost for individual Δ_Q is zero the forced quarantine cost for individual δ_{I_S+Q} must be less than 0.087, and if $\Delta_Q = 0.1$, the maximum in our consideration, δ_{I_S+Q} must be less

than 0.067. The remaining panels are presented by changing the other focal parameters $(\tau_x, \tau_y, \beta_Q \; and \; \xi)$ of the model and observed the different values for $\Delta_Q \; and \; \delta_{I_S+Q}$ to control the epidemic.

2.3.6 ASP and SED

Figure 10 shows the heatmaps of FES, time-integrated S_Q, and time-integrated Q along the cost parameters for NE (row 1) and SO (row 2). In row 3, ASP^{NE} and ASP^{SO} are presented along with the SED for the standard set of parameters. Here, we observe that increasing the value of δ_{I_S+Q} brings higher FES (because of less incentive to quarantine), while increasing the value of Δ_Q has less effect on FES in NE. In SO, we can observe less FES because the maximum flux of $x = 1.0$ and $y = 1.0$ brings the minimum FES, and most people are moving to the S_Q state. Consequently, the ASP^{SO} is very close to zero. Thus, SED is similar to ASP^{NE}. We observe that increasing the value of δ_{I_S+Q} brings more positive value to SED; thus, the social dilemma increases.

Note that the SED is featured with a larger sensitivity in δ_{I_S+Q} direction than that in Δ_Q direction. It is paraphrased by the allegation that the government could solve a more severe social dilemma than that imposed on each individual around whether he/she is committing self-quarantine by increasing the government's effort to let more infected individuals be forcefully quarantined. Thus, the social dilemma acting on the government level (through the provision of forced quarantine) is more severe than another social dilemma acting on an individual level (around self-quarantine). This is because governmental intervention through forced quarantine is more effective in preventing disease from spreading. This fact might be conceivable because self-quarantine works in an 'ex-post' way where infected people who quarantine never get infected again (they must stay at Q; see Figure 1). However, self-quarantine only works as pre-emptive; an individual once self-quarantined may (may not) get infected sooner or later.

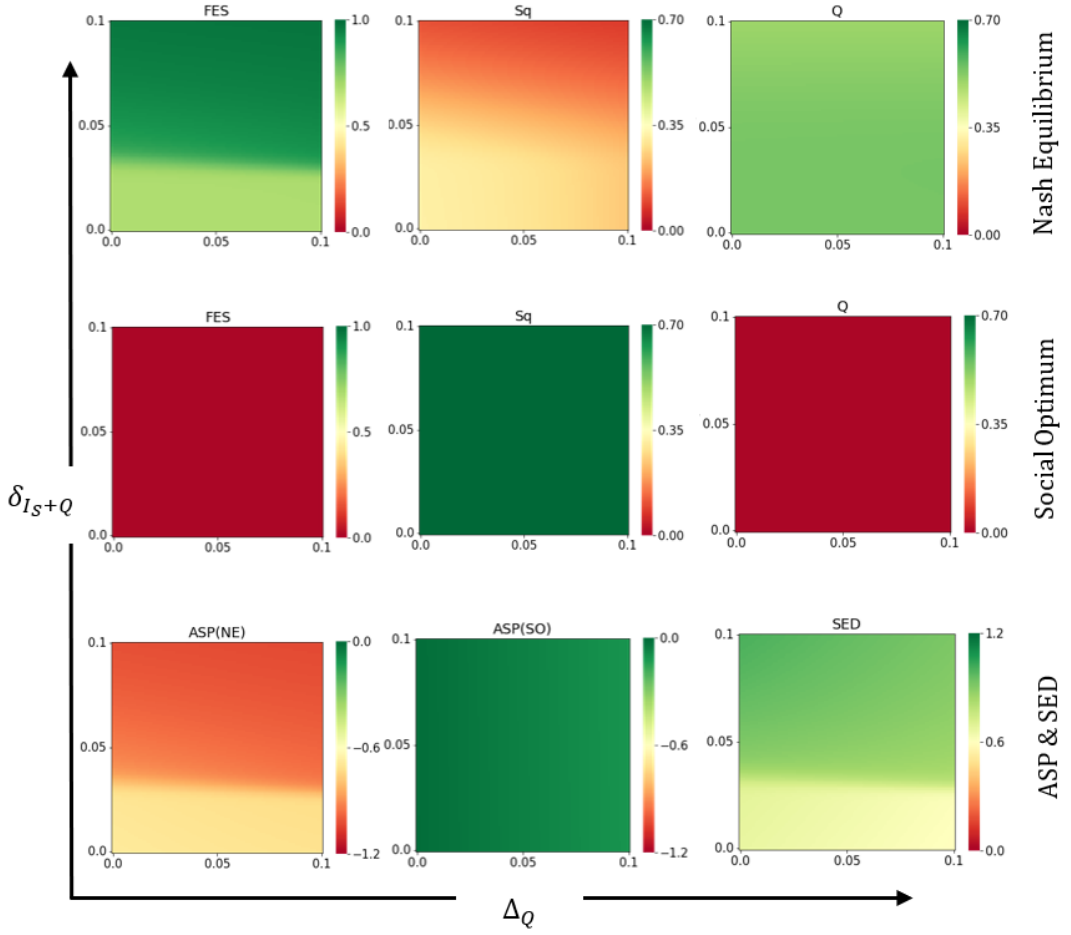

Figure 10: FES, $\sum S_Q$, $\sum Q$, ASP at NE, SO, and SED to observe the social dilemma. In this figure, the FES, time-integrated S_Q, and time-integrated Q are represented in the first two rows for the case of Nash equilibrium and social optimum in terms of the cost parameters Δ_Q *and* δ_{I_S+Q}. FES panels are displayed with a color bar ranging from 0 to 1, whereas S_Q and Q panels are displayed with a color bar ranging from 0 to 0.7. In the third row, ASP at NE and SO are displayed with a color bar ranging from -1.2 to 0.0, and SED is displayed with a color bar ranging from 0.0 to 1.2. The governmental intervention cost seems more influential in reducing the disease prevalence and social efficiency deficit.

Figure 11 shows some other combinations for ASP^{NE} and corresponding SED. For the first case (1st and 3rd panels of row 1), if $\tau_x = 0.5$, i.e., the effort rate of self-quarantine is reduced, then ASP^{NE} and SED almost behave the same as the standard case, meaning that increasing the forced quarantine costs for individuals increases the social dilemma. However, if τ_y is reduced (2nd and 4th panels of row 1), ASP^{NE} is getting lower bringing SED higher; thus, the social dilemma increases more than the standard case, which is not an ideal situation to control the epidemic. If the transmission rate β_Q reduces (1st and 3rd panels of row 2), more people stay in the S_Q state, resulting in a dilemma that reduces more than the standard case. Similarly increasing β_Q (2nd and 4th panels of row 2) increases the value of FES, and

more people are going to be infected; thus, reducing reduces the dilemma more than the standard case. If the asymptomatic infection rate (ξ) increased (row 3), FES also increased, and the value of SED gets closer to zero, meaning that there is no dilemma when most of the people are asymptomatic.

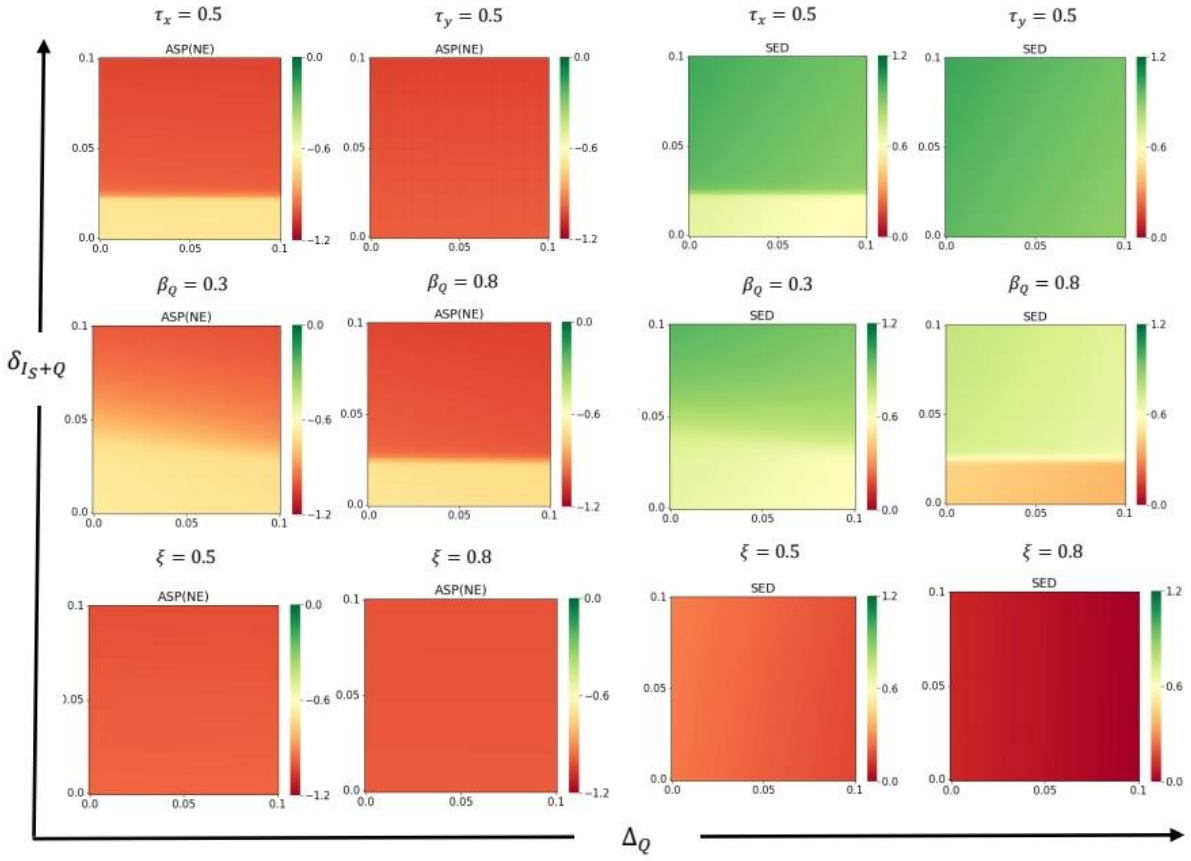

Figure 11: ASP at NE and corresponding SED to observe the social dilemma. In this figure, different ASPs at NE are displayed along with the corresponding SED with a color bar ranging from -1.2 to 0.0 and 0.0 to 1.2, respectively. All panels are drawn in terms of the cost parameters Δ_Q *and* δ_{I_S+Q}.

2.4 Conclusion

In this study, we developed an epidemiological model based on SEIR dynamics that considers dynamic human behavior for individuals and governments regarding self-quarantine and forced quarantine, respectively. The aim was to observe the interplay between both provisions towards controlling disease spreading. In general, imposing compulsory quarantine by the government seems more effective in containing the disease than self-quarantine. We also demonstrated that increasing the government's compulsory quarantine rate can considerably reduce the value of the basic reproduction number. Additionally, we observed that a proactive authoritative measure (quantified by a higher sensitivity to forced quarantine) upsurges the fraction of self-quarantine (Fig. 4), which intuitively indicates that the government's increased effort made people more aware of the importance of self-quarantine. In terms

of cost parameters, we observed that the government must keep the cost of forced quarantine under control, whereas the cost of self-quarantine does not need to be regulated.

We further demonstrated the impact of both provisions in reducing the social efficiency deficit, which is quantified by the gap between the overall payoff at the social optimum and equilibrium. Our results suggest that authoritative intervention (i.e., forced quarantine) is more effective in reducing such deficit. The analysis of SED reveals that there are rich and complex dynamics depending on the cost of forced quarantine for individuals, but not so much on the cost of self-quarantine for individuals. Also, by observing the features at NE with the prediction of our behavior model, human decisions have an inertial influence which allows humans to take certain preventive measures to slow the disease from spreading.

We intend to expand our models in the future. We might add a vaccine compartment, where people can choose their immunization to limit the danger of a pandemic. The government should focus on overall vaccination coverage to lower the death rate. We are also looking into how the inclusion of multi-strain epidemic models affects social behavior, such as self-quarantine or vaccination.

References

[1] M. Alam, K.M.A. Kabir, J. Tanimoto, Based on mathematical epidemiology and evolutionary game theory, which is more effective: Quarantine or isolation policy, J. Stat. Mech. Theory Exp. 2020 (2020). https://doi.org/10.1088/1742-5468/ab75ea.

[2] N. Nkire, K. Mrklas, M. Hrabok, A. Gusnowski, W. Vuong, S. Surood, A. Abba-Aji, L. Urichuk, B. Cao, A.J. Greenshaw, V.I.O. Agyapong, COVID-19 Pandemic: Demographic Predictors of Self-Isolation or Self-Quarantine and Impact of Isolation and Quarantine on Perceived Stress, Anxiety, and Depression, Front. Psychiatry. 12 (2021) 1–8. https://doi.org/10.3389/fpsyt.2021.553468.

[3] M.S. Aronna, R. Guglielmi, L.M. Moschen, A model for COVID-19 with isolation, quarantine and testing as control measures, Epidemics. 34 (2021) 100437. https://doi.org/10.1016/j.epidem.2021.100437.

[4] C.R. Wells, P. Sah, S.M. Moghadas, A. Pandey, A. Shoukat, Y. Wang, Z. Wang, L.A. Meyers, B.H. Singer, A.P. Galvani, Impact of international travel and border control measures on the global spread of the novel 2019 coronavirus outbreak, Proc. Natl. Acad. Sci. U. S. A. 117 (2020) 7504–7509. https://doi.org/10.1073/pnas.2002616117.

[5] I. Yen-Hao Chu, P. Alam, H.J. Larson, L. Lin, Social consequences of mass quarantine during epidemics: A systematic review with implications for the COVID-19 response, J. Travel Med. 27 (2020) 1–14. https://doi.org/10.1093/JTM/TAAA192.

[6] D. Meidan, N. Schulmann, R. Cohen, S. Haber, E. Yaniv, R. Sarid, B. Barzel, Alternating

quarantine for sustainable epidemic mitigation, Nat. Commun. 12 (2021) 1–12. https://doi.org/10.1038/s41467-020-20324-8.

[7] G. De Meijere, V. Colizza, E. Valdano, C. Castellano, Effect of delayed awareness and fatigue on the efficacy of self-isolation in epidemic control, Phys. Rev. E. 104 (2021) 1–8. https://doi.org/10.1103/PhysRevE.104.044316.

[8] K.M.A. Kabir, T. Risa, J. Tanimoto, Prosocial behavior of wearing a mask during an epidemic: an evolutionary explanation, Sci. Rep. 11 (2021) 1–14. https://doi.org/10.1038/s41598-021-92094-2.

[9] M.A. Amaral, M.M. d. Oliveira, M.A. Javarone, An epidemiological model with voluntary quarantine strategies governed by evolutionary game dynamics, Chaos, Solitons and Fractals. 143 (2021) 110616. https://doi.org/10.1016/j.chaos.2020.110616.

[10] K.A. Kabir, A. Chowdhury, J. Tanimoto, An evolutionary game modeling to assess the effect of border enforcement measures and socio-economic cost: Export-importation epidemic dynamics, Chaos, Solitons and Fractals. 146 (2021) 110918. https://doi.org/10.1016/j.chaos.2021.110918.

[11] W. Adiyoso, Wilopo, Social distancing intentions to reduce the spread of COVID-19: The extended theory of planned behavior, BMC Public Health. 21 (2021) 1–12. https://doi.org/10.1186/s12889-021-11884-5.

[12] A. Chowdhury, K.M.A. Kabir, J. Tanimoto, How quarantine and social distancing policy can suppress the outbreak of novel coronavirus in developing or under poverty level countries: a mathematical and statistical analysis., Biometrics Biostat. Int. J. 10 (2020) 145–152. https://doi.org/10.21203/rs.3.rs-20294/v1.

[13] A. Aleta, D. Martín-Corral, A. Pastore y Piontti, M. Ajelli, M. Litvinova, M. Chinazzi, N.E. Dean, M.E. Halloran, I.M. Longini, S. Merler, A. Pentland, A. Vespignani, E. Moro, Y. Moreno, Modelling the impact of testing, contact tracing and household quarantine on second waves of COVID-19, Nat. Hum. Behav. 4 (2020) 964–971. https://doi.org/10.1038/s41562-020-0931-9.

[14] M. Jusup, P. Holme, K. Kanazawa, M. Takayasu, I. Romić, Z. Wang, S. Geček, T. Lipić, B. Podobnik, L. Wang, W. Luo, T. Klanjšček, J. Fan, S. Boccaletti, M. Perc, Social physics, Phys. Rep. 948 (2022) 1–148. https://doi.org/10.1016/j.physrep.2021.10.005.

[15] D. Helbing, D. Brockmann, T. Chadefaux, K. Donnay, U. Blanke, O. Woolley-Meza, M. Moussaid, A. Johansson, J. Krause, S. Schutte, M. Perc, Saving Human Lives: What Complexity Science and Information Systems can Contribute, 2015. https://doi.org/10.1007/s10955-014-1024-9.

[16] T. Lee, H.D. Kwon, J. Lee, The effect of control measures on COVID-19 transmission in South Korea, PLoS One. 16 (2021) 1–18. https://doi.org/10.1371/journal.pone.0249262.

[17] J. Tanimoto, Fundamentals of evolutionary game theory and its applications, Springer (Tokyo), 2015.

[18] J. Tanimoto, Sociophysics approach to epidemics, Springer (Tokyo), 2021.

[19] J. Tanimoto, Evolutionary games with sociophysics: Analysis of traffic flow and epidemics, Springer (Tokyo), 2019.

[20] A. Babaei, M. Ahmadi, H. Jafari, A. Liya, A mathematical model to examine the effect of quarantine on the spread of coronavirus, Chaos, Solitons and Fractals. 142 (2021) 33–37. https://doi.org/10.1016/j.chaos.2020.110418.

[21] G. Pietrabissa, S.G. Simpson, Psychological Consequences of Social Isolation During COVID-19 Outbreak, Front. Psychol. 11 (2020) 9–12. https://doi.org/10.3389/fpsyg.2020.02201.

[22] V. Nenchev, Optimal quarantine control of an infectious outbreak, Chaos, Solitons and Fractals. 138 (2020) 110139. https://doi.org/10.1016/j.chaos.2020.110139.

[23] C.E. Madubueze, S. Dachollom, I.O. Onwubuya, Controlling the Spread of COVID-19: Optimal Control Analysis, Comput. Math. Methods Med. 2020 (2020). https://doi.org/10.1155/2020/6862516.

[24] K.M. Ariful Kabir, M. Jusup, J. Tanimoto, Behavioral incentives in a vaccination-dilemma setting with optional treatment, Phys. Rev. E. 100 (2019) 1–13. https://doi.org/10.1103/PhysRevE.100.062402.

[25] M. Ahsan Habib, M. Tanaka, J. Tanimoto, How does conformity promote the enhancement of cooperation in the network reciprocity in spatial prisoner's dilemma games? Chaos, Solitons and Fractals. 138 (2020) 109997. https://doi.org/10.1016/j.chaos.2020.109997.

[26] M.R. Arefin, J. Tanimoto, Evolution of cooperation in social dilemmas under the coexistence of aspiration and imitation mechanisms, Phys. Rev. E. 102 (2020) 32120. https://doi.org/10.1103/PhysRevE.102.032120.

[27] J. Tanimoto, H. Sagara, Relationship between dilemma occurrence and the existence of a weakly dominant strategy in a two-player symmetric game, BioSystems. 90 (2007) 105–114. https://doi.org/10.1016/j.biosystems.2006.07.005.

[28] K.M. Ariful Kabir, J. Tanimoto, Modelling and analyzing the coexistence of dual dilemmas in the proactive vaccination game and retroactive treatment game in epidemic viral dynamics, Proc. R. Soc. A Math. Phys. Eng. Sci. 475 (2019). https://doi.org/10.1098/rspa.2019.0484.

[29] M.R. Arefin, K.M.A. Kabir, M. Jusup, H. Ito, J. Tanimoto, Social efficiency deficit deciphers social dilemmas, Sci. Rep. 10 (2020) 1–9. https://doi.org/10.1038/s41598-020-72971-y.

[30] A. Szolnoki, M. Perc, Conformity enhances network reciprocity in evolutionary social dilemmas, J. R. Soc. Interface. 12 (2015) 2–9. https://doi.org/10.1098/rsif.2014.1299.

[31] C. Ohajunwa, K. Kumar, P. Seshaiyer, Mathematical modeling, analysis, and simulation of the COVID-19 pandemic with explicit and implicit behavioral changes, Comput. Math. Biophys. 8 (2020) 216–232. https://doi.org/10.1515/cmb-2020-0113.

[32] U. Foryś, Mathematical models in epidemiology and immunology, 2000. https://doi.org/10.14708/ma.v28i42/01.1879.

[33] D. Stipic, M. Bradac, T. Lipic, B. Podobnik, Effects of quarantine disobedience and mobility restrictions on COVID-19 pandemic waves in dynamical networks, Chaos, Solitons and Fractals. 150 (2021) 111200. https://doi.org/10.1016/j.chaos.2021.111200.

[34] M.A. Safi, A.B. Gumel, Dynamics of a model with quarantine-adjusted incidence and quarantine of susceptible individuals, J. Math. Anal. Appl. 399 (2013) 565–575. https://doi.org/10.1016/j.jmaa.2012.10.015.

[35] M.A. Safi, A.B. Gumel, The effect of incidence functions on the dynamics of a quarantine/isolation model with time delay, Nonlinear Anal. Real World Appl. 12 (2011) 215–235. https://doi.org/10.1016/j.nonrwa.2010.06.009.

[36] M.U.G. Kraemer, C.H. Yang, B. Gutierrez, C.H. Wu, B. Klein, D.M. Pigott, L. du Plessis, N.R. Faria, R. Li, W.P. Hanage, J.S. Brownstein, M. Layan, A. Vespignani, H. Tian, C. Dye, O.G. Pybus, S. V. Scarpino, The effect of human mobility and control measures on the COVID-19 epidemic in China, Science (80-.). 368 (2020) 493–497. https://doi.org/10.1126/science.abb4218.

[37] K.M.A. Kabir, J. Tanimoto, Evolutionary game theory modeling to represent the behavioral dynamics of economic shutdowns and shield immunity in the COVID-19 pandemic: Economic shutdowns and shield immunity, R. Soc. Open Sci. 7 (2020). https://doi.org/10.1098/rsos.201095rsos201095.

[38] K.M.A. Kabir, K. Kuga, J. Tanimoto, Analysis of SIR epidemic model with information spreading of awareness, Chaos, Solitons and Fractals. 119 (2019) 118–125. https://doi.org/10.1016/j.chaos.2018.12.017.

[39] M. Martcheva, An Introduction to Mathematical Epidemiology, 2013.

[40] C.T. Deressa, Y.O. Mussa, G.F. Duressa, Optimal control and sensitivity analysis for

transmission dynamics of Coronavirus, Results Phys. 19 (2020) 103642. https://doi.org/10.1016/j.rinp.2020.103642.

[41] K. Miyaji, J. Tanimoto, A co-evolutionary model combined mixed-strategy and network adaptation by severing disassortative neighbors promotes cooperation in prisoner's dilemma games, Chaos, Solitons and Fractals. 143 (2021) 110603. https://doi.org/10.1016/j.chaos.2020.110603.

[42] Z. Feng, Final and Peak Epidemic Sizes for Seir Models, Math. Biosci. Eng. 4 (2007) 675–686.

[43] T. Hussain, M. Ozair, F. Ali, S. ur Rehman, T.A. Assiri, E.E. Mahmoud, Sensitivity analysis and optimal control of COVID-19 dynamics based on SEIQR model, Results Phys. 22 (2021) 103956. https://doi.org/10.1016/j.rinp.2021.103956.

[44] J. Fan, Q. Yin, C. Xia, M. Perc, Epidemics on multilayer simplicial complexes, Proc. R. Soc. A Math. Phys. Eng. Sci. 478 (2022). https://doi.org/10.1098/rspa.2022.0059.

[45] H.J. Li, W. Xu, S. Song, W.X. Wang, M. Perc, The dynamics of epidemic spreading on signed networks, Chaos, Solitons and Fractals. 151 (2021) 111294. https://doi.org/10.1016/j.chaos.2021.111294.

[46] C.T. Bauch, Imitation dynamics predict vaccinating behavior, Proc. R. Soc. B Biol. Sci. 272 (2005) 1669–1675. https://doi.org/10.1098/rspb.2005.3153.

[47] C.T. Bauch, S. Bhattacharyya, Evolutionary game theory and social learning can determine how vaccine scares unfold, PLoS Comput. Biol. 8 (2012). https://doi.org/10.1371/journal.pcbi.1002452.

[48] A. Deka, S. Bhattacharyya, The effect of human vaccination behavior on strain competition in an infectious disease: An imitation dynamic approach, Theor. Popul. Biol. 143 (2022) 62–76. https://doi.org/10.1016/j.tpb.2021.12.001.

[49] M.R. Arefin, T. Masaki, J. Tanimoto, Vaccinating behavior guided by imitation and aspiration: Vaccinating behavior. - Imit. And asp., Proc. R. Soc. A Math. Phys. Eng. Sci. 476 (2020). https://doi.org/10.1098/rspa.2020.0327rspa20200327.

[50] M.R. Arefin, K.M.A. Kabir, J. Tanimoto, A mean-field vaccination game scheme to analyze the effect of a single vaccination strategy on a two-strain epidemic spreading, J. Stat. Mech. Theory Exp. 2020 (2020). https://doi.org/10.1088/1742-5468/ab74c6.

[51] M.R. Arefin, J. Tanimoto, Imitation and aspiration dynamics bring different evolutionary outcomes in feedback-evolving games, Proc. R. Soc. A Math. Phys. Eng. Sci. 477 (2021). https://doi.org/10.1098/rspa.2021.0240.

[52] J.K. Taubenberger, D.M. Morens, 1918 Influenza: the Mother of All Pandemics, Emerg. Infect. Dis. 12 (2006) 15–22. https://doi.org/10.3201/eid1209.050979.

[53] E. Schneider, Severe Acute Respiratory Syndrome (SARS), Netter's Infect. Dis. (2012) 537–543. https://doi.org/10.1016/B978-1-4377-0126-5.00089-6.

[54] R. Tori, J. Tanimoto, A study on prosocial behavior of wearing a mask and self-quarantining to prevent the spread of diseases underpinned by evolutionary game theory, Chaos, Solitons Fractals Interdiscip. J. Nonlinear Sci. Nonequilibrium Complex Phenom. 158 (2022) 112030. https://doi.org/10.1016/j.chaos.2022.112030.

[55] O. Diekmann, J.A.P. Heesterbeek, J.A.J. Metz, On the definition and the computation of the basic reproduction ratio R0 in models for infectious diseases in heterogeneous populations, J. Math. Biol. 28 (1990) 365–382. https://doi.org/10.1007/BF00178324.

[56] D. Niño-Torres, A. Ríos-Gutiérrez, V. Arunachalam, C. Ohajunwa, P. Seshaiyer, Stochastic modeling, analysis, and simulation of the COVID-19 pandemic with explicit behavioral changes in Bogotá: A case study, Infect. Dis. Model. 7 (2022) 199–211. https://doi.org/10.1016/j.idm.2021.12.008.

Chapter 3

Time delay of the appearance of a new strain can affect vaccination behavior and disease dynamics: An evolutionary explanation

Abstract

The emergence of a novel strain during a pandemic, like the current COVID-19, is a major concern to the healthcare system. The most effective strategy to control this type of pandemic is vaccination. Many previous studies suggest that the existing vaccine may not be fully effective against the new strain. Additionally, the new strain's late arrival has a significant impact on the disease dynamics and vaccine coverage. Focusing on these issues, this study presents a two-strain epidemic model in which the new strain appears with a time delay. We considered two vaccination provisions, namely preinfection and postinfection vaccinations, which are governed by human behavioral dynamics. In such a framework, individuals have the option to commit vaccination before being infected with the first strain. Additionally, people who forgo vaccination and become infected with the first train have the chance to be vaccinated (after recovery) in an attempt to avoid infection from the second strain. However, a second strain can infect vaccinated and unvaccinated individuals. People may have additional opportunities to be vaccinated and to protect themselves from the second strain due to the time delay. Considering the cost of the vaccine, the severity of the new strain, and the vaccine's effectiveness, our results indicated that delaying the second strain decreases the peak size of the infected individuals. Finally, by estimating the social efficiency deficit, we discovered that the social dilemma for receiving immunization decreases with the delay in the arrival of the second strain.

3.1 Introduction

Multistrain infection models are essential tools for studying and predicting infection dynamics in the presence of many active strains. Many illnesses, including human immunodeficiency virus (HIV), dengue fever, tuberculosis (TB), and even the current COVID-19, can arise when two or more strains coexist. For example, H1N1 flu virus infection is considered a seasonal influenza mutation, whereas COVID-19 is categorized as a novel SARS-CoV-1 strain. This mutation process can result in the emergence of new strains, especially if an effective medication has yet to be developed [1–3]. In the epidemic's propagation phase, the time it takes for a new strain to arise also plays a crucial role [4–6]. In the meantime, the cost of immunization and the vaccine's efficiency against the new strain significantly influence worldwide epidemic dynamics [7–12].

Most compartmental models, which are a negotiable instrument in the study of disease transmission and well-being administration frameworks, are as often as possible utilized to look at any epidemic process or pandemic. The SIR model, designed by Kermack and Mckendrick, is the most extensively used epidemiological model [13]. It has been altogether investigated and extended to see an assortment of speculations and circumstances. Simply put, this show portrays how ailment voyages in individuals from the susceptible compartment (S) to the infected compartment (I) and after that to the recovered compartment (R), where individuals construct insusceptibility to reinfection. Exposed (E), quarantine (Q), hospitalized (H), and asymptomatic (A) compartments can be used in some epidemics to adequately examine disease dynamics [4–6,8,14–31]. Examination of supervision and moderation measures, like immunization, establishing of vector-borne maladies, and the impact of birthing and passing elements is an extra application of compartmental models in the study of disease transmission [8–11, 15,17,30,32–39]. Misinformation dissemination, corruption, and resource misuse are factors that might be examined in SIR dynamics. However, most of these models focus on the evolution of the illness instead of the individual's behavioral response to the situation. However, numerous irresistible infection control approaches depend on human and organizational decision-making [9–12,17,30,34,40]. In, this context, the new field of behavioral epidemiology that incorporates psychology and game theory into epidemiology attracted significant attention [29,33,36,41–45]. Individual behavior, rather than a static role, is considered in behavioral epidemiology. Sociophysics, a cutting-edge discipline that combines statistical physics with evolutionary game theory (EGT) to better explain human behavior, is the ideal discipline for this situation [39,41–43]. Bauch combined the SIR model with EGT to study the vaccine decision-making dynamics in a novel approach [34,46,47]. Any individual can choose their immunization based on disease dynamics, vaccination cost, and vaccine effectiveness [7,9–11,15,30,32,34,38,48]. This later evolved into the "vaccination game" concept [7,9,10,16,33,37,38,41,43,44,49]. As a result of this technique, several observations and predictions in vaccination operations have been made. However, compared to investigations of the dynamical behaviors of multistrain epidemic models with vaccination and time delays, early studies have received little attention. The dynamics of a two-strain epidemic model were studied in [9,15,18–20,22–25,38,50–54]. Epidemic models with time delay were studied in [4,5,20,21,26,35,50,55,56]. Multistrain models with vaccination behaviors were studied in [9,12,15,18,34,37,38,56]. Stability analysis of multistrain models was found in [19–21,23,38,52,53,56,57].

Here, we propose an epidemic model with two strains in which the first strain is active from the start of the disease and the second strain emerges after a while. People can be vaccinated in one of two ways: before they become infected with strain 1 or after recovering from it. The new strain can infect vaccinated and unvaccinated individuals. When people's preferred alternatives are to take a vaccination or not, as well as when to take a vaccine, the behavior model gives a framework for describing individual behavior. We also demonstrated the impact of the new strain's introduction on disease

dynamics and individual vaccination behavior, as well as the total vaccine coverage considering the time delay. The concept of social efficiency deficit (SED), which is the difference between Nash equilibrium (NE) and the social optimum, is incorporated into our model (SO), to generate a social dilemma, taking into account the vaccine's efficacy and cost [7,17,39,41–43,58-62].

3.2 Model Formulation

3.2.1 Epidemic Model

Here we suggest a nine-compartmental two-strain epidemiological model based on the SVIR (susceptible, vaccination, infectious, recovered) dynamics. We also introduce two behaviors: preinfection and postinfection vaccinations of individuals. Depiction of the proposed model is shown in Figure 1. The formulation of the model is given as follows:

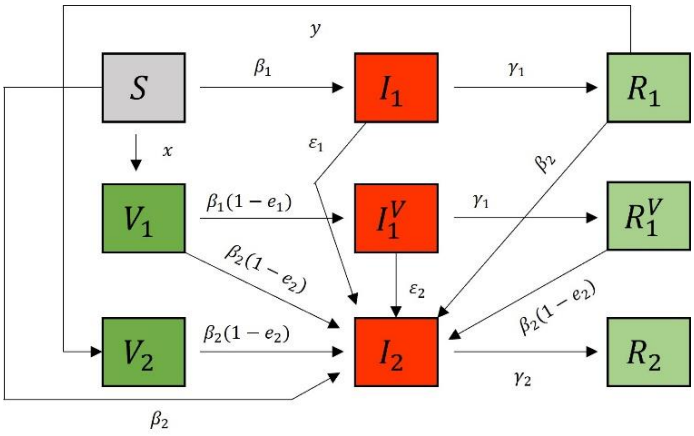

Figure 1: Depiction of the proposed model.

$$\dot{S} = -xS - \beta_1 S(I_1 + I_1^V) - \beta_2 S I_2 H, \quad (1)$$

$$\dot{V_1} = xS - \beta_1(1-e_1)(I_1 + I_1^V)V_1 - \beta_2(1-e_2)I_2 H V_1, \quad (2)$$

$$\dot{V_2} = yR_1 - \beta_2(1-e_2)I_2 H V_2, \quad (3)$$

$$\dot{I_1} = \beta_1 S(I_1 + I_1^V) - \gamma_1 I_1 - \varepsilon_1 H I_1, \quad (4)$$

$$\dot{I_1^V} = \beta_1(1-e_1)(I_1 + I_1^V)V_1 - \gamma_1 I_1^V - \varepsilon_2 H I_1^V, \quad (5)$$

$$\dot{I_2} = \beta_2 S I_2 H + \beta_2(1-e_2)I_2 H V_1 + \beta_2(1-e_2)I_2 H V_2 + \varepsilon_1 I_1 + \varepsilon_2 I_1^V + \beta_2 R_1 I_2 H + \beta_2(1-e_2)R_1^V I_2 H - \gamma_2 I_2 H, \quad (6)$$

$$\dot{R_1} = \gamma_1 I_1 - yR_1 - \beta_2 R_1 I_2 H, \quad (7)$$

$$\dot{R_1^V} = \gamma_1 I_1^V - \beta_2(1-e_2)R_1^V I_2 H, \quad (8)$$

$$\dot{R_2} = \gamma_2 I_2 H, \quad (9)$$

$$H(t-T) = \begin{cases} 0, t < T \\ 1, t \geq T \end{cases}, \quad T = \text{time delay of the appearance of strain 2}, \quad (10)$$

$$S(t) + V_1(t) + V_2(t) + I_1(t) + I_1^V(t) + I_2(t) + R_1(t) + R_1^V(t) + R_2(t) = 1, \quad (11)$$

where $S, V_1, V_2, I_1, I_1^V, I_2, R_1, R_1^V$, and R_2 are the fractions of individuals of susceptible, preinfected vaccinated, postinfected vaccinated, nonvaccinated and infected with strain 1, vaccinated and infected with strain 1, infected with strain 2, nonvaccinated and recovered from strain 1, vaccinated and recovered from strain 1, and recovered from strain 2, respectively. The total population is normalized to 1. Initially, every person is considered as susceptible. Individuals can choose vaccination and can move to the compartment V_1. Both the susceptible and vaccinated people can be infected with strain 1 since strain 1 is effective from the initial time of disease spreading. Those people who are not vaccinated at the first stage but got infected can take the vaccination after recovery from the strain 1 infection and can move to the V_2 compartment. In our study, we have considered a single type of vaccine whose efficiency is already known against the first strain but different for the second strain. All the vaccinated and nonvaccinated individuals can be infected by strain 2 when it appears. The Heaviside function H(t-T) is used to control the time delay of the appearance of strain 2. β_1 and β_2 are the transmission rates of strain 1 and strain 2 respectively. We consider $\beta_1 < \beta_2$ because the new strain is highly transmissible [20, 23]. We also demonstrate the dynamics for the opposite scenario. γ_1 and γ_2 are the recovery rates from strain 1 and strain 2 respectively. Additionally, we consider $\gamma_1 > \gamma_2$, i.e., the recovery time for strain 2 is higher [20, 23]. e_1 and e_2 are the vaccine efficacy values for strain 1 and strain 2, respectively. We have taken into account the fixed efficacy of the vaccine for strain 1, but we vary the efficacy for the new strain to demonstrate the vaccination behavior and the social dilemma. ε_1 and ε_2 are the mutation rates from nonvaccinated strain 1 and vaccinated strain 1 to strain 2, respectively. We have considered a very low mutation rate from strain 1 to strain 2. T represents the time delay of the emergence of strain 2. We didn't consider any co-infection of strain 1 and strain 2 in our work [9, 23, 38, 53]. Table 1 presents all parameters and their meaning.

3.2.2 Behavior Model

We discuss the idea of the behavior model, which explains the flux changing throughout time from susceptible (S) to preinfection vaccination (V_1) denoted by x and from the infected but recovered from strain 1 (R_1) to postinfected vaccination (V_2) denoted by y [34, 46, 47]. We illustrate the following two dynamical equations:

$$\dot{x} = t_x\, x\,(1-x)\{c_i\,(m_1 I_1 + m_1 I_1^V + m_2 I_2 H) - k\,c\}, \quad (12)$$

$$\dot{y} = t_y\, y\,(1-y)\{c_i\, m_2 I_2 H - k\,c\}, \quad (13)$$

where t_x and t_y are the inertial effects for the rate of the vaccinations; c_i and c are the disease cost and vaccination cost, respectively; $m_1$and m_2 are the severity effects of strains 1 and 2, respectively; and k is the relative sensitivity to taking the vaccination due to its cost. We have considered $c_i = 1.0$

throughout our study. Most earlier models included the total number of infected people at any given time, the cost of the disease, and the cost of vaccination when calculating the dynamics of vaccines [17,39]. The severity effect m_1, m_2 of the strains is considered in our study with the other parameters. The new strain frequently appears to be more severe and highly transmissible in most cases, such as the current COVID-19. To assess the dynamics of vaccination, the severity effect is also a crucial parameter. For the preinfection vaccination, we considered all infected individuals at any given time in equation (12). However, for the postinfection vaccination, we only take into account the total population of individuals infected with strain 2 in equation (13). This is because individuals who did not receive the vaccine the first time may be persuaded to do so by the emergence of a highly contagious and more severe strain.

Table 1: Model parameters and their description

Parameters	Description
β_1	Rate of strain 1's disease transmission
β_2	Rate of strain 2's disease transmission
e_1	Efficacy of the vaccine to strain 1
e_2	Efficacy of the vaccine to strain 2
γ_1	Recovery proportion for strain 1
γ_2	Recovery proportion for strain 2
ε_1	Mutation rate from strain 1 to strain 2 for nonvaccinated
ε_2	Mutation rate from strain 1 to strain 2 for vaccinated
t_x	Inertial effect on preinfection vaccination
t_y	Inertial effect on postinfection vaccination
m_1	Severity effect of strain 1
m_2	Severity effect of strain 2
c_i	Disease cost
c	Vaccination cost
k	Relative sensitivity due to the cost of vaccination

3.2.3 Primary Reproduction Number

We calculated the primary reproduction numbers for both strains using the next-generation matrix approach [24, 63–65]. For this, by considering the infection equations (4–6), we have

$$F = \begin{pmatrix} \beta_1 S I_1 + \beta_1 S I_1^V \\ \beta_1 V_1(1\text{-}e_1) I_1 + \beta_1 V_1(1\text{-}e_1) I_1^V \\ (\varepsilon_1 I_1 + \varepsilon_2 I_1^V + (\beta_2 S + \beta_2(1\text{-}e_2)V_2 + \beta_2 R_1 + \beta_2(1\text{-}e_2)R_1^V + \beta_2(1\text{-}e_2)V_1) I_2) H \end{pmatrix},$$

$$\nu = \begin{pmatrix} (\gamma_1 + \varepsilon_1 H) I_1 \\ (\gamma_1 + \varepsilon_2 H) I_1^V \\ \gamma_2 I_2 H \end{pmatrix},$$

Then, from F and ν, we calculate the matrices as follows:

$$F = \begin{pmatrix} \beta_1 S & \beta_1 S & 0 \\ \beta_1 V_1(1\text{-}e_1) & \beta_1 V_1(1\text{-}e_1) & 0 \\ \varepsilon_1 H & \varepsilon_2 H & (\beta_2 S + \beta_2(1\text{-}e_2)V_2 + \beta_2 R_1 + \beta_2(1\text{-}e_2)R_1^V + \beta_2(1\text{-}e_2)V_1) H \end{pmatrix},$$

$$V = \begin{pmatrix} \gamma_1 + \varepsilon_1 H & 0 & 0 \\ 0 & \gamma_1 + \varepsilon_2 H & 0 \\ 0 & 0 & \gamma_2 H \end{pmatrix},$$

$$V^{-1} = \begin{pmatrix} \frac{1}{\gamma_1 + \varepsilon_1 H} & 0 & 0 \\ 0 & \frac{1}{\gamma_1 + \varepsilon_2 H} & 0 \\ 0 & 0 & \frac{1}{\gamma_2 H} \end{pmatrix}.$$

Then, the next-generation matrix becomes,

$$M = FV^{-1} = \begin{pmatrix} \frac{\beta_1 S}{\gamma_1 + \varepsilon_1 H} & \frac{\beta_1 S}{\gamma_1 + \varepsilon_2 H} & 0 \\ \frac{\beta_1 V_1(1\text{-}e_1)}{\gamma_1 + \varepsilon_1 H} & \frac{\beta_1 V_1(1\text{-}e_1)}{\gamma_1 + \varepsilon_2 H} & 0 \\ \frac{\varepsilon_1 H}{\gamma_1 + \varepsilon_1 H} & \frac{\varepsilon_2 H}{\gamma_1 + \varepsilon_2 H} & \frac{(\beta_2 S + \beta_2(1\text{-}e_2)V_2 + \beta_2 R_1 + \beta_2(1\text{-}e_2)R_1^V + \beta_2(1\text{-}e_2)V_1) H}{\gamma_2 H} \end{pmatrix}.$$

Finally, by calculating the eigenvalues of the matrix M, we have the following expressions for the primary reproduction number of strains 1 and 2.

$$R_{o1} = \frac{\beta_1 S}{\gamma_1 + \varepsilon_1 H} + \frac{\beta_1 V_1(1\text{-}e_1)}{\gamma_1 + \varepsilon_2 H}, \tag{14}$$

$$R_{o2} = \frac{(\beta_2 S + \beta_2(1\text{-}e_2)V_2 + \beta_2 R_1 + \beta_2(1\text{-}e_2)R_1^V + \beta_2(1\text{-}e_2)V_1)}{\gamma_2}, \tag{15}$$

3.2.4 Final Epidemic Size (FES), Average Social Payoff (ASP), and Social Efficiency Deficit (SED)

In this study, we calculated the FES in three ways [56]: FES of only strain 1 (FESOS1), FES of only strain 2 (FESOS2), and FES of both strains (FESBoth). The expressions for the FESs are defined as follows:

$$FESOS1 = R_1(\infty) + V_2(\infty), \quad (16)$$

$$FESOS2 = \int_{t=0}^{\infty} (\beta_2 S I_2 H + \beta_2 (1 - e_2) V_1 I_2 H)\ dt, \quad (17)$$

$$FESBoth = \int_{t=0}^{\infty} (\beta_2 R_1 I_2 H + \beta_2 (1 - e_2) V_2 I_2 H + \beta_2 (1 - e_2) R_1^V I_2 H + \varepsilon_1 I_1 H + \varepsilon_2 I_1^V H)\ dt, \quad (18)$$

where the symbol ∞ denotes a state of equilibrium (let's name it NE) at $t = \infty$.

The vaccination coverages preinfected v_x and postinfected v_y and the total vaccination coverage v_c are defined as

$$v_x = \int_{t=0}^{\infty} xS\ dt, \quad (19)$$

$$v_y = \int_{t=0}^{\infty} yR_1\ dt, \quad (20)$$

Then,

$$v_c = v_x + v_y. \quad (21)$$

The average social payoff (ASPNE) in the model can be defined as follows:

$$ASPNE = c_i\ (FESOS1 + FESOS2 + 2\ FESBoth) - c\ v_c, \quad (22)$$

where the first item on the right-hand side represents the overall disease cost when combining the affected individuals with either one strain or both strains, and the second term represents the entire vaccine cost. Individuals' disease cost for each strain c_i is taken as 1.0 in this study. Those afflicted with both strains must pay twice the disease cost.

By referring to the original SED idea [58], which evaluates the discrepancy between ASP at NE and ASP at SO to determine whether a social dilemma underlies the current social-dynamical system or not. If the x and y evolutionary processes are properly controlled, SED demonstrates how to increase the system's ASP from an evolutionary final state (NE) to a hypothetical perfect society to attain the highest ASPSO imaginable. It is defined as follows:

$$\text{SED} = \text{ASPSO-ASPNE}, \quad (23)$$

The social optimal state is a time-constant vector $(x\ (\text{for SO}), y\ (\text{for SO}))$, with both elements in the range $[0,1]$. Thus, we have

$$SO = arg\ max\ [ASP(x\ (for\ SO), y\ (for\ SO))]. \quad (24)$$

When NE agrees with SO, SED implies zero. Meanwhile, when SED is positive but not zero, there is a social dilemma.

3.3 Results and Discussions

3.3.1 Standard (Basic) Case:

The time series graph for the proposed model employing the common (basic) parameters set is shown in Figure 2(a). The initial value for the compartments and vaccination rates, as well as the common values for the parameters, are shown in Tables 2 and 3 respectively. We considered that the transmission rate of strain 1 (β_1) is lower than the transmission rate of strain 2 (β_2). We also considered the efficacy of the vaccine for strain 1 (e_1) is higher than the efficacy of the vaccine for strain 2 (e_2). The mutation rates $\varepsilon_1, \varepsilon_2$ from strain 1 to strain 2 were taken quite low. In the standard case, we considered the appearance of strain 2 after $T = 60$ days after the appearance of strain 1. Figure 2(b) shows that the transmission rate of strain 2 is lower than that of strain 1 (reversing the values of β_1 and β_2), with all the remaining parameters, kept the same.

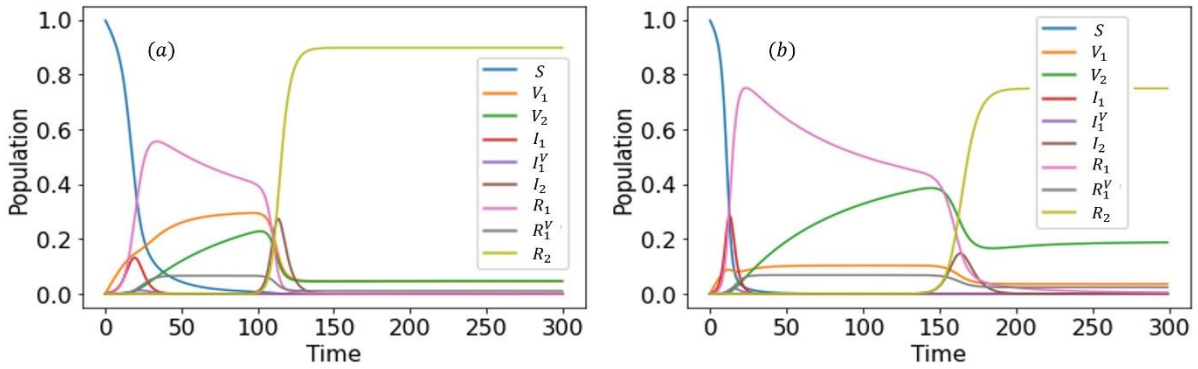

Figure 2: Time series of the compartments for a common case. Here, the blue line indicates the susceptible people; the orange and green lines indicate the vaccinated people before and after being infected with strain 1, respectively; red, violet, and brown indicate the infected people with strain 1 (nonvaccinated and vaccinated, respectively) and strain 2; pink and gray indicate the recovered people infected with strain 1 (nonvaccinated and vaccinated, respectively); and yellow indicates the recovered people infected with strain 2. In Figure 2(a), the peak infection for strain 1 is approximately 0.15 and the peak infection for strain 2 is approximately 0.3. However, in Figure 2(b), the peak infection for strain 1 is approximately 0.3 whereas the peak infection for strain 2 is approximately 0.15. In Figure 2(a), almost 90% of the people are infected with strain 2 because the transmission rate of strain 2 is higher. However, in Figure 2(b), nearly 80% of the people are infected with strain 2 because the transmission rate of strain 2 is lower.

Table 2: Values of the parameters (common case)

Parameter	Value	Parameter	Value
β_1	0.7	$\varepsilon_1, \varepsilon_2$	0.0001
β_2	1.0	t_x, t_y	1.0
e_1	0.7	m_1, m_2	1.0
e_2	0.5	c_i	1.0
γ_1	0.33	c	0.1
γ_2	0.25	k	0.1

Table 3: Initial values for the compartments and vaccination rate

State	At $t = 0$	State/Rate	At $t = 0$
S	0.997	I_2	0.00
V_1	0.001	R_1	0.00
V_2	0.00	R_1^V	0.00
I_1	0.001	R_2	0.00
I_1^V	0.001	x, y	0.01

3.3.2 Time Delay Effect on Primary Reproduction Number, R_o

Figure 3 shows the time delay effect on Primary reproduction numbers R_{o1} and R_{o2}. We considered four cases. The appearance of strain 2 happens after $T = 1, 60, 120, \text{and } 240$ days. For strain 1, the primary reproduction number always starts from the same point, approximately 2.2, and decreases with time. However, for strain 2, the starting point for the primary reproduction number decreases with time. Thus, if strain 2 appears at $T = 1$ days, i.e., almost simultaneous with strain 1, the initial value of the primary reproduction number starts from approximately 4.0 because strain 2 has a larger transmission rate. If the time delay for strain 2 is 60 days, the initial value of the primary reproduction number is approximately 3.1. Similarly, for $T = 120, 240$, the initial value of the primary reproduction number starts from 2.9 and 2.8 and decreases with the spent time.

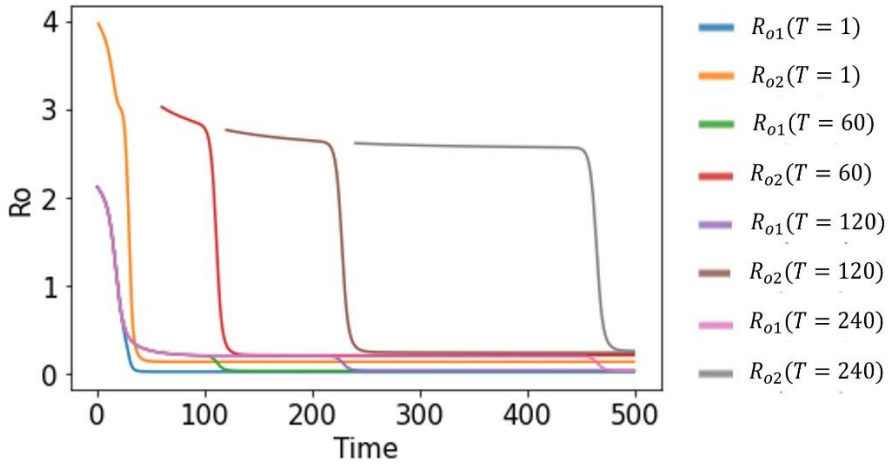

Figure 3: Time series of primary reproduction numbers with different time delays of the appearance of strain 2. The values of the parameters are the same as those for the standard case. For strain 1, the starting points of R_{o1} is the same with different T values and they decrease with the spent time. However, the starting points of R_{o2} decrease with the delayed appearance of strain 2 and decrease with time.

3.3.3 Time Delay Effect on Infection and Vaccination:

Figure 4 shows the infection and vaccination time series using four distinct time delays of strain 2 emergence. The total infection for strain 1 (vaccinated and nonvaccinated) is shown in panel (a). We can see that the total infection of strain 1 is unaffected because of the time delay in the appearance of strain 2. The total infection peak is the same for $T = 1,60,120,240$ (approximately 0.15). Infection for strain 2 is displayed in panel (b) showing that the infection peak decreases when the arrival of strain 2 is delayed. When $T = 1$ day, i.e., both strains are active practically concurrently from the start, the infection peak for strain 2 is the highest (approximately 0.35). However, when $T = 60,120,240$, the infection peaks for strain 2 are 0.28, 0.25, and 0.23, respectively. Panel (c) is made up of panels (a) and (b). As shown in these panels, the delay in the appearance of strain 2 does not affect the infection of strain 1 but it does diminish the peak size of strain 2, implying that strain 2 becomes weaker as time passes.

Preinfection, postinfection, and entire vaccination time series are illustrated in panels (d), (e), and (f). If $T = 1$, there is less time for vaccination instead of infection in panel (d). If $T = 60,120,240$ persons have time to be vaccinated, approximately 30% of them (vaccination peak always occurs at approximately 0.3) received their vaccination before becoming sick with any strain. In panel (e), the vaccination peak increases as the arrival of strain 2 is delayed. After being infected with strain 1 for $T = 240$, over 35% of persons (peaking at approximately 0.35) can be vaccinated. The entire vaccination time series is presented in panel (f). We can see that delaying the appearance of strain 2 increases the possibility of postinfection vaccination and hence overall vaccination, lowering the risk of infection with strain 2, which is complementary to panels (a)-(c).

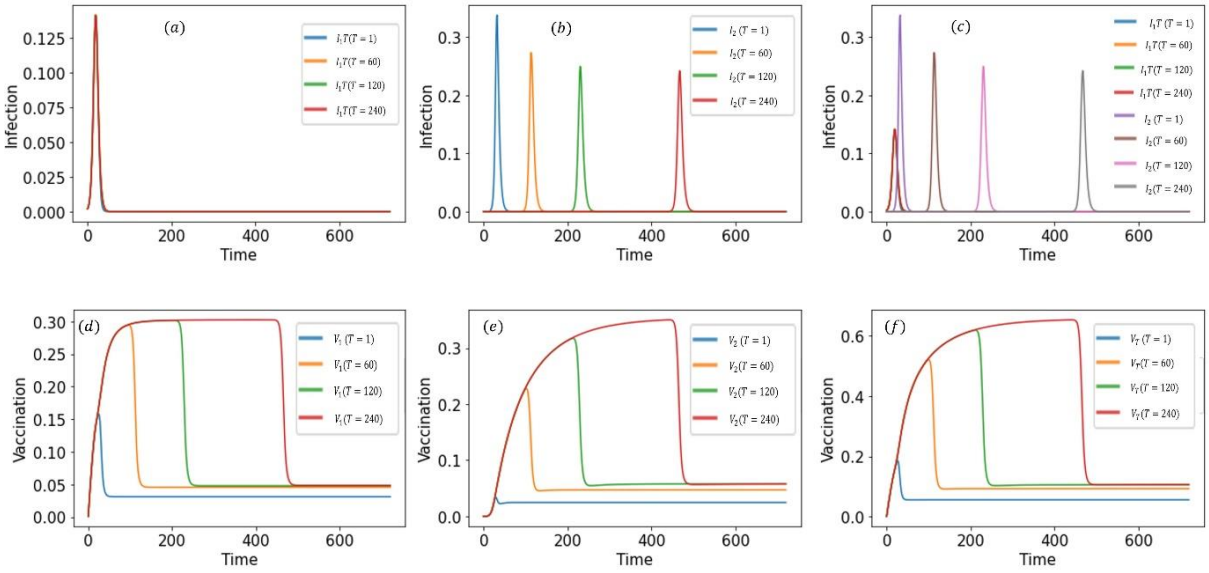

Figure 4: Time series of infection and vaccination with a time delay of the appearance of strain 2. Panel (a) shows the total infection (I_1T) due to strain 1, and panel (b) shows the total infection due to strain 2 (I_2). Both (a) and (b) show the four different time delays of the appearance of strain 2. Panel (c) is the combination of (a) and (b). Panel (d)-(f) represent the time series of preinfected vaccinated (V_1), postinfected vaccinated (V_2), and total vaccinated (V_T), respectively. Here, time delay T is taken as 1,60,120,240 days, and all parameters and initial values are kept the same as those of the standard case. We can observe from the panels that the time delay of the appearance can give people more chances to be vaccinated and can reduce the risk of infection from strain 2.

3.3.4 Time Delay and Inertial Effects on Vaccination

Figure 5 shows the inertial and time delay effects on vaccination. Here, we considered three-time delays $T = 60, 120, 240$, and three sets of inertial effects $(t_x, t_y) = (0.1,0.1), (0.5,0.5), (1.0,1.0)$ on vaccination. For $T = 60$, panels (a)-(c) show the time series of preinfection vaccination, postinfection vaccination, and total vaccination. In panel (a), we can observe that preinfection vaccination is less with the less inertial effect and it is high with maximum inertial effect. This is obvious when the high inertial effect is active, i.e., people giving maximum effort, the preinfected vaccinees is maximum. However, the behavior of postinfection vaccination is the opposite. We can see from panel (b), that a less inertial effect gives maximum vaccines whereas a high inertial effect gives fewer vaccines. This is because, with a high inertial effect, most people take the vaccine before they are infected with strain 1 and fewer people who can take the vaccine after being infected with strain 1 remain. Meanwhile, if fewer people take the vaccine earlier (when the less inertial effect has been considered), there will be more people remaining, who can be infected with strain 1 and can take the vaccine to become safe from strain 2. A combination of (a) and (b) shows in panel (c), that the total vaccination looks similar, but for the less inertial effect the peak of the total vaccination seems higher.

For $T = 120$, panels (d)-(f) are displayed. In panel (d), we can see similar behavior in preinfection vaccination time series like panel (a) which means that less inertial effect implies fewer people choose vaccination before being infected with strain 1. In panel (e), similar behavior is observed in panel (b), less inertial effect implies more people take the vaccine after being infected with strain 1. However, the infection peaks in all three cases in panel (e) are much higher than the corresponding peaks in panel (b). Consequently, the combination of panels (d) and (e) i.e., panel (f), shows that the total vaccination peaks are also much higher than those in panel (c). This is because the time delay of the appearance of strain 2 gives much time to the people who are not vaccinated before being infected with strain 1. These people can take a vaccine when strain 2 emerges or is present.

For $T = 240$, panels (g)-(i) look almost similar to the corresponding panels (d)-(f). However, peaks in panels (h) and(i) are higher than the corresponding peaks of panels (e) and (f) because of the time delay of the appearance of strain 2. Thus, we can see that the time delay of the appearance of strain 2 can increase the chance of taking a vaccine, which can reduce the risk of infection. Additionally, a less inertial effect may help to get more people vaccinated.

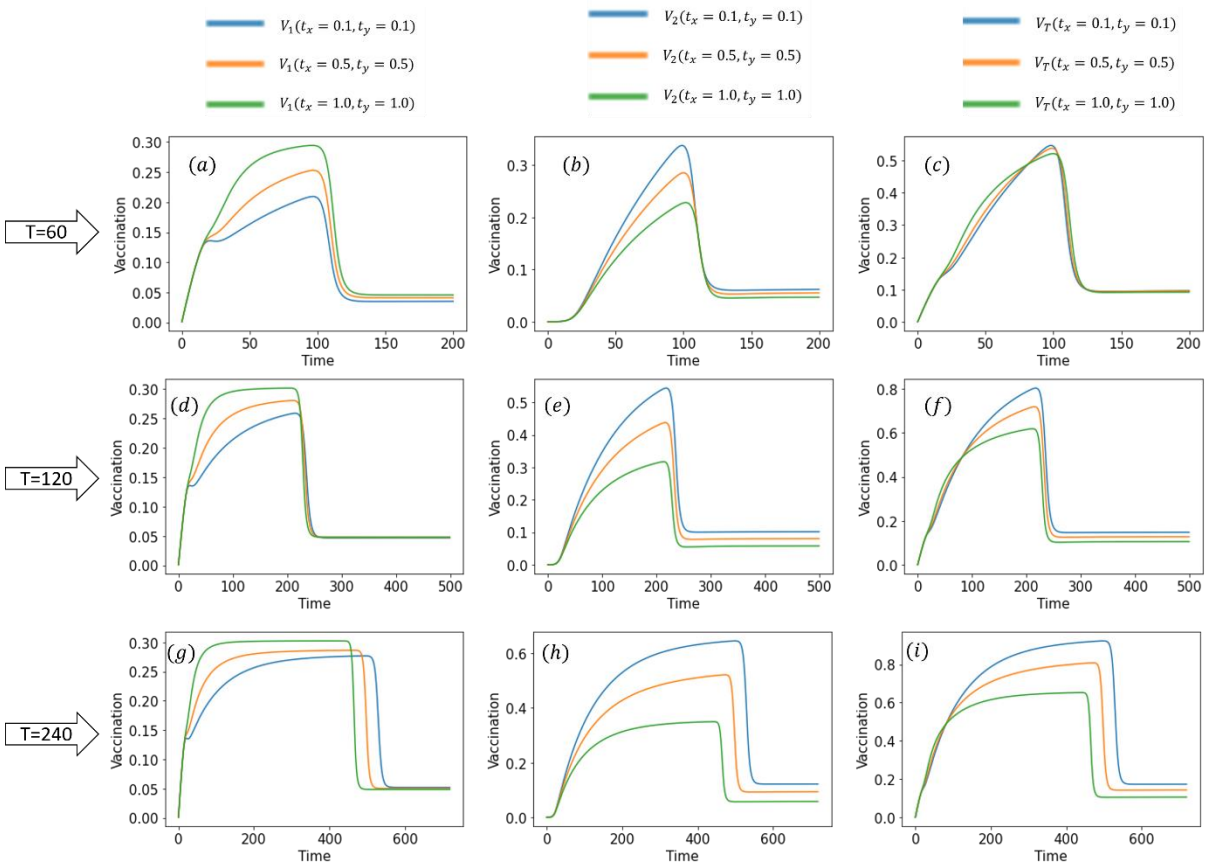

Figure 5: Time series of preinfected vaccinated (V_1), postinfected vaccinated (V_2), and total vaccinated (V_T) People are presented with three sets of inertial effect $(t_x, t_y) = (0.1,0.1), (0.5,0.5), (1.0,1.0)$ along with $T = 60,120,240$ days. The remaining parameters are taken as standard ones. These figures show

that the time delay of the emergence of the second strain can help people be vaccinated more and less inertial effect can increase the total number of vaccinated people as a whole.

3.3.5 Time Delay and Severity Effects on Vaccination

Figure 6 shows the severity and time delay effects of vaccination. Here, we considered three-time delays $T = 60, 120, 240,$ and three sets of severity effect $(m_1, m_2) = (0.1,0.1), (0.5,0.5), (1.0,1.0)$ on vaccination. For $T = 60$, panels (a)-(c) show the time series of preinfected vaccination, postinfected vaccination, and total vaccination. In panel (a), we observed that the vaccination peak is highest when the severity effect is maximum. This is obvious because if the severity is higher for any strain, people must go for the vaccination as early as it is available. In panel (b), we observed almost a similar behavior with different severity effects because after being infected with strain 1, every person tries to take the vaccination to remain safer from strain 2. Panel (c) is the combination of panels (a) and (b), which reflects that more severity implies more vaccination.

For $T = 120$, panels (d)-(f) have similar behavior corresponding to panels (a)-(c). In panel (d), the peaks of the vaccination compared to panel (a) are similar, but in panel (e), peaks are much higher than those in panel (b). This is because the time delay of the appearance of strain 2 gives more time for people to be vaccinated. Consequently, panel (f) shows that the peak of the total vaccinated people is higher than that in panel (c).

For $T = 240$, panels (g)-(i) also behave similarly compared to panels (d)-(f). However, the postinfection vaccination peak is a little higher in panels (h) and (i) than in panels (e) and (f) because of the time delay of the appearance of strain 2. Therefore these panels show that more severe diseases can increase the chance of vaccination and more time delay increases the chance of vaccination, which can reduce the risk of infection.

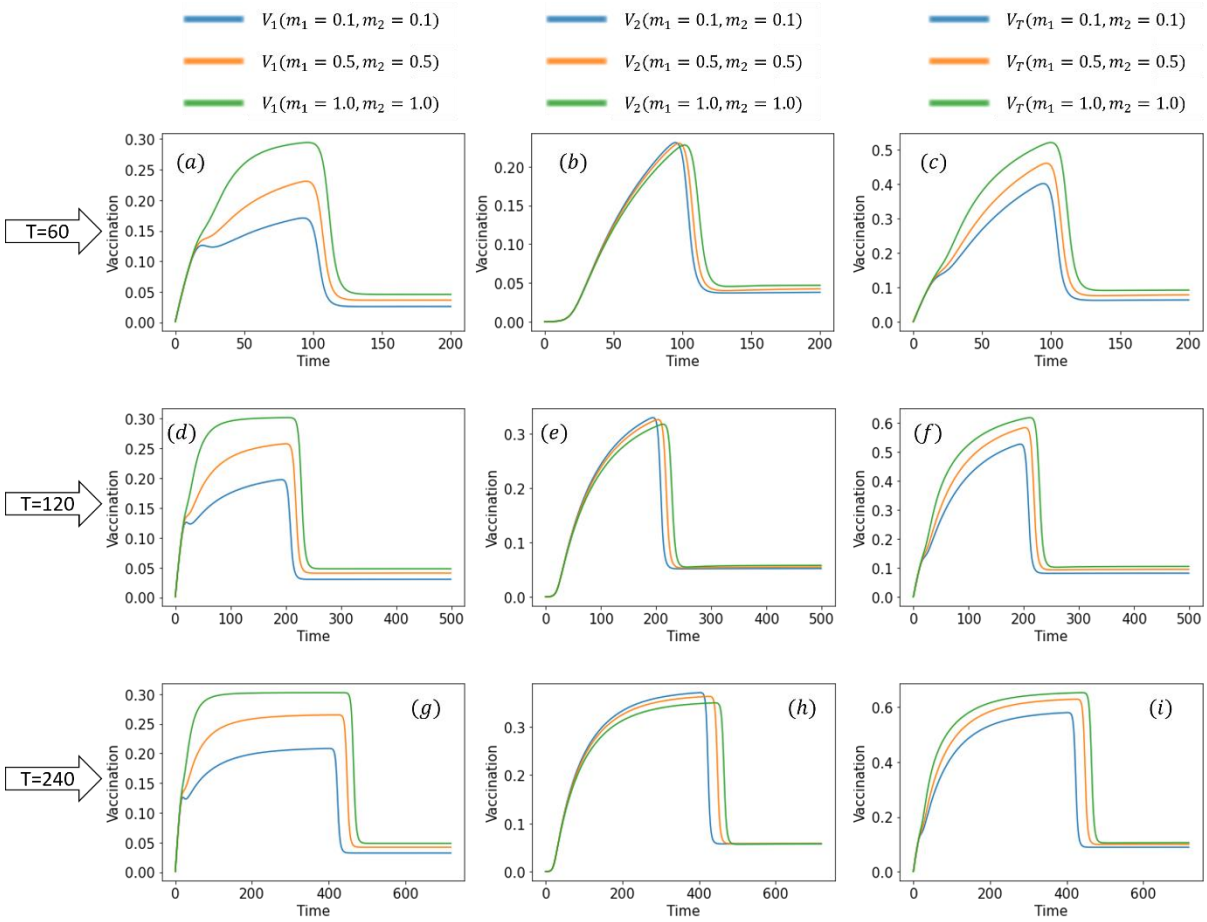

Figure 6: Time series of preinfected vaccinated (V_1), postinfected vaccinated (V_2), and total vaccinated (V_T) People are presented with three sets of severity effects $(m_1, m_2) = (0.1,0.1), (0.5,0.5), (1.0,1.0)$ along with $T = 60,120,240$ days. The remaining parameters are taken as standard ones. These figures, show that the time delay of the emergence of a second strain can help people be vaccinated more and a higher severity effect can also increase the total number of vaccinated people.

3.3.6 Time Delay Effect on ASP and SED

In this subsection, We investigate the impact of the time delay on the ASP and SED to observe the social dilemma of the proposed model. We also considered four distinct time delay effects: $T = 1,60,120,240$. Heatmaps were created using the vaccine's cost c as the x-axis and its effectiveness e_2 to strain 2 as the y-axis.

Figure 7.1 shows the heatmaps of the final epidemic sizes for only strain 1, only strain 2, both strains, vaccination coverage, and the average social payoff for NE and SO cases, as well as the SED for the time delay $T = 1$, i.e., both strains almost effective for the entire time. The situation for NE is depicted in panels (a)-(e), whereas the case for SO is depicted in panels (f)-(j). SED is depicted in panel (k) with the difference between (j) and (e). To explain the general context of the case, we divided the SED region into two different regions (panel (k)).

When the efficacy is high and the cost of vaccination is low, we may see a light red corner in the left upper region in panel (a) in the NE case. The remaining region is dark red, indicating that when the efficacy is high and the cost is low, only a small percentage of the population will remain infected with only strain 1. When the efficacy is high and the cost is low, a dark red region appears in the left upper region in panel (b), indicating that only a small percentage of people will be infected with only strain 2. When the time delay for strain 2 is 1 day, panel (c) shows that more than 50% of people will be infected with both strains. Panel (d) shows very little vaccination coverage for this case. Panel (e) illustrates the average social reward for the NE case when all of these panels ((a)-(d)) are combined. We can see that the average social payoff is low when the vaccination cost is low and the efficacy is high. We can also observe that in the SO situation, there are nearly no persons (panel (f)) who become infected with only strain 1, and vaccine coverage is at its highest (panel (i)). Additionally, there is a critical line between the value $e_2 = 0.75$ (panel (g)). No one will be infected with solely strain 2 beyond this critical line, and people will be infected with strain 2 below the line because of the vaccines' reduced efficiency against strain 2. Furthermore, the SO predicted that no one would be infected by both strains (panel (h)). Consequently, in the SO, the average social payoff produces two zones separated by the critical line. SED is shown in panel (k) with the difference between panels (j) and (e). The critical line separates regions (1) and (2) in the context of SED. We found a monotonic decline in the value of SED along the direction of vaccination cost in the region (1) (green to yellow). As the cost of vaccination increases, people will opt out. Similar behavior can be seen in Region 2. However, the monotonic reduction occurs (light red to dark red) in the diagonal direction, implying that when vaccine efficacy is poor and vaccination costs are high, no one will be vaccinated. Thus, raising the price of less effective vaccines does not create a broader social dilemma.

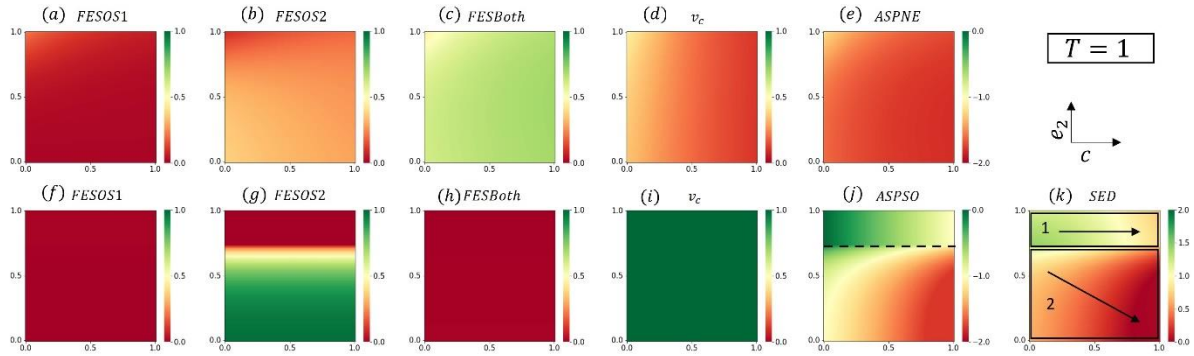

Figure 7.1: This graph shows the FESs, vaccination coverage, ASP, and SED. For NE cases (panels (a)-(e)), the final epidemic sizes for only strain 1, only strain 2, both strains, vaccination coverage, and average social payoff are shown in the first row, whereas the instances for SO are shown in the second row (panels (f)-(j). SED is depicted in panel (k). The cost of the vaccination c is plotted on the x-axis, whereas the efficacy of the vaccine e_2 against strain 2 is plotted on the y-axis, both ranging from 0 to 1. Except for these two, all other settings are set to their default values. The ranges of the FESs and

vaccine coverage are taken from 0 to 1. The ASP panel range is taken from -2.0 to 0.0 and the SED panel is depicted with a range from 0.0 to 2.0. At approximately $e_2 = 0.75$, a critical line is detected for the SO case, dividing the SED region into two sections. The arrival of strain 2 is given a time delay of $T = 1$ day.

Figure 7.2 shows the case when the time delay, $T = 60$ days. Similar to the panels in Figure 7.1, all panels are depicted with the same values of the parameters. Here, we can see that a triangular (green and yellow) region occurs in the upper left corner in panel (a), representing the FES of only strain 1. This means that with the high efficacy of strain 2, the low cost of the vaccine, and delayed appearance, some people have the chance not to be infected with strain 2. The dark red region of panels (b) and (c) compliments the scenario of the panel (a). In panel (d), with low cost and high efficacy, we see that most people go for vaccination because they also have 60 days to become vaccinated. As a combination of panels (a)-(d), panel (e) presented the ASP for the NE case where the ASP is lower in the left upper triangular region, i.e., people will take a vaccine rather than be infected with strain 2. In SO (panels (f)-(j)), similar behaviors are observed in Figure 7.2, like in Figure 7.1. SO suggested maximum vaccination, which also shows that no person will remain infected with only strain 1. We also observed a triangular region in SED (panel (k)) due to the triangular region occurring in the ASP at the NE. Therefore we divide the SED region into three parts using the observed critical line (panel (j)). Region 1 is light red because when the efficacy is high and the cost is low, most people will go for the vaccination and there will be a very less social dilemma. In Region 2, increasing the cost of the vaccination decreases the social dilemma monotonically because as the price increases, people will not go for the vaccination. In region 3, the monotonic decreasing behavior is observed diagonally, as shown in Figure 7.1. This implies that with low efficacy and high cost, people will lose interest in taking the vaccine and the social dilemma also decreases monotonically.

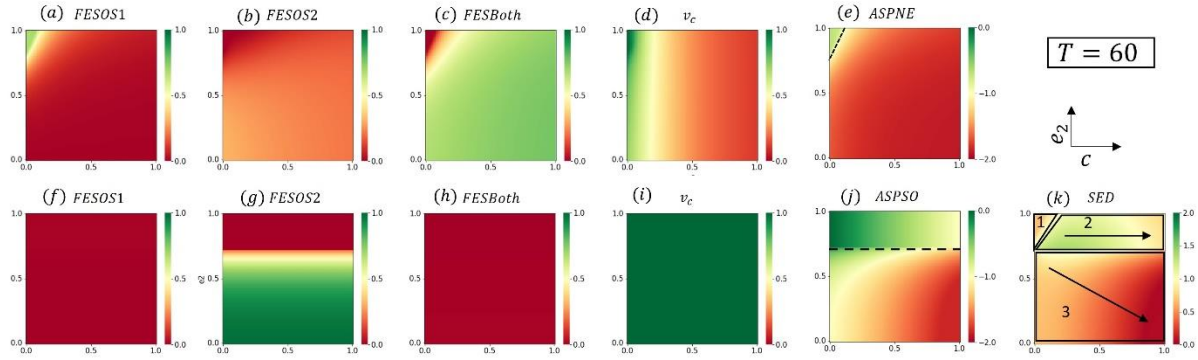

Figure 7.2: This graph shows the FESs, vaccination coverage, ASP, and SED. For the NE case (panels (a)-(e)), the first row shows the final epidemic sizes for only strain 1, only strain 2, both strains, vaccination coverage, and average social payoff whereas, the second row (panels (f)-(j) shows the instances of SO. The SED was depicted in panel (k). The cost of the vaccination c is plotted on the x-

axis, whereas the efficacy of the vaccine e_2 against strain 2 is plotted on the y-axis both ranging from 0 to 1. Except for these two, all other settings are set to their default values. The ranges of the FESs and vaccine coverage are taken from 0 to 1. The ASP panels range is taken from -2.0 to 0.0 and the SED panel is depicted with a range from 0.0 to 2.0. At approximately $e_2 = 0.75$, a critical line is detected for the SO case and combined with the triangular region in the NE case, dividing the SED region into three sections. The arrival of strain 2 is given a time delay of $T = 60$ days.

Figure 7.3 depicts the situation where the time delay, $T = 120$ days. All panels are depicted with identical parameter values as those of the panels in Figures 7.1 and 7.2. In panel (a), we can also see a triangle (green and yellow) zone in the left upper corner. This represents the FES of only strain 1, implying that owing to the vaccine's great efficiency against strain 2, low cost, and delayed appearance, some people may avoid becoming infected with strain 2. The triangular region of panel (a) in Figure 7.3 is slightly larger than that of the panel (a) in Figure 7.2, indicating that with an additional 60-day time delay, reduced efficacy, and a higher cost may be appropriate to avoid infection with strain 2. Panels (b) and (c) have a dark red section that matches the scene in panel (a). Additionally, vaccine coverage in panel (d) of Figure 7.3 is higher than that of panel (d) in Figure 7.2, indicating that an extra 60 days can vaccinate more people. Panel (e), which contains a similar triangular green region when the vaccination cost is low and efficacy is high, is the average social payoff for the NE when panels (a)-(d) are combined. Figure 7.3 shows comparable features to Figures 7.1 and 7.2 in the SO (panels (f)-(j)). The SO for the maximum vaccination has been proposed, demonstrating that no one will remain infected with only strain 1. The critical line is also visible, indicating that if the vaccine efficiency is greater than 0.75, no one will be infected with strain 2. We have seen triangular and trapezium-shaped regions in SED (panel (k)) above the critical line because of the triangular region in the ASP at the NE and the critical line in the SO (panel (j)). Consequently, we partition the SED region into three regions using the observed critical line. Region 1 is light red because when vaccination efficiency is high and the cost is low, most people will opt for it and there will be a less social dilemma. In Region 2, increasing the cost of vaccination reduces the social problem monotonically because people will not be vaccinated as the price rises. In Region 3, as shown in Figures 7.1 and 7.2, the monotonic declining behavior is exhibited diagonally, indicating that with low efficacy and high cost, people will lose interest in taking the vaccine and the social dilemma will also diminish monotonically.

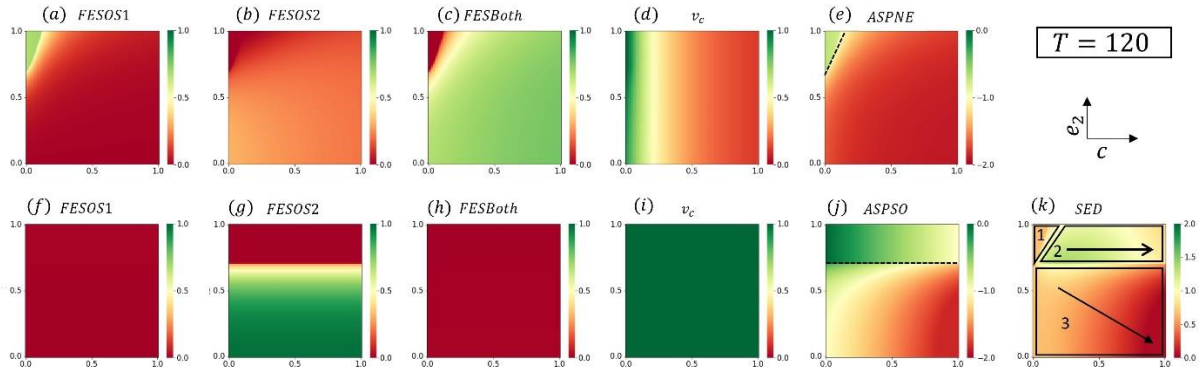

Figure 7.3: This graph shows the FESs, vaccination coverage, ASP, and SED. The final epidemic sizes for only strain 1, only strain 2, both strains, vaccination coverage, and average social payoff are shown in the first row for NE (panels (a)-(e)), whereas the examples for SO are shown in the second row (panels (f)-(j)). The SED was depicted in panel (k). The cost of vaccination c is plotted, on the x-axis, whereas the efficacy of vaccine e_2 against strain 2 is plotted on the y-axis, both ranging from 0 to 1. All other parameters, except for these two, are left at their default values. FESs and vaccination coverage are measured on a scale of 0 to 1. The ASP panels range from -2.0 to 0.0, whereas the SED panels range from 0.0 to 2.0. For the SO case, a critical line is discovered at approximately $e_2 = 0.75$, dividing the SED region into three halves with the triangular region in NE. The arrival of strain 2 is given a time delay of $T = 120$ days.

Figure 7.4 shows the time delay $T = 240$ days. All of these panels are depicted with identical parameter values to the panels in Figures 7.1-7.3. A triangle (green and yellow) zone in the left upper corner of the panel (a) indicates the FES of only strain 1, indicating that some people may escape becoming infected with strain 2 due to the vaccine's high efficacy against strain 2, low cost, and delayed appearance. The triangular region of panel (a) in Figure 7.4 is much larger than that of panel (a) in Figure 7.3, showing that avoiding infection with strain 2 may be possible with an extra 120-day time delay but at a higher cost. A dark red portion appears in panels (b) and (c), corresponding to the scene in panel (a). Vaccine coverage in panel (d) of Figure 7.4 is greater than that in panel (d) of Figure 7.3, showing that an extra 120 days can vaccinate more people. It also exhibits a monotonically declining vaccine coverage with increasing vaccination costs, but less sensitivity with increasing vaccine efficacy. When panels (a)-(d) are merged, the average social payoff for the NE is panel (e), which has a comparable triangular green zone when the vaccine cost is low and efficacy is high. Figure 7.4 in SO (panels (f)-(j)) has aspects that are similar to figures 7.1-7.3 in SO. It has been proposed that the SO for maximum vaccination is established, proving that no one will remain infected with only strain 1. The critical line, which indicates that no one will be infected with strain 2 if the vaccine efficacy is greater than 0.7, is also apparent. Because of the triangular region in the ASP at the NE and the critical line in SO, there are two trapezium-shaped regions in SED (panel (k)) above the critical line and one triangular and one trapezium-shaped region below the critical line. Consequently, we use the critical line to divide

the SED region into four portions. When vaccine efficiency is high and the cost is cheap, most people will choose it and there will be fewer social dilemmas. In Region 2, increasing the cost of vaccination lessens the social problem over time because people will refuse to be vaccinated as the cost increases. A dark red triangular section appears in Region 3, indicating almost no dilemma issue. Using a $T = 240$-days time delay, some people may need to be vaccinated with a vaccine that is less expensive and has a lower efficiency (approximately 0.5). The monotonic falling behavior is displayed diagonally in Region 4, as illustrated in Figures 7.1-7.3, which means that with low efficacy and high cost, people will lose interest in taking the vaccine, and the social dilemma will also reduce monotonically.

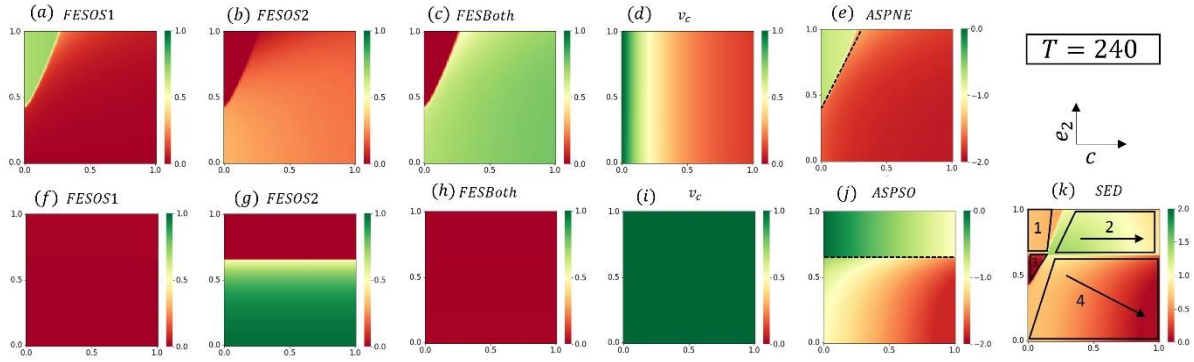

Figure 7.4: This graph shows the FESs, vaccination coverage, ASP, and SED. In the first row for NE (panels (a)-(e)), the final epidemic sizes for only strain 1, only strain 2, both strains, vaccination coverage, and average social payoff are provided, whereas the examples for SO are shown in the second row (panels (f)-(j)). Panel (k) depicts the SED. The cost of vaccination c is plotted on the x-axis, whereas the efficacy of the vaccine e_2 against strain 2 is plotted on the y-axis, with both values ranging from 0 to 1. Except for these two, all other parameters are left at their default levels. FESs and vaccination coverage are rated on a scale of 0 to 1. The ASP panels range from -2.0 to 0.0, while the SED panels range from 0.0 to 2.0. For the SO case, a critical line is discovered at approximately $e_2 = 0.75$, dividing the SED region into four parts, with the triangular region in NE. The arrival of strain 2 is given a time delay of $T = 240$ days.

3.4 Conclusion

The emergence of new strains creates a new challenge to the healthcare system. However, the time lag between the appearances of the resident and new strains can be substantially influential in determining the disease dynamics, especially for the second strain. Although vaccine efficacy against the new strain may be reduced, its late appearance increases the possibility of higher vaccination coverage, inevitably reducing the infection peak (as well as epidemic size) concerning the new strain. This study investigated such a context by employing a two-strain epidemic model with preinfection and postinfection vaccinations. More precisely, individuals who forgo vaccination and are infected with the resident strain have the chance to be vaccinated after recovery. As vaccination is mostly voluntary, we consider

behavioral dynamics to model individuals' vaccination behavior. The decision to be vaccinated is influenced by the timing of the emergence of the new strain, its severity, transmission rate, and the cost and effectiveness of the vaccine. Most previous studies concerning two-strain or multi-strain epidemic models focused on stability analysis with non-monotone incidence rates, complex network with latency, general incidence rate, age structure and mutation [19,50,53,56], competitive coexistence with periodic infection rate [54], optimal control with general incidence function and time delay, imperfect vaccination, covid-19 application [5,48,65], vaccination behavior with imitation dynamic approach, social distance effect, covid-19 modeling, awareness decay [10,11,15,30], and disease dynamics with cross-immunity, in patchy environments, generic approach [14,22,25,51], etc.

Our primary concern was to observe the effect of vaccination and the time delay of the emergence of a new strain on controlling disease spreading. We have considered four-time delays of the appearance of new strains which has a huge impact on global disease dynamics and vaccination behavior which is not discussed in any other prior studies. Generally, vaccination is effective in reducing the disease spreading. We also demonstrated that the time delay of the advent of a new strain could considerably reduce the corresponding basic reproduction number. Our results further suggest that the larger the time delay is, the higher the vaccination coverage, reducing the peak and the final epidemic size of the new strain. In terms of the cost and efficacy of the vaccine, we observed that higher efficacy and a lower cost increase vaccination uptake, which is quite comprehensible.

Later, we presented the SED analysis of our model which showed how the social dilemma situation acts with the emergence of new strain along with time delay. We found that SED, measured by the difference between the average payoff at the SO and equilibrium, can be reduced by vaccination and the increase in time delay. Our findings imply that vaccination and time delay are substantial in reducing SED. The lesser SED demonstrates that the evolutionary outcomes are closer to the SO. Also, as the time delay rises, we can see from figures (7.1–7.4) that the SED regions can be separated into additional sections to describe the social dilemma with various costs and levels of efficacy, which is a little bit intriguing.

In our model, we merely used a straightforward ODE model (mean-field approximation) technique to study the dynamics of vaccination behavior and social dilemma, and the social context lends credibility to our data. In future studies, we will investigate the result multiagent simulation approach. We will also include a single vaccination in our model with varying efficacy for the different strains. Furthermore, we will strive to expand our approach to include different vaccinations at various price points in addition to multidose vaccination. We considered the constant time delay of the appearance of a new strain in our work. Next, we will focus on how a time-variant time delay can affect disease dynamics, vaccination behavior, and social dilemmas in our future study.

References

[1] A.E. Gorbalenya, S.C. Baker, R.S. Baric, R.J. de Groot, C. Drosten, A.A. Gulyaeva, B.L.

Haagmans, C. Lauber, A.M. Leontovich, B.W. Neuman, D. Penzar, S. Perlman, L.L.M. Poon, D. V. Samborskiy, I.A. Sidorov, I. Sola, J. Ziebuhr, The species severe acute respiratory syndrome-related coronavirus: Classifying 2019-nCoV and naming it SARS-CoV-2, Nat. Microbiol. 5 (2020) 536–544. https://doi.org/10.1038/s41564-020-0695-z.

[2] S.M. Halstead, Dengue and dengue hemorrhagic fever, Handb. Zoonoses, Second Ed. Sect. B Viral Zoonoses. 11 (2017) 89–99. https://doi.org/10.1201/9780203752463.

[3] J.M. Brenchley, D.A. Price, T.W. Schacker, T.E. Asher, G. Silvestri, S. Rao, Z. Kazzaz, E. Bornstein, O. Lambotte, D. Altmann, B.R. Blazar, B. Rodriguez, L. Teixeira-Johnson, A. Landay, J.N. Martin, F.M. Hecht, L.J. Picker, M.M. Lederman, S.G. Deeks, D.C. Douek, Microbial translocation is a cause of systemic immune activation in chronic HIV infection, Nat. Med. 12 (2006) 1365–1371. https://doi.org/10.1038/nm1511.

[4] W. Ma, Y. Takeuchi, T. Hara, E. Beretta, Permanence of a SIR epidemic model with distributed time delays, Tohoku Math. J. 54 (2002) 581–591. https://doi.org/10.2748/tmj/1113247650.

[5] M. Barro, A. Guiro, D. Ouedraogo, Optimal control of a SIR epidemic model with general incidence function and time delays, Cubo. 20 (2018) 53–66. https://doi.org/10.4067/s0719-06462018000200053.

[6] W. Xia, S. Kundu, S. Maitra, Dynamics of a delayed SEIQ epidemic model, Adv. Differ. Equations. 2018 (2018). https://doi.org/10.1186/s13662-018-1791-8.

[7] K.M. Ariful Kabir, J. Tanimoto, Modelling and analyzing the coexistence of dual dilemmas in the proactive vaccination game and retroactive treatment game in epidemic viral dynamics, Proc. R. Soc. A Math. Phys. Eng. Sci. 475 (2019). https://doi.org/10.1098/rspa.2019.0484.

[8] J.M. Epstein, E. Hatna, J. Crodelle, Triple contagion: A two-fears epidemic model, J. R. Soc. Interface. 18 (2021). https://doi.org/10.1098/rsif.2021.0186.

[9] M. Rajib Arefin, T. Masaki, K.M. Ariful Kabir, J. Tanimoto, Interplay between cost and effectiveness in influenza vaccine uptake: A vaccination game approach, Proc. R. Soc. A Math. Phys. Eng. Sci. 475 (2019). https://doi.org/10.1098/rspa.2019.0608.

[10] A. Deka, S. Bhattacharyya, The effect of human vaccination behavior on strain competition in an infectious disease: An imitation dynamic approach, Theor. Popul. Biol. 143 (2022) 62–76. https://doi.org/10.1016/j.tpb.2021.12.001.

[11] M. Dashtbali, M. Mirzaie, A compartmental model that predicts the effect of social distancing and vaccination on controlling COVID-19, Sci. Rep. 11 (2021) 1–11. https://doi.org/10.1038/s41598-021-86873-0.

[12] C. Zuo, F. Zhu, Z. Meng, Y. Ling, Y. Zheng, X. Zhao, Analyzing the COVID-19 vaccination behavior based on an epidemic model with awareness-information, Infect. Genet. Evol. 98 (2022) 105218. https://doi.org/10.1016/j.meegid.2022.105218.

[13] William Ogilvy Kermack and A. G. McKendrick, A contribution to the mathematical theory of epidemics, Proc. R. Soc. A Math. Phys. Eng. Sci. 115 (1927) 700–721. https://doi.org/https://doi.org/10.1098/rspa.1927.0118.

[14] J. Amador, D. Armesto, A. Gómez-Corral, Extreme values in SIR epidemic models with two strains and cross-immunity, Math. Biosci. Eng. 16 (2019) 1992–2022. https://doi.org/10.3934/mbe.2019098.

[15] U.A.P. de León, E. Avila-Vales, K. Lin Huang, Modeling COVID-19 dynamic using a two-strain model with vaccination, Chaos, Solitons and Fractals. 157 (2022) 111927. https://doi.org/10.1016/j.chaos.2022.111927.

[16] M.A. Amaral, M.M. d. Oliveira, M.A. Javarone, An epidemiological model with voluntary quarantine strategies governed by evolutionary game dynamics, Chaos, Solitons and Fractals. 143 (2021) 110616. https://doi.org/10.1016/j.chaos.2020.110616.

[17] K.M.A. Kabir, T. Risa, J. Tanimoto, Prosocial behavior of wearing a mask during an epidemic: an evolutionary explanation, Sci. Rep. 11 (2021) 1–14. https://doi.org/10.1038/s41598-021-92094-2.

[18] M.M. and C.C.-C. M. Nuño, Z. Feng, Dynamics of Two-Strain Influenza with Isolation and Partial Cross-Immunity, SIAM J. Appl. Math. 65 (2005) 964–982. https://doi.org/10.1137/S003613990.

[19] A. Meskaf, O. Khyar, J. Danane, K. Allali, Global stability analysis of a two-strain epidemic model with non-monotone incidence rates, Chaos, Solitons and Fractals. 133 (2020) 109647. https://doi.org/10.1016/j.chaos.2020.109647.

[20] E.M. Farah, S. Amine, K. Allali, Dynamics of a time-delayed two-strain epidemic model with general incidence rates, Chaos, Solitons and Fractals. 153 (2021) 111527. https://doi.org/10.1016/j.chaos.2021.111527.

[21] J. Dong, T. Li, C. Wan, X. Liu, The analysis of a SEIRS epidemic model with time delay on complex networks, OALib. 04 (2017) 1–10. https://doi.org/10.4236/oalib.1103901.

[22] C. Li, J. Wang, J. Xu, Y. Rong, The Global dynamics of a SIR model considering competitions among multiple strains in patchy environments, Math. Biosci. Eng. 19 (2022) 4690–4702. https://doi.org/10.3934/mbe.2022218.

[23] O. Khyar, K. Allali, Global dynamics of a multi-strain SEIR epidemic model with general incidence rates: application to COVID-19 pandemic, Nonlinear Dyn. 102 (2020) 489–509. https://doi.org/10.1007/s11071-020-05929-4.

[24] X.Z. Li, J.X. Liu, M. Martcheva, An age-structured two-strain epidemic model with super-infection, Math. Biosci. Eng. 7 (2010) 123–147. https://doi.org/10.3934/mbe.2010.7.123.

[25] T. Lazebnik, S. Bunimovich-Mendrazitsky, Generic approach for a mathematical model of multi-strain pandemics, PLoS One. 17 (2022) 1–20. https://doi.org/10.1371/journal.pone.0260683.

[26] E. Beretta, D. Breda, An SEIR epidemic model with constant latency time and infectious period, Math. Biosci. Eng. 8 (2011) 931–952. https://doi.org/10.3934/mbe.2011.8.931.

[27] F.A. Rihan, H.J. Alsakaji, C. Rajivganthi, Stochastic SIRC epidemic model with time-delay for COVID-19, Adv. Differ. Equations. 2020 (2020). https://doi.org/10.1186/s13662-020-02964-8.

[28] A. Khan, R. Ikram, A. Din, U.W. Humphries, A. Akgul, Stochastic COVID-19 SEIQ epidemic model with time-delay, Results Phys. 30 (2021) 104775. https://doi.org/10.1016/j.rinp.2021.104775.

[29] D. Niño-Torres, A. Ríos-Gutiérrez, V. Arunachalam, C. Ohajunwa, P. Seshaiyer, Stochastic modeling, analysis, and simulation of the COVID-19 pandemic with explicit behavioral changes in Bogotá: A case study, Infect. Dis. Model. 7 (2022) 199–211. https://doi.org/10.1016/j.idm.2021.12.008.

[30] C. Zuo, F. Zhu, Y. Ling, Analyzing COVID-19 vaccination behavior using a SEIRM/V epidemic model with awareness decay, Front. Public Heal. 10 (2022) 1–12. https://doi.org/10.3389/fpubh.2022.817749.

[31] M. Li, X. Liu, An SIR epidemic model with time delay and general nonlinear incidence rate, Abstr. Appl. Anal. 2014 (2014). https://doi.org/10.1155/2014/131257.

[32] D. Helbing, D. Brockmann, T. Chadefaux, K. Donnay, U. Blanke, O. Woolley-Meza, M. Moussaid, A. Johansson, J. Krause, S. Schutte, M. Perc, Saving human lives: What complexity science and information systems can contribute, 2015. https://doi.org/10.1007/s10955-014-1024-9.

[33] M. Jusup, P. Holme, K. Kanazawa, M. Takayasu, I. Romić, Z. Wang, S. Geček, T. Lipić, B. Podobnik, L. Wang, W. Luo, T. Klanjšček, J. Fan, S. Boccaletti, M. Perc, Social physics, Phys. Rep. 948 (2022) 1–148. https://doi.org/10.1016/j.physrep.2021.10.005.

[34] Q. Yin, Z. Wang, C. Xia, C.T. Bauch, Impact of co-evolution of negative vaccine-related

information, vaccination behavior and epidemic spreading in multilayer networks, Commun. Nonlinear Sci. Numer. Simul. 109 (2022) 106312. https://doi.org/10.1016/j.cnsns.2022.106312.

[35] Y. Nakata, R. Omori, Delay equation formulation for an epidemic model with waning immunity: An application to mycoplasma pneumoniae, IFAC-PapersOnLine. 28 (2015) 132–135. https://doi.org/10.1016/j.ifacol.2015.11.024.

[36] G. Lobinska, A. Pauzner, A. Traulsen, Y. Pilpel, M.A. Nowak, Evolution of resistance to COVID-19 vaccination with dynamic social distancing, Nat. Hum. Behav. 6 (2022) 193–206. https://doi.org/10.1038/s41562-021-01281-8.

[37] D. Han, X. Li, On Evolutionary vaccination game in activity-driven networks, IEEE Trans. Comput. Soc. Syst. (2022) 1–11. https://doi.org/10.1109/TCSS.2021.3137724.

[38] S. Tchoumi, J.M. Tchuenche, Dynamic of a two-strain COVID-19 model with vaccination vaccination, Res. Sq. (2021) 1–15. https://doi.org/https://doi.org/10.21203/rs.3.rs-553546/v1.

[39] R. Tori, J. Tanimoto, A study on prosocial behavior of wearing a mask and self-quarantining to prevent the spread of diseases underpinned by evolutionary game theory, Chaos, Solitons and Fractals. 158 (2022) 112030. https://doi.org/10.1016/j.chaos.2022.112030.

[40] P. Poletti, B. Caprile, M. Ajelli, A. Pugliese, S. Merler, Spontaneous behavioral changes in response to epidemics, J. Theor. Biol. 260 (2009) 31–40. https://doi.org/10.1016/j.jtbi.2009.04.029.

[41] J. Tanimoto, Evolutionary games with sociophysics: Analysis of traffic flow and epidemics, Springer (Tokyo), 2019.

[42] J. Tanimoto, Fundamentals of evolutionary game theory and its applications, Springer (Tokyo), 2015.

[43] J. Tanimoto, Sociophysics approach to epidemics, Springer (Tokyo), 2021.

[44] K.M.A. Kabir, How evolutionary game could solve the human vaccine dilemma, Chaos, Solitons and Fractals. 152 (2021) 111459. https://doi.org/10.1016/j.chaos.2021.111459.

[45] F.B. Agusto, I. V. Erovenko, A. Fulk, Q. Abu-Saymeh, D. Romero-Alvarez, J. Ponce, S. Sindi, O. Ortega, J.M. Saint Onge, A.T. Peterson, To isolate or not to isolate: the impact of changing behavior on COVID-19 transmission, BMC Public Health. 22 (2022) 1–20. https://doi.org/10.1186/s12889-021-12275-6.

[46] C.T. Bauch, Imitation dynamics predict vaccinating behavior, Proc. R. Soc. B Biol. Sci. 272 (2005) 1669–1675. https://doi.org/10.1098/rspb.2005.3153.

[47] C.T. Bauch, S. Bhattacharyya, Evolutionary game theory and social learning can determine how vaccine scares unfold, PLoS Comput. Biol. 8 (2012). https://doi.org/10.1371/journal.pcbi.1002452.

[48] T. Li, Y. Guo, Modeling and optimal control of mutated COVID-19 (Delta strain) with imperfect vaccination, Chaos, Solitons and Fractals. 156 (2022). https://doi.org/10.1016/j.chaos.2022.111825.

[49] A. Szolnoki, M. Perc, Conformity enhances network reciprocity in evolutionary social dilemmas, J. R. Soc. Interface. 12 (2015) 2–9. https://doi.org/10.1098/rsif.2014.1299.

[50] J. Yang, Y. Chen, J. Liu, Stability analysis of a two-strain epidemic model on complex networks with latency, Discret. Contin. Dyn. Syst. - Ser. B. 21 (2016) 2851–2866. https://doi.org/10.3934/dcdsb.2016076.

[51] P. Theprungsimankul, S. Junsank, A. Abdulloh, W. Chinviriyasit, The effect of cross-immunity in a multi-strain epidemic model, Kasetsart J. - Nat. Sci. 45 (2011) 563–570.

[52] A. Khatua, D. Pal, T. K. Kar, Global dynamics of an epidemic model with a non-monotonic incidence rate, Iran J Sci Technol Trans Sci. 10 (2014) 71–77. https://doi.org/10.9790/5728-10277177.

[53] S. Allali, A. Amine, Stability analysis of a fractional-order two-strain epidemic model with general incidence rates, Commun. Math. Biol. Neurosci. 43 (2022). https://doi.org/https://doi.org/10.28919/cmbn/7297.

[54] C. Li, Y. Zhang, Y. Zhou, Competitive coexistence in a two-strain epidemic model with a periodic infection rate, Discret. Dyn. Nat. Soc. 2020 (2020). https://doi.org/10.1155/2020/7541861.

[55] G. Nastasi, C. Perrone, S. Taffara, G. Vitanza, A time-delayed deterministic model for the spread of COVID-19 with calibration on a real dataset, Mathematics. 10 (2022) 1–14. https://doi.org/10.3390/math10040661.

[56] J. Yang, F. Zhang, Stability of a two-strain epidemic model with an age structure, J. Appl. Math. Informatics. 30 (2012) 183–200.

[57] P.K. Tiwari, R.K. Rai, S. Khajanchi, R.K. Gupta, A.K. Misra, Dynamics of coronavirus pandemic: effects of community awareness and global information campaigns, Eur. Phys. J. Plus. 136 (2021). https://doi.org/10.1140/epjp/s13360-021-01997-6.

[58] M.R. Arefin, K.M.A. Kabir, M. Jusup, H. Ito, J. Tanimoto, Social efficiency deficit deciphers social dilemmas, Sci. Rep. 10 (2020) 1–9. https://doi.org/10.1038/s41598-020-72971-y.

[59] J. Huang, J. Wang, C. Xia, Role of vaccine efficacy in the vaccination behavior under myopic update rule on complex networks, Chaos, Solitons and Fractals. 130 (2020). https://doi.org/10.1016/j.chaos.2019.109425.

[60] Z. wang, C. Xia, Co-evolution spreading of multiple information and epidemics on two-layered networks under the influence of mass media. Nonlinear Dynamics, 2020, 102: 3039-3051, https://doi.org/10.1007/s11071-020-06021-7.

[61] M.M.U.R. Khan, M.R. Arefin, J. Tanimoto, Investigating the trade-off between self-quarantine and forced quarantine provisions to control an epidemic: An evolutionary approach, Appl. Math. Comput. 432 (2022) 127365, https://doi.org/10.1016/j.amc.2022.127365.

[62] M.M.U.R. Khan, M.R. Arefin, J. Tanimoto, Investigating vaccination behavior and disease dynamics of a time-delayed two-strain epidemic model : An evolutionary approach, Proc. Int. Exch. Innov. Conf. Eng. Sci. 8 (2022) 147–154.

[63] M. Martcheva, An Introduction to Mathematical Epidemiology, Springer International Publishing, 2013.

[64] M. Martcheva, A non-autonomous multi-strain SIS epidemic model, J. Biol. Dyn. 3 (2009) 235–251. https://doi.org/10.1080/17513750802638712.

[65] E.F. Arruda, S.S. Das, C.M. Dias, D.H. Pastore, Modelling and optimal control of multi-strain epidemics, with application to COVID-19, PLoS One. 16 (2021) 1–18. https://doi.org/10.1371/journal.pone.0257512.

Chapter 4

Investigating the social dilemma of an epidemic model with provaccination and antivaccination groups: an evolutionary approach

Abstract

In this study, an epidemiological model with the provaccination and antivaccination susceptible groups is proposed, and the social dilemma of the model is analyzed. During a pandemic, such as the current COVID-19, many individuals get confused about choosing the option of adopting a provaccination or antivaccination strategy based on the number of infected people and the payoff of being infected. In the proposed model, people can obtain immunity either through vaccination or by getting infected with the disease which is known as natural immunity. In addition, increasing the waning immunity influences the choice of adopting the provaccination or antivaccination strategy. We used the behavior model to analyze the choice of the two strategies, where any individual can choose a strategy based on the number of infected individuals from each group. Moreover, individuals who are already infected can choose their strategy based on the payoff of their disease cost or vaccination cost. Our results show that, at Nash equilibrium, individuals in both groups behave the same. Further, from our numerical results, increasing the number of vaccinations can reduce the social dilemma whereas an increase in the waning immunity rate increases the social dilemma.

4.1 Introduction

The best method for preventing any infectious disease is vaccination. However, people do not always choose to get vaccinated. Some people develop immunity to infectious diseases after contracting them or develop a natural herd immunity. Some people would rather receive the vaccination after each season, such as influenza. Moreover, the current COVID-19 seems to resemble seasonal influenza, where people may require vaccination because of the decreasing effects of protection after a specific amount of time [1–7]. Thus, the entire human population can be split into two groups when vaccination becomes voluntary provaccination and antivaccination groups−meaning getting vaccinated and not getting vaccinated respectively. The decisions of individuals toward vaccination are influenced by the overall number of infected people in each group and the total payoff of both groups' illnesses[8–12].

In analyzing infectious disease models, compartmental models are the most useful tool for scientists and healthcare management authorities. The most extensively used model is the SIR model, which was developed by Kermach and Mckendrick [13] and is regarded as a pioneer in this field. This model depicts the path that disease takes in humans as it moves from the susceptible compartment (S) to the infected compartment (I) and then to the recovered compartment (R), where people develop resistance to reinfection. However, in certain instances, the recovered individual relapses, a condition known as

the waning of immunity. Exposed (E), quarantine (Q), hospitalized (H), and asymptomatic (A) compartments can be used in some epidemics to adequately examine disease dynamics [2, 4, 5, 11, 14–36]. An additional application of compartmental models in the research of disease transmission is the examination of supervision and moderation methods, such as immunization, and the impact of birthing and passing factors. SIR dynamics may analyze elements such as resource exploitation, corruption, and the spread of false information. However, most models emphasize more on how the illness develops than how a person behaves in a given circumstance. Nevertheless, various irresistible infection control strategies rely on organizational and human decision-making [8, 10, 15, 23, 24, 37–48]. The emerging discipline of behavioral epidemiology, which integrates game theory and psychology with epidemiology, has garnered considerable attention in this setting. Behavioral epidemiology considers individual behavior as opposed to a fixed role. The best discipline for this situation is sociophysics, a cutting-edge field that uses "Evolutionary Game Theory" (EGT) and statistical physics to better understand the behavior of humans. In a unique method, Bauch studied the dynamics of vaccine decision-making by combining the SIR model with EGT. Based on the disease dynamics, the total number of infected people, infection cost, vaccination cost, and vaccine efficacy, anybody can obtain their vaccination. Later, this developed into the idea of the "vaccination game." This method has led to several findings and predictions regarding vaccination campaigns [14, 49–55].

In this study, we propose a behavior epidemic model based on SIRS dynamics with two susceptible population groups: provaccination and antivaccination groups. Any individual can choose the strategy of committing provaccination or antivaccination based on the total number of infected individuals in each group before they got infected. However, any individual can choose their strategy based on the total payoff during each time step after being infected and recovering. We used the behavior model to analyze how people choose their strategies before infection and after recovery. Finally, for analyzing the social dilemma of the model based on transmission rate, vaccination rate, waning rate against immunity, and individual cost of vaccination or infection, we calculated the Social Efficiency Deficit (SED), which is the difference between the payoffs at the Nash Equilibrium (NE) and Social Optimum (SO).

4.2 Model Depiction

4.2.1 Epidemic Model

We suggested a 6-compartmental epidemic model based on the SIRS process. In the model, the entire population is split into two susceptible groups: the provaccination group P and the antivaccination group A. Individuals of P are willing to take part in the vaccination or prefer the provaccination strategy with some payoff. Meanwhile, the antivaccination group A includes individuals who are not willing to take part in the vaccination or prefer the antivaccination strategy. I_P and I_A denote the infected compartments of individuals who are infected from the provaccination and antivaccination groups,

respectively. Similarly, R_P and R_A denote the recovered individuals from the provaccination and antivaccination groups, respectively. Figure 1 depicts the flow diagram of the proposed model; the model formation is as follows:

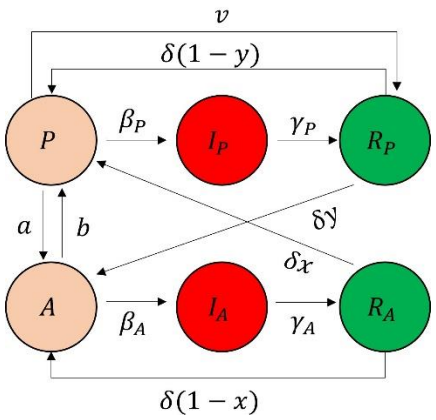

Figure 1: The compartments and their transition of the proposed model.

$$\dot{P} = -\beta_P P(I_A + I_P) + bA + \delta(1-y)R_P + \delta x R_A - aP - vP \quad (1)$$

$$\dot{A} = -\beta_A A(I_A + I_P) - bA + \delta(1-x)R_A + \delta y R_P + aP \quad (2)$$

$$\dot{I_P} = \beta_P P(I_A + I_P) - \gamma_P I_P \quad (3)$$

$$\dot{I_A} = \beta_A A(I_A + I_P) - \gamma_A I_A \quad (4)$$

$$\dot{R_P} = \gamma_P I_P - \delta(1-y)R_P - \delta y R_P + vP \quad (5)$$

$$\dot{R_A} = \gamma_A I_A - \delta(1-x)R_A - \delta x R_A \quad (6)$$

$$P(t) + A(t) + I_P(t) + I_A(t) + R_P(t) + R_A(t) = 1 \quad (7)$$

where, β_P and β_A denote the transmission rate of susceptible individuals in the provaccination and antivaccination groups, respectively. We consider $\beta_P < \beta_A$ because individuals in the provaccination group always have less risk of infection in the global context. γ_P and γ_A denote the recovery rate from provaccination and antivaccination infected groups, respectively. We consider $\gamma_P < \gamma_A$, i.e., the recovery time for individuals in the provaccination group is lower, to keep the basic reproduction number fixed for the proposed model. Table 1 shows all parameters with their meanings. δ denotes the waning rate against immunity, and v denotes the vaccination rate. To keep the model simple we have neglected the parameters which involve the birth and death issues [5, 11, 15, 16, 17, 22, 40, 55].

4.2.2 Behavior Model

We present the idea of the behavior model, which counts for the time-dependent flux from the susceptible provaccination group (P) to the susceptible antivaccination group (A) by a, the susceptible antivaccination group (A) to the susceptible provaccination group (P) by b, recovered from the

provaccination group (R_P) to the susceptible antivaccination group (A) by y and recovered from the antivaccination group (R_A) to the susceptible provaccination group (P) by x [53]. We define the following four dynamic equations:

$$\dot{a} = t_a\, a\,(1-a)\{I_P - I_A\} \tag{8}$$

$$\dot{b} = t_b\, b\,(1-b)\{I_A - I_P\} \tag{9}$$

$$\dot{x} = t_x\, x\,(1-x)\{c_a R_A - c_p R_P\} \tag{10}$$

$$\dot{y} = t_y\, y\,(1-y)\{c_p R_P - c_a R_A\} \tag{11}$$

where, t_a, t_b, t_x, and t_y are the inertial effects of the migration rate; c_a denotes the individual cost of committing an antivaccination strategy, i.e., the cost of infection from the antivaccination group; c_p denotes the individual cost of committing to a provaccination strategy, i.e., the cost of either vaccination or infection from a provaccination strategy. We consider $c_a > c_p$. Individuals can choose their strategy twice: before infection and after recovery. Before infection, individuals will consider the total number of infected individuals from both susceptible groups. If the infection from P, i.e., I_P increases, individuals will prefer to commit A, whereas if the infection from A, i.e., I_A increases, the individual will prefer P. After recovery, individuals choose their strategy based on the payoff during their infection period and the total number of recovered people from the provaccination and antivaccination groups. The total payoff at each time interval is calculated with the product of individual costs and recovered people. If the payoff from the antivaccination group increases, individuals will prefer the provaccination strategy, whereas if the payoff from the provaccination group increases individuals will prefer the antivaccination strategy.

Table 1: Description of the model parameters

Parameter symbol	Parameter Description
β_P	Disease Transference rate of provaccination group
β_A	Disease Transference rate of antivaccination group
γ_P	The recovery rate from the provaccination group
γ_A	The recovery rate from the antivaccination group
t_a	Inertial effect on migration from P to A
t_b	Inertial effect on migration from A to P
t_x	Inertial effect on migration from R_A to P
t_y	Inertial effect on migration from R_P to A
c_p	Individual cost due to choice of provaccination strategy
c_a	Individual cost due to choice of antivaccination strategy
δ	Waning rate against immunity
v	Vaccination rate

4.2.3 Basic Reproduction Number, Total infection, Average Social payoff (ASP), SED

In this model, we considered the basic reproduction number, $R_0 = \frac{\beta_P}{\gamma_P} = \frac{\beta_A}{\gamma_A} = 2.5$ [5, 11, 15, 40].

The total numbers of infected individuals from the provaccination and antivaccination groups are, respectively, defined as follows:

$$I_P T = \int_0^\infty \beta_P P(I_A + I_P)\, dt \tag{12}$$

$$I_A T = \int_0^\infty \beta_A A(I_A + I_P)\, dt \tag{13}$$

where $t = \infty$ denotes a state of equilibrium (we say it, NE).

The ASP at NE is defined as follows:

$$ASP_{NE} = -I_P T * c_p - I_A T * c_a \tag{14}$$

where the first and second terms on the right-hand side indicate the total payoffs of the individuals who commit the provaccination and antivaccination strategies, respectively.

By referring to the original definition of SED, we evaluate the discrepancy between ASP at NE and ASP at SO to determine whether a social dilemma underlies the current social-dynamical system (ASP_{SO}). It illustrates the way to increase the system's ASP from an evolutionary closing state (NE) to a theoretically optimal society to fulfill the highest ASP_{SO} plausible if all $a, b, x,$ and y evolutionary processes are properly controlled [25, 56]. It is defined as follows:

$$SED = ASP_{SO} - ASP_{NE} \tag{15}$$

The SO state is a time-constant vector $(a(for\ SO), b(for\ SO), x\ (for\ SO), y\ (for\ SO))$, with a, b ranging in [0.0,0.5] and x, y ranging in [0.0,1.0]. Thus,

$$\boldsymbol{SO} = \arg\max\ [ASP(a(for\ SO), b(for\ SO), x\ (for\ SO), y\ (for\ SO))] \tag{16}.$$

When NE equals SO, SED implies zero. However, when the SED is positive but not zero, there is a social dilemma.

4.3 Results and Discussion

4.3.1 Timeseries depiction:

Figure 2(a) shows the timeseries of all compartments taking the standard (basic) parameter values. Table 2 represents the parameters' standard values. Table 3 represents the initial values of the compartments and migration rates. We used the explicit finite difference method to solve the model [Equations (1)−(11)] numerically. Time step dt is taken as 1.0 in Figure 2. We have also checked the numerical simulation by using different time steps, where we observed that taking larger time steps (such as $dt =$

2.0) brings the NE faster whereas taking small time steps (such as $dt = 0.5$) brings NE slower. Because of this reason, we have used $dt = 1.0$ throughout the study. We assume the disease transmission rate β_P from the provaccination group is lower than the disease transmission rate β_A from the antivaccination group. In addition, we assume the recovery rate γ_P from the provaccination group is lower than the recovery rate γ_A from the antivaccination group to keep the basic reproduction number fixed at $R_0 = 2.5$. From Figure 2(a), at NE, graphs of both provaccination and antivaccination compartments (blue and orange, respectively) coincide with each other. Thus, we can say that the provaccination and antivaccination groups behave similarly at NE. Further, the NE graphs of the infected compartments from both the provaccination and antivaccination groups (red and green, respectively) coincide with each other. The number of people remaining in the recovered compartment from the provaccination group R_P (violet graph) is much higher than the people remaining in the recovered compartment from the antivaccination group R_A (brown graph). Figures 2(b) and 2(c) show the rates from the compartments that are proposed by the behavior model. In Figure 2(b), at NE, b is approximately 0.17, whereas a is close to zero. This is because, during the oscillating period, infection from the antivaccination group is mostly higher than the infection from the provaccination group; thus, most people will prefer to go to the provaccination state before infection. In Figure 2(c), rate y is almost close to 1.0 and x is almost close to 0.0 at NE. This is because, during the oscillating period, people staying in the recovered compartment from the provaccination group is always higher than the people staying in the recovered compartment from the antivaccination group; thus, most people will prefer to migrate to A as the total payoff $c_p R_P$ is always higher than the total payoff $c_a R_A$.

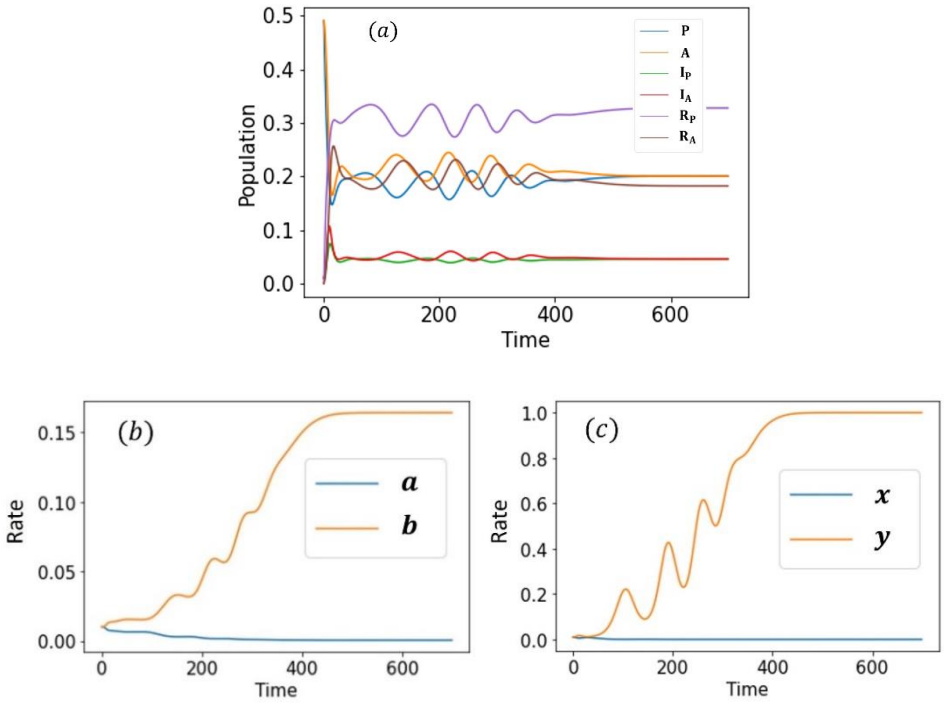

Figure 2: Timeseries of the compartments and rates for the standard case. In 2(a), the blue and orange lines depict the people of provaccination and antivaccination compartments, respectively; the green and red lines represent the infection compartments from provaccination and antivaccination groups, respectively; the violet and brown lines depict the recovered people from provaccination and antivaccination groups, respectively. Migration rates are depicted in 2(b) and 2(c). From 2(b), the moving rate from A to P is much lower than the moving rate from P to A. In 2(c), the moving rate from R_P to A is much higher than the moving rate from R_A to P. From the graph, the provaccination and antivaccination compartments coincide with each other at NE. In addition, their infection graphs coincide. The number of recovered from the provaccination group remains higher than that of those recovering from the antivaccination group at NE.

Table 2: Standard values of the parameters [11, 15, 16, 17, 40]

Parameter	Value	Parameter	Value
β_P	0.7	t_x, t_y	1.0
β_A	1.0	c_p	0.7
γ_P	0.28	c_a	1.0
γ_A	0.40	v	0.1
t_a, t_b	1.0	δ	0.1

Table 3: Initial values for the compartments and migration rates [11, 15, 16, 17, 40]

State	At $t = 0$	State/Rate	At $t = 0$
P	0.49	R_A	0.00
A	0.49	a	0.01
I_P	0.01	b	0.01
I_A	0.01	x	0.01
R_P	0.00	y	0.01

4.3.2 ASP and SED in Terms of Vaccination and Waning Immunity

The first row of Figure 3 shows the total number of infected people from the provaccination and antivaccination groups at the equilibrium state and the ASP for the NE state. The second row shows the total number of infected people from both the provaccination and antivaccination groups, ASP for the SO state, and the SED. All panels are drawn in terms of the waning immunity rate (δ) along the $x-$axis and vaccination rate (v) along the $y-$axis, both ranging from 0 to 0.5. From panel (a), if the waning immunity rate increases, the total number of infected people increases (yellow to blue). In addition, if the vaccination rate increases, the total number of infected people decreases (blue to yellow). Similar phenomena occur in panel (b). However, the total number of infected people is less than in panel (a)

because people will prefer the provaccination strategy to the antivaccination strategy during the total period to reach NE. Panel (c) shows the total payoff at NE, which is the combination of panels (a) and (b) multiplied by their payoffs. In panel (d), the total number of infected people is quite low for all combinations of vaccination rate and waning immunity rate. Meanwhile, in panel (e), a high vaccination rate gives low infection, whereas higher waning immunity gives higher infection, which is similar to panels (a) and (b). This is because as the provaccination strategy has a lower payoff than the antivaccination strategy, SO will go for the minimum cost, i.e., most people will prefer the provaccination strategy, and the flow into the provaccination group will be maximum. Thus most infections will be from the provaccination group. Therefore, we can say that most infections will come from the provaccination group at SO. Panel (f) presents the total payoff for the SO case, and the payoff is less than the payoff for the NE case. Considering the difference between the SO and NE states, we show the SED in panel (g). From the SED, we can observe that increasing the vaccination rate causes fewer social dilemmas, i.e., the payoff in the NE and SO states are very close to each other. However, if the waning rate increases, the social dilemma will also increase because most people will get confused in choosing their strategy if the immunity through vaccination or infection is not high. If both the waning immunity and vaccination are maximum, the social dilemma will be maximum.

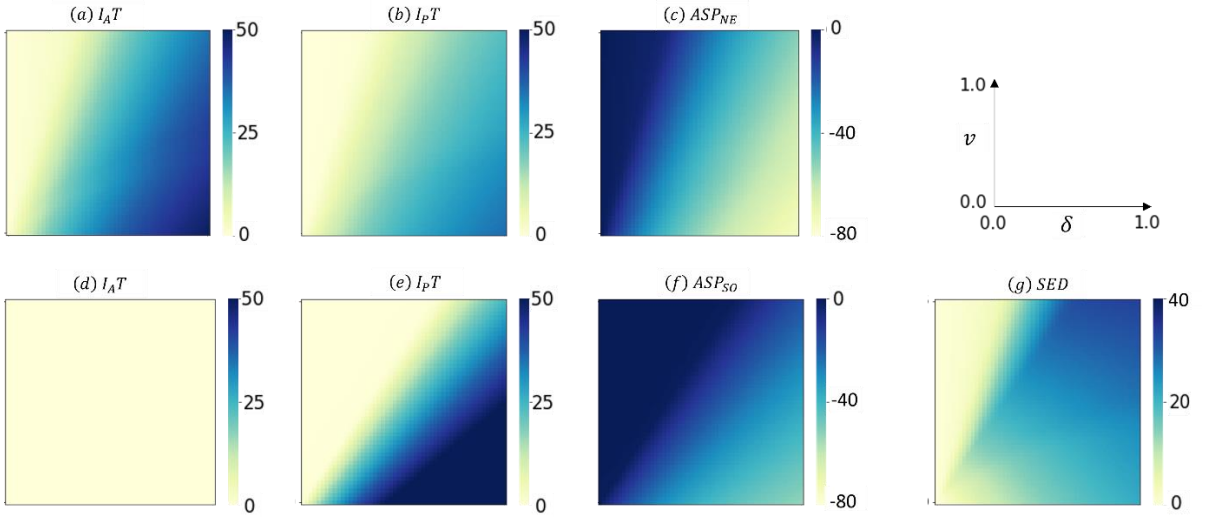

Figure 3: Total number of infected people from the provaccination and antivaccination groups, ASP, and SED. Panels (a) $-$(c) are for the NE case, and panels (d) $-$ (f) are for the SO case. Panel (g) represents the SED, which is the difference between panels (f) and (c). All the panels are drawn concerning vaccination rate (v) along the $y-$axis and waning immunity rate (δ) along the $x-$axis, both ranging from 0 to 0.5. The range of the total number of infected people is set from 0 to 50. The ASPs range from -80 to 0 and the SED range is set from 0 to 40. The remaining parameters are the same as in the standard case. From the figure, we can see if the wanning rate and vaccination rate are the maximum social dilemma will also be maximum.

4.3.3 ASP and SED in Terms of Individual Payoff

The first row of Figure 4 shows the total number of infected people from the provaccination and antivaccination groups in the NE state and also the ASP for the NE state. The second row shows the total number of infected people from both the provaccination and antivaccination groups, ASP for the SO state, and the SED. Each panel has been drawn in terms of the individual cost due to committing an antivaccination strategy (c_a) along the x −axis ranging from 0 to 1, and individual cost due to committing a provaccination strategy (c_p) along the y −axis ranging from 0 to c_a. In panel (a), the total number of infected people will be high if c_a and as c_p are high. In panel (b), a similar attitude is observed, but the total number of infected people is lower than in panel (a). Thus, the total number of infections will be greater in the antivaccination group than in the provaccination group. However, in the SO case, there are fewer infected people from the antivaccination group than from the provaccination group. Because the SO case is based on the total minimum payoff, the provaccination strategy is preferred due to its low payoff. Panels (c) and (f) represent the total average payoff of the provaccination and antivaccination groups, respectively, and from their difference, we can observe the SED in panel (g). In the NE case, increasing both costs increases the total payoff. In panel (f), the same phenomena are observed. As a result, the SED panel shows that increasing the price raises the value of SED, creating a social dilemma. The social dilemma will be maximum if both costs are at the maximum level.

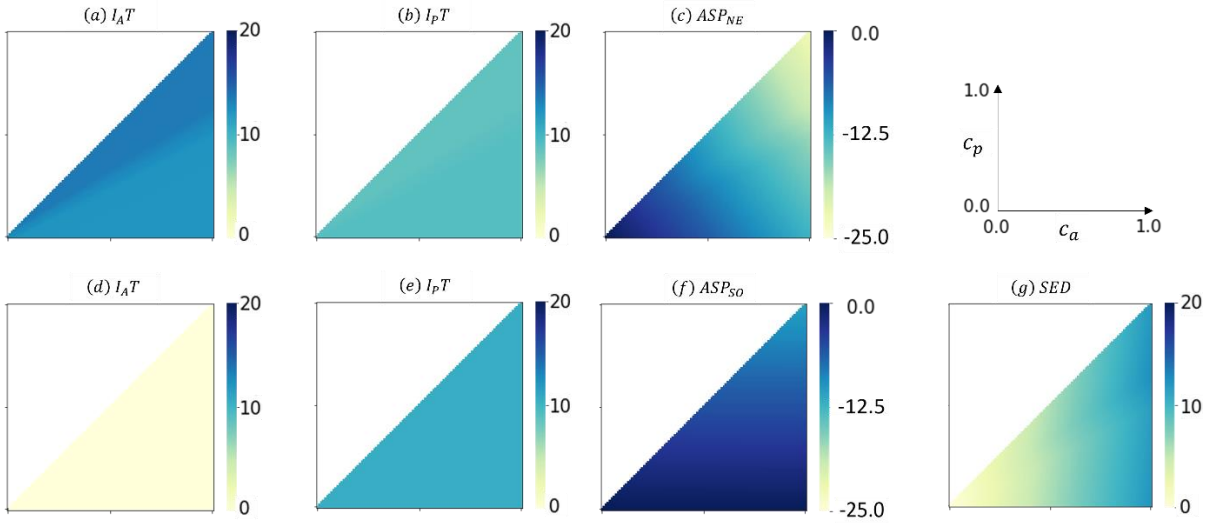

Figure 4: Total number of infected people from provaccination and antivaccination groups, ASP, and SED. Panels (a) − (c) are for the NE case, and panels (d) − (f) are for the SO case. Panel (g) represents the SED, which is the difference between panels (f) and (c). All the panels are drawn in terms of the individual cost due to committing an antivaccination strategy (c_a) along the x −axis ranging from 0 to 1 and individual cost due to committing a provaccination strategy (c_p) along the y − axis ranging from 0 to c_a. The total number of infected people is depicted with a range from 0 to 20, the ASPs are depicted with a range from −25 to 0, and the SED is depicted with a range from 0 to 20. The other parameters

are the same as in the basic case. From the figures, the social dilemma will be maximum if both the costs are at maximum level.

4.3.4 ASP and SED in Terms of Transmission Rate

The first row of Figure 5 shows the total number of infected people from the provaccination and antivaccination groups in the NE state and the ASP for the NE state. The second row shows the total number of infected people from both groups, the ASP for the SO state, and the SED. Each panel has been drawn in terms of the transmission rate from the antivaccination group (β_a) along the $x-$axis ranging from 0 to 1 and the transmission rate from the provaccination group (β_p) along the $y-$ axis ranging from 0 to β_a. In panel (a), the total number of infected people will be high if β_a and β_p are high. In panel (b), a similar attitude is observed, but the total number of infected people is higher than in panel (a). Thus, the total number of infections will be larger in the provaccination group than in the antivaccination group. Because the transmission rate is the same for both groups, more people will choose the strategy of provaccination because of less payoff. For the SO case, there is a very low number of infected people from the antivaccination group but a high number of infected people from the provaccination group. Because the SO case is based on the total minimum payoff, the provaccination strategy is preferred due to its low payoff. Panels (c) and (f) represent the total average payoffs of the provaccination and antivaccination groups, respectively; from their difference, we can see the SED in panel (g). In the NE case in panel (c), increasing of transmission rate increases the total payoff. In panel (f), the same phenomena are observed. Thus, from the SED panel, when β_a is high (greater than 0.5), increasing β_P increases the dilemma and there is a peak dilemma (dark blue) approximately at $\beta_P = 0.7$. Afterward, the peak dilemma decreases because, if β_P is more than 0.7, and infection from both groups becomes the same. Therefore, there will be fewer social dilemmas when the two transmission rates are the same.

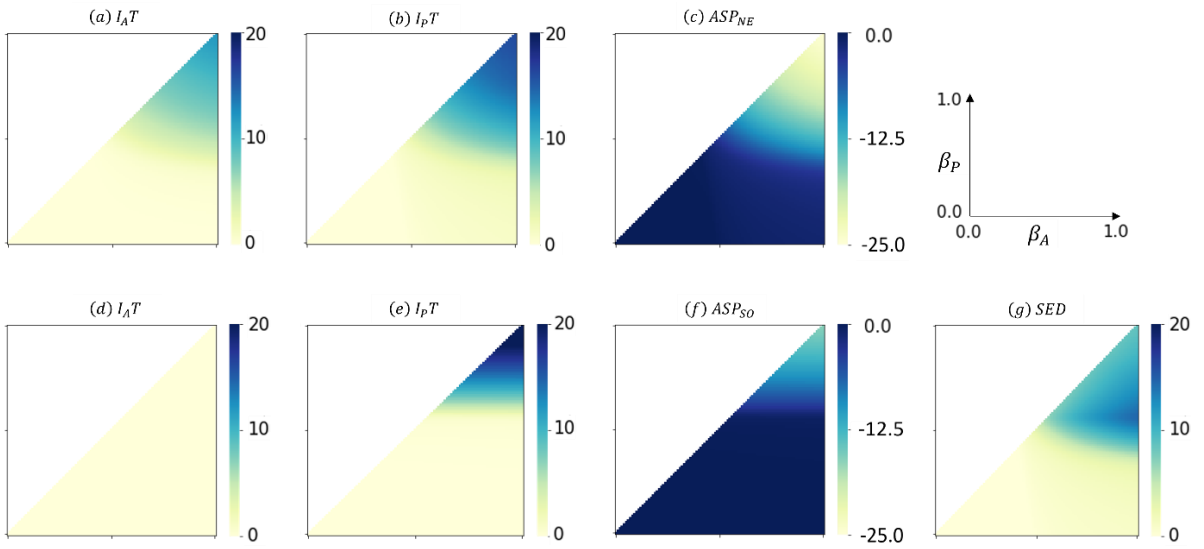

Figure 5: The total number of infected people from provaccination and antivaccination groups, ASP, and SED. Panels (a) − (c) are for the NE case and panels (d) − (f) are for the SO case. Panel (g) represents the SED, which is the difference between panels (f) and (c). All the panels are drawn in terms of the transmission rate from the antivaccination group (β_a) along the x −axis ranging from 0 to 1 and the transmission rate from the antivaccination group (β_p) along the $y-$ axis both ranging from 0 to β_a. The total number of infected people is depicted with a range from 0 to 20, the ASPs are depicted with a range from −25 to 0, and the SED is depicted with a range from 0 to 20. The other parameters are the same as in the basic case. From the figures, we see that the social dilemma reached a peak level with the increasing transmission rate of the provaccination group and then started to decrease.

4.4 Conclusion

Any infectious disease dynamics are always influenced by how people behave. People determine their approach to maintaining protection to fend off infectious diseases based on available therapy, vaccinations, and other preventative measures. In a model of an epidemic where all susceptible people are split into provaccination and antivaccination groups, we consider disease dynamics. Decisions are examined in light of dynamic human behavior. Depending on the total number of infections from each group, any individual can take a provaccination or antivaccination strategy before infection. However, once infected, individuals can adopt a strategy by considering the benefits accrued throughout the infection phase and the overall number of recovered members of each group. Some analytic and numerical results of an epidemic model containing the pro- and anti-vaccine groups were presented in [12]. Group behavior towards the provaccination or antivaccination groups was analyzed in [8]. The vaccination behavior of humans and the waning immunity effect in epidemic models were also analyzed in [4, 6, 10, 18].

The proposed model's disease dynamics were our focus. We considered whether behavior equations suggested an NE state while maintaining the fundamental reproduction number at a fixed value.

According to our findings, the overall number of people using the two strategies and the total number of diseases originating from each group were equal at NE. Thus, we can conclude that both groups behave similarly when the situation is balanced. Our next issue is to examine the social dilemma of the model using suggested key elements. When considering vaccination rates and the waning immunity effect, we find that increasing the vaccination rates decreases the payoff gap between the NE state and the SO state, thereby alleviating the social dilemma of adopting the provaccination strategy. In addition, reducing the waning immunity rate lessens the social pressure to adopt the provaccination strategy. Social dilemma grows as the payoffs for adopting the two strategies increase from an individual perspective. In terms of the transmission rate for both groups, the social dilemma increases monotonically as the transmission rate from the provaccination group increases and reaches a peak value. Following the peak, the social dilemma declines are monotonic with the increase in the provaccination group's transmission rate.

The disease dynamics and social dilemma were studied in our model using a simple ordinary differential equation model (mean-field approximation) technique, and the social context gives our data credibility. We will use a multiagent simulation approach to analyze the results in further investigations.

References

[1] M. V. Boven, H.E. De Melker, J.F.P. Schellekens, M. Kretzschmar, Waning immunity and sub-clinical infection in an epidemic model: Implications for pertussis in The Netherlands, Math. Biosci. 164 (2000) 161–182. https://doi.org/10.1016/S0025-5564(00)00009-2.

[2] G. Webb, A COVID-19 epidemic model predicting the effectiveness of vaccination in the US, Infect. Dis. Rep. 13 (2021) 654–667. https://doi.org/10.3390/IDR13030062.

[3] Y. Nakata, R. Omori, Delay equation formulation for an epidemic model with waning immunity: An application to mycoplasma pneumoniae, IFAC-PapersOnLine. 28 (2015) 132–135. https://doi.org/10.1016/j.ifacol.2015.11.024.

[4] M. Turkyilmazoglu, An extended epidemic model with vaccination: Weak-immune SIRVI, Phys. A Stat. Mech. It's Appl. 598 (2022) 127429. https://doi.org/10.1016/j.physa.2022.127429.

[5] Y. Tatsukawa, M.R. Arefin, S. Utsumi, J. Tanimoto, Investigating the efficiency of dynamic vaccination by consolidating detecting errors and vaccine efficacy, Sci. Rep. 12 (2022) 1–12. https://doi.org/10.1038/s41598-022-12039-1.

[6] D. Hamami, R. Cameron, K.G. Pollock, C. Shankland, Waning immunity is associated with periodic large outbreaks of mumps: A mathematical modeling study of Scottish data, Front. Physiol. 8 (2017) 1–11. https://doi.org/10.3389/fphys.2017.00233.

[7] A.C.S. Chun-Miin Chen, Simulating influenza epidemics with waning vaccine immunity,

Medicine (Baltimore). (2021). https://doi.org/http://dx.doi.org/10.1097/MD.0000000000027169.

[8] J. Maciuszek, M. Polak, K. Stasiuk, D. Doliński, Active pro-vaccine, and anti-vaccine groups: Their group identities and attitudes toward science, PLoS One. 16 (2021) 1–15. https://doi.org/10.1371/journal.pone.0261648.

[9] F. Brauer, A simple model for behavior change in epidemics, BMC Public Health. 11 (2011) 1–5. https://doi.org/10.1186/1471-2458-11-S2-S3.

[10] E.P. Fenichela, C. Castillo-Chavezb, M.G. Ceddiac, G. Chowellb, P.A. Gonzalez Parrae, G.J. Hickling, G. Holloway, R. Horan, B. Morin, C. Perrings, M. Springborn, L. Velazquez, C. Villalobos, Adaptive human behavior in epidemiological models, Proc. Natl. Acad. Sci. U. S. A. 108 (2011) 6306–6311. https://doi.org/10.1073/pnas.1011250108.

[11] S. Utsumi, M.R. Arefin, Y. Tatsukawa, J. Tanimoto, How and to what extent does the anti-social behavior of violating self-quarantine measures increase the spread of disease?, Chaos, Solitons and Fractals. 159 (2022). https://doi.org/10.1016/j.chaos.2022.112178.

[12] G.S. Harari, L.H.A. Monteiro, An Epidemic Model with Pro and Anti-vaccine Groups, Acta Biotheor. 70 (2022) 1–13. https://doi.org/10.1007/s10441-022-09443-5.

[13] W. O. Kermack and A. G. McKendrick, A contribution to the mathematical theory of epidemics, Proc. R. Soc. A Math. Phys. Eng. Sci. 115 (1927) 700–721. https://doi.org/https://doi.org/10.1098/rspa.1927.0118.

[14] M. Martcheva, An Introduction to Mathematical Epidemiology, 2013.

[15] R. Tori, J. Tanimoto, A study on prosocial behavior of wearing a mask and self-quarantining to prevent the spread of diseases underpinned by evolutionary game theory, Chaos, Solitons Fractals Interdiscip. J. Nonlinear Sci. Nonequilibrium Complex Phenom. 158 (2022) 112030. https://doi.org/10.1016/j.chaos.2022.112030.

[16] M.M.U.R. Khan, M. R. Arefin, J. Tanimoto, Investigating the trade-off between self-quarantine and forced quarantine provisions to control an epidemic: An evolutionary approach, Appl. Math. Comput. 432 (2022) 127365, /https://doi.org/10.1016/j.amc.2022.127365.

[17] M. M. U. R. Khan, M.R. Arefin, J. Tanimoto, Investigating vaccination behavior and disease dynamics of a time-delayed two-strain epidemic model : An evolutionary approach, Proc. Int. Exch. Innov. Conf. Eng. Sci. 8 (2022) 147–154.

[18] C. Fahdilla, A. R. Putri, H. Haripamyu, Bifurcation analysis of epidemic model waning immunity, J. Phys. Conf. Ser. 1940 (2021) 012014. https://doi.org/10.1088/1742-

6596/1940/1/012014.

[19] Q. Sun, Z. Wang, D. Zhao, C. Xia, and M. Perc, “Diffusion of resources and their impact on epidemic spreading in multilayer networks with simplicial complexes,” *Chaos, Solitons and Fractals*, vol. 164, no. August, 2022, doi: 10.1016/j.chaos.2022.112734.

[20] J. Fan, Q. Yin, C. Xia, and M. Perc, “Epidemics on multilayer simplicial complexes,” *Proc. R. Soc. A Math. Phys. Eng. Sci.*, vol. 478, no. 2261, May 2022, doi: 10.1098/rspa.2022.0059.

[21] H. J. Li, W. Xu, S. Song, W. X. Wang, and M. Perc, “The dynamics of epidemic spreading on signed networks,” *Chaos, Solitons and Fractals*, vol. 151, p. 111294, 2021, doi: 10.1016/j.chaos.2021.111294.

[22] K. M. A. Kabir, K. Kuga, J. Tanimoto, Analysis of SIR epidemic model with information spreading of awareness, Chaos, Solitons and Fractals. 119 (2019) 118–125. https://doi.org/10.1016/j.chaos.2018.12.017.

[23] M. Cabrera, F. Córdova-Lepe, J.P. Gutiérrez-Jara, K. Vogt-Geisse, An SIR-type epidemiological model that integrates social distancing as a dynamic law based on point prevalence and socio-behavioral factors, Sci. Rep. 11 (2021) 1–16. https://doi.org/10.1038/s41598-021-89492-x.

[24] R. Ghostine, M. Gharamti, S. Hassrouny, I. Hoteit, Ghostine-2021-An extended seir model with vacc.pdf, Mathematics. 9 (2021) 636.

[25] M. R. Arefin, T. Masaki, K.M. Ariful Kabir, J. Tanimoto, Interplay between cost and effectiveness in influenza vaccine uptake: A vaccination game approach, Proc. R. Soc. A Math. Phys. Eng. Sci. 475 (2019). https://doi.org/10.1098/rspa.2019.0608.

[26] K. M. A. Kabir, M. Jusup, J. Tanimoto, Behavioral incentives in a vaccination-dilemma setting with optional treatment, Phys. Rev. E. 100 (2019) 1–13. https://doi.org/10.1103/PhysRevE.100.062402.

[27] S. Tyagi, S. Gupta, S. Abbas, K. P. Das, and B. Riadh, “Analysis of infectious disease transmission and prediction through SEIQR epidemic model,” *Nonautonomous Dyn. Syst.*, vol. 8, no. 1, pp. 75–86, 2021, doi: 10.1515/msds-2020-0126.

[28] R. Kiran, M. Roy, S. Abbas, and A. Taraphder, “Effect of population migration and punctuated lockdown on the spread of infectious diseases,” *Nonautonomous Dyn. Syst.*, vol. 8, no. 1, pp. 251–266, 2021, doi: 10.1515/msds-2020-0137.

[29] S. Tyagi, S. C. Martha, S. Abbas, and A. Debbouche, “Mathematical modeling and analysis for controlling the spread of infectious diseases,” *Chaos, Solitons and Fractals*, vol. 144, p. 110707, 2021, doi: 10.1016/j.chaos.2021.110707.

[30] M. Kumar and S. Abbas, “Age-Structured SIR Model for the Spread of Infectious Diseases Through Indirect Contacts,” *Mediterr. J. Math.*, vol. 19, no. 1, pp. 1–18, 2022, doi: 10.1007/s00009-021-01925-z.

[31] J. Huang, J. Wang, C. Xia, Role of vaccine efficacy in the vaccination behavior under myopic update rule on complex networks, Chaos, Solitons and Fractals. 130 (2020). https://doi.org/10.1016/j.chaos.2019.109425.

[32] M. Turkyilmazoglu, “Explicit formulae for the peak time of an epidemic from the SIR model,” *Phys. D Nonlinear Phenom.*, vol. 422, p. 132902, 2021, doi: 10.1016/j.physd.2021.132902.

[33] M. Turkyilmazoglu, “A restricted epidemic SIR model with elementary solutions,” *Phys. A Stat. Mech. its Appl.*, vol. 600, p. 127570, 2022, doi: 10.1016/j.physa.2022.127570.

[34] Q. Yin, Z. Wang, C. Xia, M. Dehmer, F. Emmert-Streib, Z. Jin, A novel epidemic model considering demographics and intercity commuting on complex dynamical networks, Appl. Math. Comput. 386 (2020) 125517. https://doi.org/10.1016/j.amc.2020.125517.

[35] F. Calleri, G. Nastasi, V. Romano, Continuous-time stochastic processes for the spread of COVID-19 disease simulated via a Monte Carlo approach and comparison with deterministic models, J. Math. Biol. 83 (2021) 1–26. https://doi.org/10.1007/s00285-021-01657-4.

[36] G. Nastasi, C. Perrone, S. Taffara, G. Vitanza, A Time-Delayed Deterministic Model for the Spread of COVID-19 with Calibration on a Real Dataset, Mathematics. 10 (2022) 1–14. https://doi.org/10.3390/math10040661.

[37] Y. Wei, Y. Lin, B. Wu, Vaccination dilemma on an evolving social network, J. Theor. Biol. 483 (2019). https://doi.org/10.1016/j.jtbi.2019.08.009.

[38] C. Zuo, F. Zhu, Z. Meng, Y. Ling, Y. Zheng, X. Zhao, Analyzing the COVID-19 vaccination behavior based on epidemic model with awareness-information, Infect. Genet. Evol. 98 (2022) 105218. https://doi.org/10.1016/j.meegid.2022.105218.

[39] J.M. Epstein, E. Hatna, J. Crodelle, Triple contagion: A two-fears epidemic model, J. R. Soc. Interface. 18 (2021). https://doi.org/10.1098/rsif.2021.0186.

[40] K.M.A. Kabir, T. Risa, J. Tanimoto, Prosocial behavior of wearing a mask during an epidemic:

an evolutionary explanation, Sci. Rep. 11 (2021) 1–14. https://doi.org/10.1038/s41598-021-92094-2.

[41] C. Zuo, F. Zhu, Y. Ling, Analyzing COVID-19 Vaccination Behavior Using an SEIRM/V Epidemic Model With Awareness Decay, Front. Public Heal. 10 (2022) 1–12. https://doi.org/10.3389/fpubh.2022.817749.

[42] K.M.A. Kabir, K. Kuga, J. Tanimoto, Effect of information spreading to suppress the disease contagion on the epidemic vaccination game, Chaos, Solitons and Fractals. 119 (2019) 180–187. https://doi.org/10.1016/j.chaos.2018.12.023.

[43] K.M.A. Kabir, J. Tanimoto, Analysis of epidemic outbreaks in two-layer networks with different structures for information spreading and disease diffusion, Commun. Nonlinear Sci. Numer. Simul. 72 (2019) 565–574. https://doi.org/10.1016/j.cnsns.2019.01.020.

[44] N.F. Johnson, N. Velásquez, N.J. Restrepo, R. Leahy, N. Gabriel, S. El Oud, M. Zheng, P. Manrique, S. Wuchty, Y. Lupu, The online competition between pro- and anti-vaccination views, Nature. 582 (2020) 230–233. https://doi.org/10.1038/s41586-020-2281-1.

[45] Z. Wu, Social distancing is a social dilemma game played by every individual against his/her population, PLoS One. 16 (2021) 1–26. https://doi.org/10.1371/journal.pone.0255543.

[46] K.M.A. Kabir, How evolutionary game could solve the human vaccine dilemma, Chaos, Solitons and Fractals. 152 (2021) 111459. https://doi.org/10.1016/j.chaos.2021.111459.

[47] Y. Zhu, C.Y. Xia, Z. Wang, Z. Chen, Networked Decision-Making Dynamics Based on Fair, Extortionate and Generous Strategies in Iterated Public Goods Games, IEEE Trans. Netw. Sci. Eng. 9 (2022) 2450–2462. https://doi.org/10.1109/TNSE.2022.3164094.

[48] C. Xia, Z. Hu, D. Zhao, Costly reputation building still promotes the collective trust within the networked population, New J. Phys. 24 (2022). https://doi.org/10.1088/1367-2630/ac8898.

[49] J. Tanimoto, Sociophysics approach to epidemics, Springer (Tokyo), 2021.

[50] J. Tanimoto, Fundamentals of evolutionary game theory and its applications, Springer (Tokyo), 2015.

[51] M. Jusup, P. Holme, K. Kanazawa, M. Takayasu, I. Romić, Z. Wang, S. Geček, T. Lipić, B. Podobnik, L. Wang, W. Luo, T. Klanjšček, J. Fan, S. Boccaletti, M. Perc, Social physics, Phys. Rep. 948 (2022) 1–148. https://doi.org/10.1016/j.physrep.2021.10.005.

[52] D. Helbing, D. Brockmann, T. Chadefaux, K. Donnay, U. Blanke, O. Woolley-Meza, M. Moussaid, A. Johansson, J. Krause, S. Schutte, M. Perc, Saving Human Lives: What Complexity Science and Information Systems can Contribute, 2015. https://doi.org/10.1007/s10955-014-

1024-9.

[53] C.T. Bauch, Imitation dynamics predict vaccinating behaviour, Proc. R. Soc. B Biol. Sci. 272 (2005) 1669–1675. https://doi.org/10.1098/rspb.2005.3153.

[54] J. Tanimoto, Evolutionary games with sociophysics: Analysis of traffic flow and epidemics, Springer (Tokyo), 2019.

[55] M.A. Amaral, M.M. D. Oliveira, M.A. Javarone, An epidemiological model with voluntary quarantine strategies governed by evolutionary game dynamics, Chaos, Solitons and Fractals. 143 (2021) 110616. https://doi.org/10.1016/j.chaos.2020.110616.

[56] M.R. Arefin, K.M.A. Kabir, M. Jusup, H. Ito, J. Tanimoto, Social efficiency deficit deciphers social dilemmas, Sci. Rep. 10 (2020) 1–9. https://doi.org/10.1038/s41598-020-72971-y.

Chapter 5

Influence of Waning Immunity on Vaccination Decision-making: A Multi-Strain Epidemic Model with an Evolutionary Approach Analyzing Cost and Efficacy

Abstract

In this research, we introduce a comprehensive epidemiological model that accounts for multiple strains of an infectious disease and two distinct vaccination options. Vaccination stands out as the most effective means to prevent and manage infectious diseases. However, when there are various vaccines available, each with its costs and effectiveness, the decision-making process for individuals becomes paramount. Furthermore, the factor of waning immunity following vaccination also plays a significant role in influencing these choices. To understand how individuals make decisions in the context of multiple strains and waning immunity, we employ a behavioral model, allowing an epidemiological model to be coupled with the dynamics of a decision-making process. Individuals base their choice of vaccination on factors such as the total number of infected individuals and the cost-effectiveness of the vaccine. Our findings indicate that as waning immunity increases, people tend to prioritize vaccines with higher costs and greater efficacy. Moreover, when more contagious strains are present, the equilibrium in vaccine adoption is reached more rapidly. Finally, we delve into the social dilemma inherent in our model by quantifying the social efficiency deficit (SED) under various parameter combinations.

5.1 Introduction

Vaccination stands as the foremost strategy for preventing infectious diseases. However, the proliferation of diverse vaccines has introduced a conundrum among individuals, creating confusion in the selection process [1–4]. This dilemma is exacerbated in the context of diseases with multiple strains, accentuating the critical nature of informed vaccine selection [3,4]. The pivotal determinants in this decision-making process revolve around the economic considerations associated with vaccination cost and the efficacy of the chosen vaccine [5–10]. Despite the established efficacy of vaccination, not all individuals opt for this preventive measure. Some individuals acquire immunity through natural exposure to infectious agents or contribute to the development of natural herd immunity. In specific cases, individuals may favor periodic vaccinations, as exemplified by the seasonal administration of influenza vaccines [5,11,12]. Notably, the ongoing COVID-19 pandemic shares resemblances with seasonal influenza, warranting recurrent vaccinations due to the diminishing protective effects over time [2,13–17]. Individual choices regarding vaccination are further molded by prevailing infection rates and the financial implications of vaccine acquisition.

In the examination of infectious disease models, compartmental models emerge as the preeminent tool for scientific and healthcare management authorities. The foremost among these models is the SIR model, pioneered by Kermack and McKendrick, delineating the progression of disease in humans through sequential transitions from the susceptible compartment (S) to the infected compartment (I) and ultimately to the recovered compartment (R), where immunity to reinfection develops [18]. The phenomenon of waning immunity, manifesting as relapses in recovered individuals, introduces a nuanced consideration.

Certain epidemics necessitate the incorporation of additional compartments, such as Exposed (E), Quarantine (Q), Hospitalized (H), and Asymptomatic (A), to comprehensively investigate disease dynamics [1,19,28–30,20–27]. Furthermore, compartmental models find applicability in exploring disease transmission interventions, including the scrutiny of supervision and moderation methods like immunization, as well as the impact of demographic factors.

While SIR dynamics afford analysis of various elements such as resource exploitation, corruption, and the dissemination of misinformation, it is noteworthy that most models tend to emphasize the pathogenesis of the illness rather than individual behavior within specific circumstances. However, it is pivotal to acknowledge that numerous infectious disease control strategies hinge on organizational and human decision-making processes [1,3,14,27,31,32].

The nascent field of behavioral epidemiology, an amalgamation of game theory and psychology with epidemiology, has gained significant attention in addressing this gap. Behavioral epidemiology diverges from fixed role paradigms, focusing on individual behavior as a key determinant. In this context, sociophysics emerges as a cutting-edge discipline utilizing Evolutionary Game Theory (EGT) and statistical physics to enhance the understanding of human behavior [3,4,6,7,12,32−35].

An innovative approach, as exemplified by Bauch [36], involves the integration of the SIR model with EGT to scrutinize the dynamics of vaccine decision-making. By considering disease dynamics, total infected individuals, infection cost, vaccination cost, and vaccine efficacy, this approach facilitates personalized vaccination decisions, culminating in the concept of the “vaccination game”. The application of this method has yielded numerous insights and predictions pertinent to vaccination campaigns[5,12,30,31,37].

Aside from the standpoint of epidemiological modeling, the question of how people adopt a vaccine; whether willing to commit or to avoid it, and which vaccine is favored amid several alternatives, is important. It should be said still a difficult problem to reproduce in a mathematical model, although some field survey studies were explored (e.g. [38]).

In this investigation, we present a comprehensive behavioral epidemic model featuring multiple strains, built upon the SIRS/V dynamics and incorporating two distinct vaccination options. Our model allows

individuals to make vaccination choices based on key factors such as the total number of infected individuals, vaccination costs, and the efficacy of available vaccines with the presence of wanning immunity [11,37,39–42]. The multistrain context enables an exploration of how these behavioral dynamics influence the dominance or coexistence of the two vaccination options over time [3–5].

Through the selection of critical parameters within our proposed model, we have computed the fractions of vaccinated individuals at equilibrium, providing insights into the emergence of vaccine dominance. The behavioral model serves as a framework for guiding individual vaccination strategies.

To delve into the societal implications of our model, particularly addressing the social dilemma, we utilize essential metrics such as the basic reproduction number, waning rate of immunity, vaccination cost, inertial effect of vaccination rate, and the sensitivity of vaccination choice to cost. Specifically, we quantify the Social Efficiency Deficit (SED), representing the disparity between payoffs at the Nash Equilibrium (NE) and the Social Optimum (SO). This analysis sheds light on the societal consequences of individual vaccination decisions, offering a nuanced understanding of the interplay between individual choices and collective outcomes [3,7,8,9,12,17,22,27,31,32,43–45].

5.2 Model Depiction

5.2.1 Epidemic Model

We considered an epidemiological model that consists of two vaccination compartments and n infected compartments with the presence of n strain. All the people are considered Susceptible and initially belong to compartment S. Vaccination compartment V_1 contains those individuals who choose vaccine 1 which has a high cost and high efficacy while V_2 contains those individuals who choose vaccine 2 which is less costly and less efficacy. All the individuals will recover from strain and move to the recovered or removed compartment R. Recovered individuals can be susceptible again with the loss of immunity. The transmission rate from the susceptible compartment is $\beta_i (\beta_i < \beta_{i+1})$, where i starts from 1 to n. We consider both vaccinations imperfect so both individuals from the compartment $V_1$and V_2 can be infected with any strain. $e_{1i}$and e_{2i} are vaccine efficacy of vaccines 1 and 2. Here, the efficacy obeys the concept of effectiveness [46]. So the discounted transmission rates from vaccine 1 and vaccine 2 compartments will be $(1 - e_{1i})\beta_i$ and $(1 - e_{2i})\beta_i$ respectively. We define the efficacy ratio $e_r = \frac{e_{1i}}{e_{2i}}$ for the two vaccines for n strains to analyze the dynamics of vaccination. The recovery rates for n strains are γ_i. In addition, we considered $\gamma_i < \gamma_{i+1}$ to keep the basic reproduction number at a fixed value which makes the model simpler. With the rate ω, individuals become susceptible again which we call the waning immunity. The schematic diagram of the proposed model is shown in Figure 1 and the set of Ordinary differential equations is as follows:

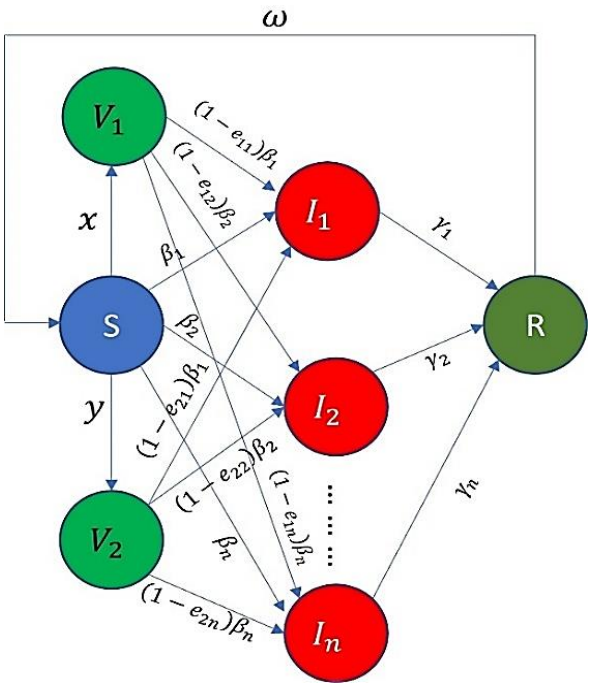

Figure 1: The compartments and their transition of the proposed model.

$$\dot{S} = -xS - yS - \sum_{i=1}^{n} \beta_i S I_i + \omega R, \tag{1}$$

$$\dot{V_1} = xS - \sum_{i=1}^{n} (1 - e_{1i}) \beta_i V_1 I_i, \tag{2}$$

$$\dot{V_2} = yS - \sum_{i=1}^{n} (1 - e_{2i}) \beta_i V_2 I_i, \tag{3}$$

$$\begin{aligned} \dot{I_1} &= (1 - e_{11}) \beta_1 V_1 I_1 + \beta_1 S I_1 + (1 - e_{21}) \beta_1 V_2 I_1 - \gamma_1 I_1, \\ \dot{I_2} &= (1 - e_{12}) \beta_2 V_1 I_2 + \beta_2 S I_2 + (1 - e_{22}) \beta_2 V_2 I_2 - \gamma_2 I_2, \end{aligned} \tag{4}$$

… … …

$$\dot{I_n} = (1 - e_{1n}) \beta_n V_1 I_n + \beta_n S I_n + (1 - e_{2n}) \beta_n V_2 I_n - \gamma_n I_n,$$

$$\dot{R} = \sum_{i=1}^{n} \gamma_i I_i - \omega R, \tag{5}$$

$$S(t) + V_1(t) + V_2(t) + \sum_{i=1}^{n} I_i(t) + R(t) = 1, \tag{6}$$

5.2.2 Behavior Model

For the vaccination flux from the susceptible to vaccination compartments, we considered the famous behavior model originated by Bauch [36]. At rates x and y susceptible individuals can choose their vaccine 1 and vaccine 2 respectively. We define the dynamical equations:

$$\dot{x} = m\,x\,(1-x)\{c\sum_{i=1}^{n} I_i - kc_{v1}\}, \quad (7)$$

$$\dot{y} = m\,y\,(1-y)\{c\sum_{i=1}^{n} I_i - kc_{v2}\}, \quad (8)$$

where m is the inertial effect constant and k is the relative sensitivity to the vaccination cost. We considered the values of m and k will be equal to keep the general tendency for two vaccinations equal. c_{v1} and c_{v2} are the vaccination cost of vaccines 1 and 2 respectively where we consider that the cost of vaccine 1 is up to 1 and always greater or equal to the cost of vaccine 2 (i.e., $0 \le c_{v1} \le 1$ and $0 \le c_{v2} \le c_{v1}$). c is the cost of disease that should be paid by every infected individual and we consider that the value of c is 1 throughout our work (i.e., $c = 1$). With the increase in the value of the summation i.e., the total number of infected individuals at any time t with all strains the above equations always increase the values of x and y i.e., the vaccination uptake while increasing the cost of the vaccinations always reduces the vaccination uptake.

Table 1: Description of the model parameters

Parameter symbol	Parameter Description
β_i	Disease Transference rate due to strain i
γ_i	The recovery rate from strain i
e_{1i}	The efficacy of the vaccine 1 to strain i
e_{2i}	The efficacy of the vaccine 2 to strain i
e_r	Efficacy ratio
m	Inertial effect on migration from S to V_1 and S to V_2
k	Sensitivity to vaccination due to cost
c	Disease cost
c_{v1}	Cost of the vaccine 1
c_{v2}	Cost of the vaccine 2
ω	Waning rate against immunity

5.2.3 Basic Reproduction Number, Vaccine Equilibrium, Fraction of vaccinated individuals, Total vaccination, Total infection, Average Social payoff (ASP), Social efficiency Deficit (SED)

In this model, we considered the standard value of the basic reproduction number, $R_0 = \frac{\beta_i}{\gamma_i} = 2.5$ [36]. However, in the latter segment of the discussion of the results, we also examined the interplay between vaccination behavior and disease dynamics across various values of the basic reproduction number.

To get the vaccine equilibrium we need to set equations (7) and (8) equal to zero. i.e.,

$$\dot{x} = m\,x\,(1-x)\{c\sum_{i=1}^{n} I_i - kc_{v1}\} = 0$$

$\dot{y} = m\, y\, (1 - y)\{c \sum_{i=1}^{n} I_i - k c_{v2}\} = 0$

Since, $m, x, c \sum_{i=1}^{n} I_i - k c_{v1}$ cannot be zero because $m = 0$ or $x = 0$ implies constant or no vaccination flow and $c \sum_{i=1}^{n} I_i$ is also nonzero, the only possibility is $(1 - x) = 0$ which implies $x = 1$.

Similarly, we can get $y = 1$.

So the equilibrium point for the vaccination is $(x, y) = (1,1)$. This is assuming I_i are nonzero, k is positive and the conditions between c_{v1} and c_{v2} $(0 \leq c_{v1} \leq 1$ and $0 \leq c_{v2} \leq c_{v1})$ are satisfied.

The fractions of vaccinated individuals for both vaccinations are defined as follows:

$$V_1R = \frac{V_1(\infty)}{V_1(\infty)+V_2(\infty)}, \tag{9}$$

$$V_2R = \frac{V_2(\infty)}{V_1(\infty)+V_2(\infty)}, \tag{10}$$

where $t = \infty$ denotes a state of equilibrium or steady state (we say it, Nash equilibrium NE).

The total number of vaccinated individuals from vaccination 1, and vaccination 2 are defined as follows:

$$V_1T = \int_0^{\infty} (xS)\, dt, \tag{11}$$

$$V_2T = \int_0^{\infty} (yS)\, dt, \tag{12}$$

$$VT = V_1T + V_2T, \tag{13}$$

The total number of infected individuals from vaccination 1, vaccination 2, and susceptible are defined as:

$$IV_1T = \int_0^{\infty} (\sum_{i=1}^{n} \beta_i (1 - e_{1i}) I_i V_1)\, dt, \tag{14}$$

$$IV_2T = \int_0^{\infty} (\sum_{i=1}^{n} \beta_i (1 - e_{2i}) I_i V_2)\, dt, \tag{15}$$

$$IST = \int_0^{\infty} (\sum_{i=1}^{n} \beta_i I_i S)\, dt, \tag{16}$$

$$IT = IV_1T + IV_2T + IST, \tag{17}$$

where $t = \infty$ denotes a state of equilibrium or steady state (we say it, Nash equilibrium NE).

The ASP at NE is defined as follows:

$$ASP_{NE} = -IT * c - V_1T * c_{v1} - V_2T * c_{v2}, \tag{18}$$

where the first term on the right-hand side indicates the total payoff due to infection and the second and third terms indicate the payoffs of the individuals who commit vaccination 1 and vaccination 2 respectively.

By referencing the original definition of the Social Efficiency Deficit (SED), we assess the disparity between the Average System Payoff (ASP) at the Nash Equilibrium (NE) and the ASP at the Social Optimum (SO), thereby discerning the potential existence of a social dilemma within the present social-dynamical system (ASP_{SO}). This analysis elucidates the means to enhance the system's ASP, transitioning from an evolutionarily stable state (NE) to a theoretically optimal societal state, maximizing the attainable ASP_{SO} when all evolutionary processes represented by variables x and y are effectively managed [44].

It is defined as follows:

$$SED = ASP_{SO} - ASP_{NE}, \tag{19}$$

The SO state is a time-constant vector $(x\ (for\ SO), y\ (for\ SO))$, with x, y ranging in [0,1]. Thus,

$$\boldsymbol{SO} = \arg\max\ [ASP(x\ (for\ SO), y\ (for\ SO))]. \tag{20}$$

When NE equals SO, SED implies zero. However, when the SED is positive but not zero, there is a social dilemma.

5.3 Results and Discussion

5.3.1 Impact of waning immunity ω on vaccination choice:

In this section, we present time series data for compartments V_1 and V_2, with a focus on analyzing the impact of waning immunity in the context of vaccination choices. The figures herein are generated using the established set of parameter values outlined in Table 2. Furthermore, Table 3 provides the initial values for each compartment and the associated flow rates. Within this framework, we examine various scenarios denoted by the parameter "n" which can take on values of 2, 3, and 4, corresponding to models featuring two, three, and four viral strains, respectively. As previously noted, these newer strains are characterized by higher transmission rates in comparison to their predecessors. In Figures 2 (a)−(c), we illustrate the vaccination compartments under the assumption of waning immunity ($\omega = 0.05$) for two, three, and four strains, respectively. The time series spans 3000 days. Across all cases in Figures 2(a)−(c), it is evident that individuals consistently favor the second vaccine option, characterized by lower cost and reduced efficacy. Figures 2(d)−(f) provide insights into the flow rates from susceptible individuals to vaccinated compartments, serving as a complementary visual representation to Figures 2(a)−(c). These figures reveal that the transition to compartment V_2 occurs more rapidly, approaching equilibrium and reaching values close to 1 before the transition to V_1. This suggests that susceptible individuals are more inclined to choose a vaccine V_2 over vaccine V_1.

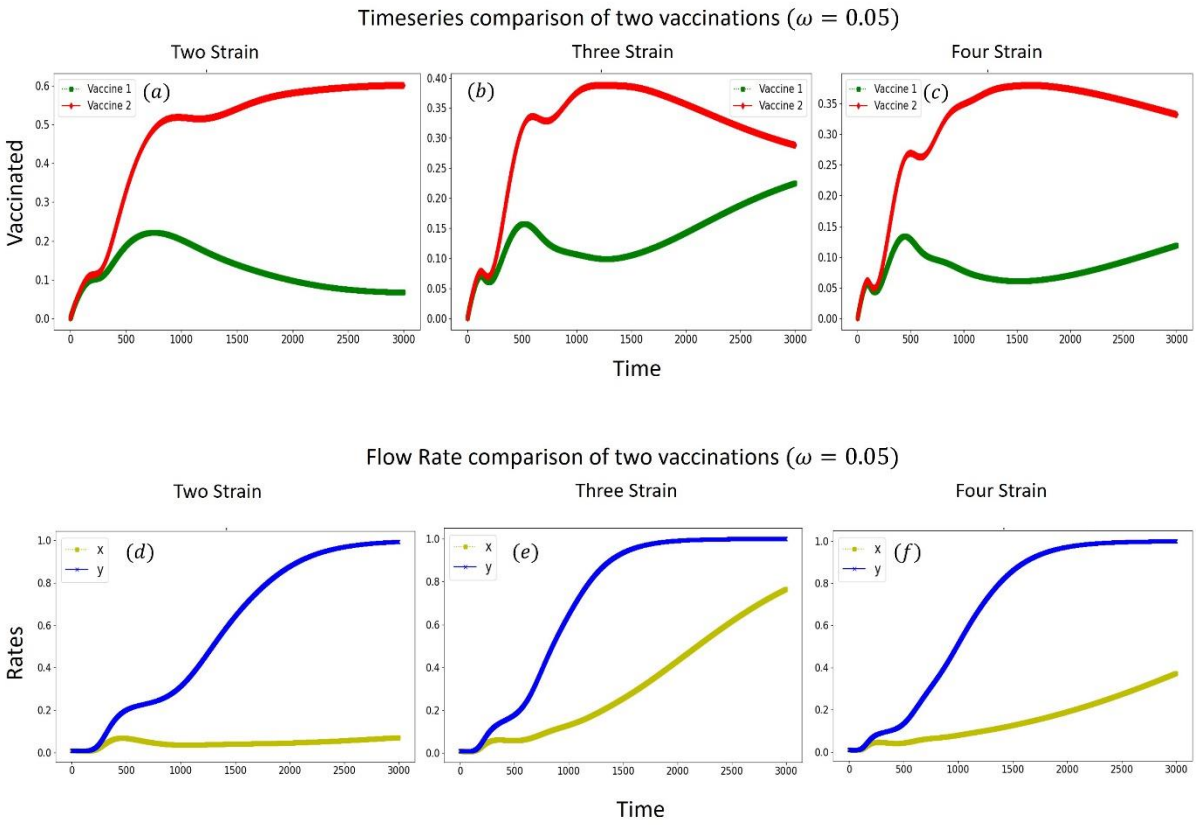

Figure 2: In the temporal evolution of the vaccination dynamics concerning two, three, and four strains with a specified value of $\omega = 0.05$, the standard parameters remain unchanged. Panels (a)−(c) illustrate timeseries data for the number of vaccinated individuals at time t, with the red curves denoting those who opted for vaccine 2 and the green curves representing individuals who selected vaccine 1. Across all scenarios, it is evident that Vaccine 2 consistently dominates throughout the entire temporal span. Moving on to panels (d)−(f), the focus shifts to the vaccination rates. Here, the observation reveals a consistent dominance of y (Vaccine 2) until the mentioned period ($T = 3000$ days). Throughout this period, y maintains superiority in the vaccination rates over other options. In summary, the visual representation of the timeseries data underscores the persistent dominance of Vaccine 2 in terms of both the number of vaccinated individuals and the vaccination rates, irrespective of the varying number of strains considered, with ω held constant at 0.05.

Figures 3(g)−(h) present time series data for compartments V_1 and V_2, considering two, three, and four strains, all under the assumption of waning immunity with a parameter value of $\omega = 0.1$. Within each panel, we observe a noteworthy phenomenon where Vaccine 1 eventually supersedes Vaccine 2 over time. Furthermore, the increasing number of strains characterized by higher transmission rates leads to an earlier preference for Vaccine 1 among individuals. Figures 3(j)−(l) display a comparative analysis of flow rates. In each case, the rates eventually converge to an equilibrium state $(x = 1, y = 1)$, with the number of strains showing a positive correlation with the speed at which equilibrium is reached.

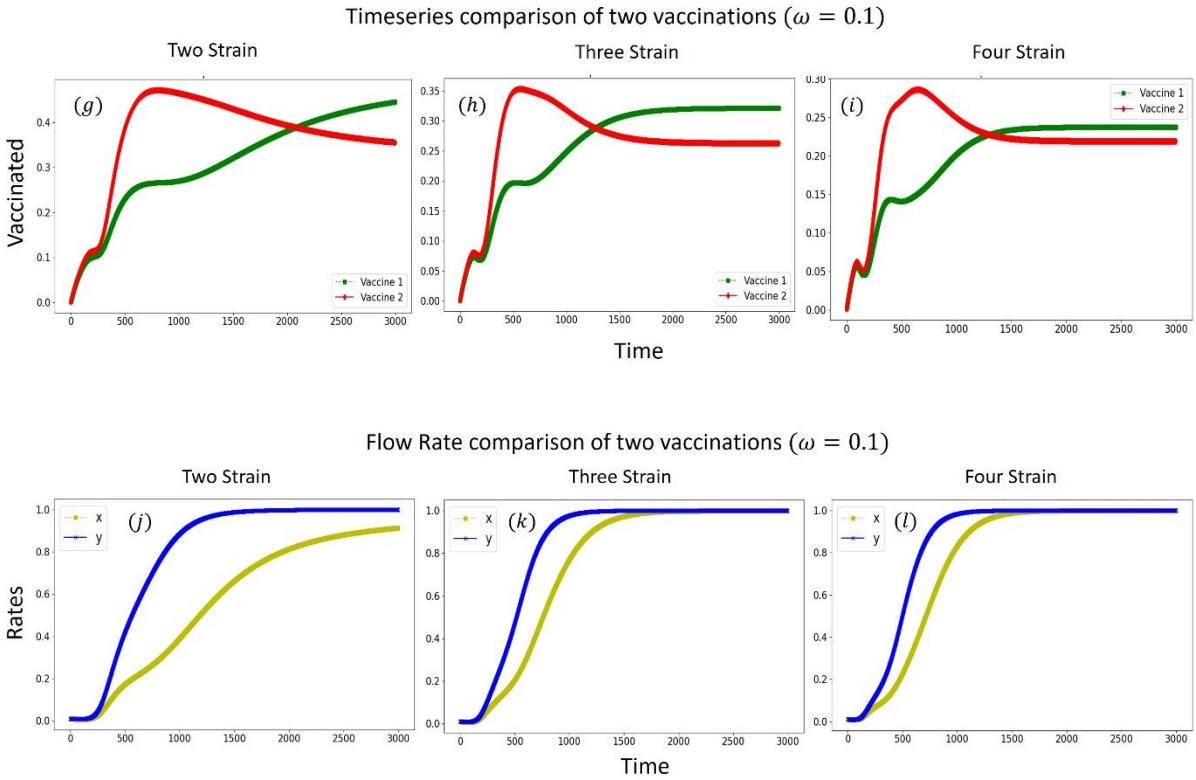

Figure 3: In the context of a specified value of $\omega = 0.1$, and with the standard parameters remaining unchanged, we examine the timeseries of vaccination compartments and rates for two, three, and four strains. Panels (g)−(i) display the number of vaccinated individuals at time t, with the red curves indicating those who opted for vaccine 2 and the green curves representing individuals who chose vaccine 1. Notably, in each scenario, a discernible shift occurs, and after a certain duration, Vaccine 1 emerges as the dominant choice. This shift in dominance is particularly pronounced in the presence of highly transmissible multiple strains, resulting in an earlier attainment of vaccine equilibrium. Turning attention to panels (j)−(l), which illustrate the vaccination rates, it is observed that both x and y reach equilibrium point 1 after a certain duration. This indicates that, despite initial variations, both vaccines eventually stabilize at the same equilibrium point over time. In summary, the timeseries analysis underscores the dynamic nature of vaccine dominance, with Vaccine 1 emerging as the dominant choice after a certain period. Additionally, the impact of highly transmissible multiple strains is evident in the accelerated arrival of the vaccine equilibrium. In terms of vaccination rates, both x and y eventually converge to equilibrium point 1, demonstrating a stabilization of the system over time.

Figures 4(m)−(n) provide a detailed analysis of time series data for compartments V_1 and V_2, taking into account two, three, and four viral strains while incorporating a waning immunity parameter of $\omega = 0.2$. In each of these panels, a consistent trend emerges where Vaccine 1 eventually surpasses Vaccine 2, underscoring the temporal dynamics. Furthermore, as the number of strains increases, each characterized by higher transmission rates, Vaccine 1 establishes its preference among individuals at an

earlier stage. Figures 4(p)−(r) present a comparative examination of flow rates. In each scenario, these rates gradually approach equilibrium ($x = 1, y = 1$), and once again, we observe that the introduction of a greater number of strains leads to an accelerated attainment of equilibrium, mirroring the pattern observed in the previous case.

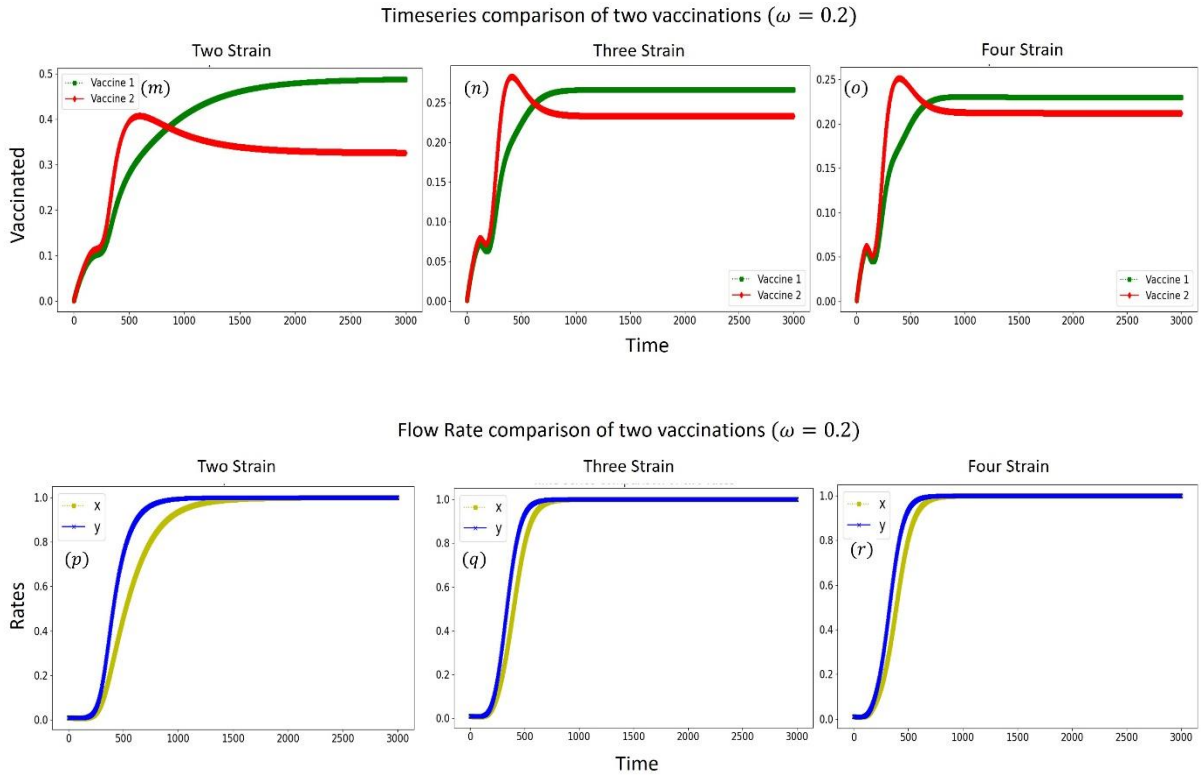

Figure 4: Temporal profiles of vaccination compartments and rates are examined for two, three, and four strains with ω held constant at 0.2, while the remaining parameters adhere to the standard configuration. In panels (m)−(o), the red curves delineate the count of individuals vaccinated at time t who selected vaccine 2, while the green curves represent those who chose vaccine 1. Notably, in each scenario, there is a discernible temporal pattern where Vaccine 1 attains dominance after a specific duration. The concurrent presence of highly transmissible multiple strains expedites the establishment of vaccine equilibrium. Turning attention to panels (p)−(r), which depict vaccination rates, it is observed that both x and y converge to equilibrium point 1 after a certain duration. In contrast to the findings in Figure 3, a notable observation is the earlier dominance of vaccine 1 in every scenario. In summary, the analysis of the timeseries data underscores the temporal dynamics of vaccine dominance and equilibrium, particularly accentuated by the presence of highly transmissible multiple strains. The acceleration of the dominance of vaccine 1 is a notable departure from the observations in Figure 3.

Table 2: Standard values of the parameters [3,4,28,47,48]

Parameter	Value	Parameter	Value	Parameter	Value	Parameter	Value
β_1	0.4	γ_1	0.16	e_{11}	0.9	e_{21}	0.6
β_2	0.6	γ_2	0.24	e_{12}	0.6	e_{22}	0.4
β_3	0.8	γ_3	0.32	e_{13}	0.3	e_{23}	0.2
β_4	1.0	γ_4	0.4	e_{14}	0.2	e_{24}	0.13
m	1.0	k	0.1	e_r	$2/3$	c	1.0
c_{v1}	0.5	c_{v2}	0.25	ω	0.1		

Table 3: Initial values for the compartments and migration rates [3,4,28,47,48]

State	At $t = 0$	State/Rate	At $t = 0$
S	0.994	R	0.00
V_1	0.001	x	0.01
V_2	0.001	y	0.01
I_i $(i = \overline{1,4})$	0.001		

5.3.2 Comparison between the fraction of vaccinated individuals at equilibrium

In the preceding section, we presented outcomes based on the consideration of 2, 3, and 4 strains. Remarkably, our findings indicated a consistent trend when utilizing more than two strains. Consequently, for the subsequent sections of the results, we exclusively employed a 4−strain configuration to conduct a comprehensive analysis of the remaining outcomes.

In this section, we delve into an examination of the equilibrium fractions of vaccinated individuals, as described by equations (9) and (10), while varying key parameters. Figure 5 visually represents the proportion of individuals at equilibrium who have chosen vaccine 1. In panels (a)−(d), we construct heatmaps by varying the values of R_0 (ranging from 0.1 to 5.1) along the y −axis and ω (ranging from 0.0 to 0.5) along the x −axis. Additionally, we introduce four distinct values of the efficacy ratio e_r (specifically, $\frac{1}{5}, \frac{1}{3}, \frac{2}{3}$, and 1) to analyze the dominance dynamics between vaccine 1 and vaccine 2. All other parameters are maintained at their standard values as outlined in Table 1.

Across every panel (a)−(d), we discern three distinct regions. The upper right region gradually transitions from red to white as e_r increases. According to the definition in EGT, these regions indicate predominance by vaccine 1, except for panel (d), where light red hues suggest that the value of V_1R is slightly more than 0.5. In panel (d), we can infer that when e_r is close to 1, both vaccines hold an equal priority (coexistence) among individuals due to their identical efficacy. In cases where R_0 and ω are

substantial, the choice of vaccination is not significantly affected, provided the efficacies of the vaccines remain equal.

Conversely, the bottom light blue regions and the dark blue regions in the middle signify predominance and dominance by vaccine 2 respectively. When R_0 falls below 1, it indicates that the disease is unlikely to spread extensively, leading individuals to opt for the more cost-effective vaccine. Efficacy holds little sway over vaccination behavior when the disease's transmission is limited. However, as R_0 surpasses 1 and ω increases, individuals tend to select the less expensive vaccine until a certain threshold is reached. Beyond this point, individuals opt for the vaccine with higher efficacy, despite the higher cost.

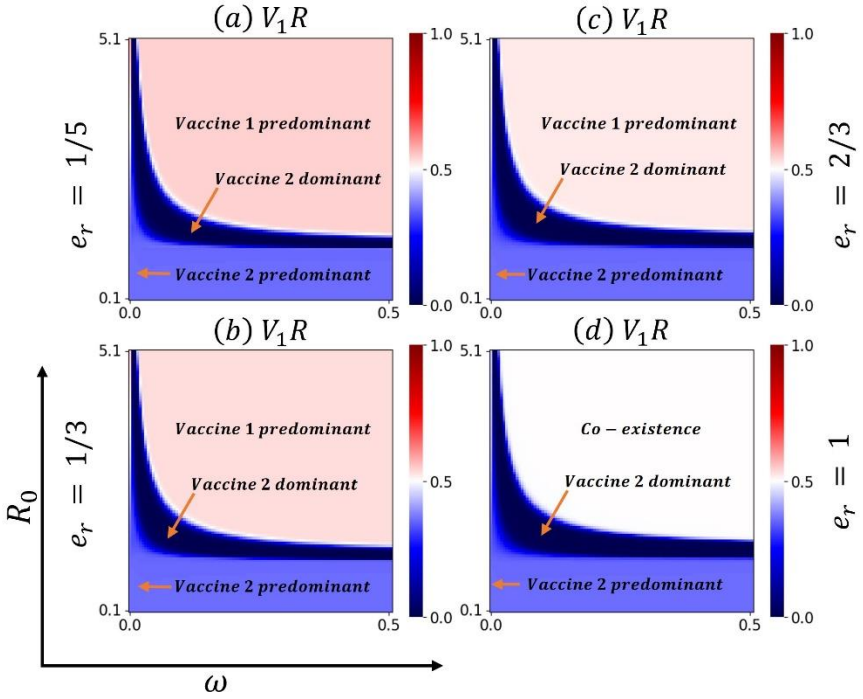

Figure 5: Heatmaps are employed as a visual tool to illustrate the proportion of individuals who have selected vaccine 1 at equilibrium. Panels (a)−(d) showcase four distinct heatmaps, each corresponding to different efficacy ratio values (e_r) of $\frac{1}{5}, \frac{1}{3}, \frac{2}{3}$, and 1. The spatial orientation is delineated by the waning immunity rate (ω) along the x-axis, ranging from 0 to 0.5, and the basic reproduction number (R_0) along the y-axis, ranging from 0.1 to 5.1. The color gradient on the heatmap scale varies from 0 to 1, with blue denoting the prevalence of vaccine 2, red indicating the dominance of vaccine 1, and white representing the co-existence of both vaccines.

Figure 6 presents a depiction of the equilibrium fractions of individuals who have opted for vaccine 1. In panels (a)−(d), we construct heatmaps by varying the cost of vaccine 1 (c_{v1}) within the range of 0.0 to 1.0 along the y −axis and the cost of vaccine 2 (c_{v2}) within the range of 0.0 to c_{v1} along the x −axis. Moreover, we consider four distinct values of the efficacy ratio (e_r) - specifically, $\frac{1}{5}, \frac{1}{3}, \frac{2}{3}$, and 1 to

analyze the dominance dynamics between vaccine 1 and vaccine 2. All other parameters are maintained at their standard values as specified in Table 1.

Across each panel (a)−(d), we observe two primary regions. The upper region gradually transitions from light to dark blue as e_r increases, predominance of vaccine 2 becomes dominant. When e_r is close to 1, individuals tend to opt for vaccine 2, which is the more cost-effective choice.

Conversely, the lower light red regions in every panel, except for panel (d), indicate the predominance of vaccine 1. In panel (d), these regions become white, signifying a coexistence of the two vaccines. Hence, when the cost of vaccine 1 becomes significantly higher, approaching the cost of managing the disease (c), individuals tend to prefer vaccine 2, regardless of whether the efficacies of the vaccines are equal or unequal.

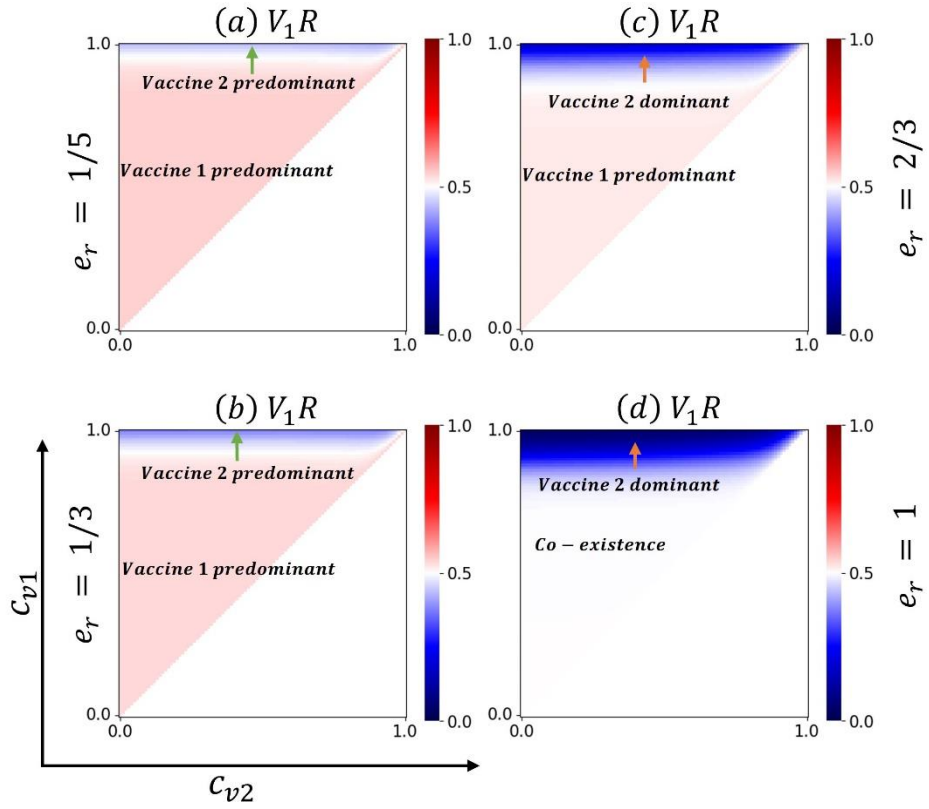

Figure 6: Heatmaps are utilized to visualize the proportion of individuals who have opted for vaccine 1 at equilibrium. Panels (a)−(d) present four distinct heatmaps corresponding to efficacy ratio values (e_r) of $\frac{1}{5}, \frac{1}{3}, \frac{2}{3}$, and 1. All the panels are drawn in terms of the cost of vaccine 1 (c_{v1}) along the y-axis ranging from 0 to 1 and the cost of vaccine 2 (c_{v2}) along the x- axis both ranging from 0 to c_{v1}. The color gradient on the heatmap scale ranges from 0 to 1, where blue indicates the dominance of vaccine 2, red signifies the dominance of vaccine 1, and white denotes the co-existence of both vaccines. Note

that there is almost no sensitivity from c_{v2}. It is conceivable just because vaccines 1 or 2 give predominant results from the ratio of those two vaccine costs, not absolute values.

Figure 7 presents an analysis of the equilibrium fractions of individuals who have chosen vaccine 1. In panels (a)−(d), we construct heatmaps by varying the parameter m within the range of 0.0 to 1.0 along the y −axis and the parameter k within the range of 0.0 to 1.0 along the x −axis. Additionally, we consider four distinct values of the efficacy ratio (e_r), specifically, $\frac{1}{5}, \frac{1}{3}, \frac{2}{3}$, and 1 to examine the dynamics of dominance between vaccine 1 and vaccine 2. All other parameters remain set at their standard values as specified in Table 1.

Across every panel (a)−(d), we observe three distinct regions. In panels (a)−(c), the left region is predominated by vaccine 1, while in panel (d), the left region becomes coexistent. As the efficacy ratio increases, there is a transition from vaccine 1 dominance to coexistence. This shift occurs because, in scenarios characterized by low sensitivity and a high level of inertial effect, individuals tend to prefer the vaccine with a higher cost. Conversely, higher relative sensitivity leads to the emergence of dark blue regions in every panel, where vaccine 2 becomes the dominant choice. In essence, high sensitivity implies a preference for the less expensive vaccination option.

Of particular interest are the regions in panels (a)−(c) and the third region, which disappears in panel (d), located in the upper right corner with dark red hues. In this region, vaccine 1 dominates, primarily due to the substantial increase in the inertial effect, leading to a heightened flow of vaccination, particularly with a high cost. However, this region diminishes as the efficacy ratio increases. In other words, when efficacy becomes equal, cost takes precedence in the choice of vaccination, favoring vaccine 2.

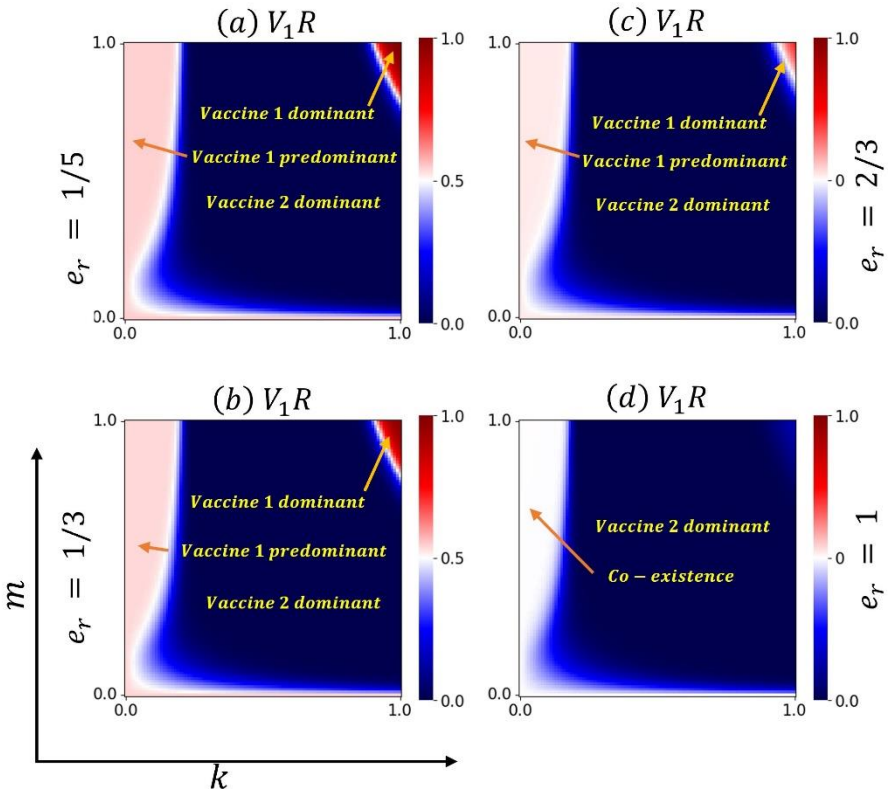

Figure 7: Heatmaps serve as a visual aid to depict the proportion of individuals choosing vaccine 1 at equilibrium. Panels (a)−(d) present four distinct heatmaps, each corresponding to various efficacy ratio values (e_r) of $\frac{1}{5}, \frac{1}{3}, \frac{2}{3}$, and 1. The spatial arrangement is determined by the impact of sensitivity to vaccination cost (k) along the x-axis, ranging from 0 to 1.0, and the influence of the inertial effect of vaccination rate (m) along the y-axis, ranging from 0.0 to 1.0. The color spectrum on the heatmap scale ranges from 0 to 1, where blue indicates the predominance of vaccine 2, red signals the dominance of vaccine 1, and white signifies the co-existence of both vaccines.

5.3.3 Analysis of Average Social Payoff (ASP) and Social Efficiency Deficit (SED)

The top row of Figure 8 provides an overview of key metrics for the NE state, including the total number of vaccinated individuals, the total number of infected individuals, and the Average Social Payoff (ASP). The second row focuses on the SO state, featuring the total number of vaccinated individuals, the total number of infected individuals, the ASP, and the Social Efficiency Deficit (SED). All panels are presented in terms of the waning immunity rate (ω) along the x −axis (ranging from 0.0 to 0.5) and the Basic Reproduction Number (R_0) along the y −axis (ranging from 0.1 to 5.1).

In panel (a), when R_0 is less than 1, the number of vaccinated individuals remains very low. Similarly, in panel (b), if R_0 is less than 1, the number of infected individuals is minimal. Combining these factors and considering their associated costs in panel (c), the ASP is also low when R_0 is less than 1. This aligns with the understanding that an R_0 less than 1 implies limited disease spread, resulting in low vaccination and infection rates, consequently yielding a low ASP.

As R_0 surpasses 1, all panels (a)−(c) demonstrate a monotonic increase in the number of vaccinated and infected individuals as both R_0 and ω increase. Consequently, the ASP exhibits a corresponding monotonic increase.

Panels (d)−(f) illustrate the social optimum cases, showcasing a similar trend to panels (a)−(c) but with relatively lower values. Panel (g), depicting the Social Efficiency Deficit (SED), highlights distinctive regions. When the basic reproduction number (R_0) is below 1 (indicated by the dark purple region), and the disease does not propagate significantly, resulting in an absence of an actual social dilemma regarding vaccination. Subsequently, a yellow region emerges with an elevation in R_0, signifying the onset of disease spread. This phase represents a transient state from a disease-free condition to a diseased state. In the presence of multiple vaccines, individuals face heightened uncertainty regarding the decision to undergo vaccination and the selection of the most beneficial vaccine. Following this transitional phase, a conventional scenario unfolds when R_0 surpasses 1. In this case, the disease becomes established, prompting individuals to opt for vaccination and reducing the social dilemma, as indicated by the purple region. Moreover, as both R_0 and the waning immunity rate (ω) increases, the social dilemma exhibits a monotonic escalation, transitioning from purple to yellow regions. The social dilemma attains its maximum magnitude when both R_0 and ω reach their peak values.

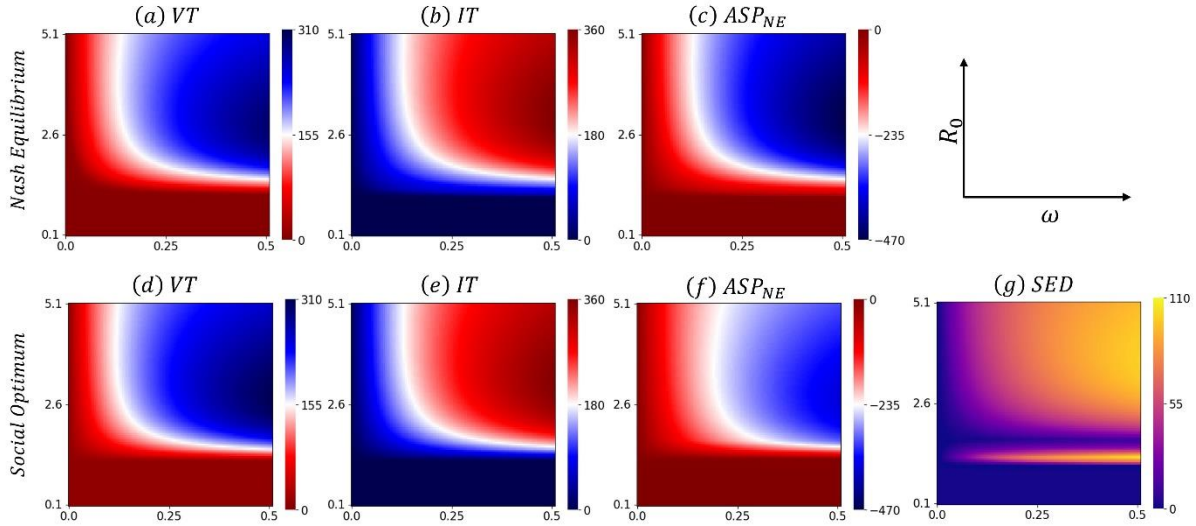

Figure 8: The total number of vaccinated people, the total number of infected people, ASP, and SED. Panels (a) − (c) are for the NE case and panels (d) − (f) are for the SO case. Panel (g) represents the SED, which is the difference between panels (f) and (c). All the panels are drawn in terms of the waning immunity rate (ω) along the x −axis ranging from 0 to 0.5 and the basic reproduction number (R_0) along the $y-$ axis both ranging from 0.1 to 5.1 The total number of vaccinated people is depicted with a range from 0 to 310, the total number of infected people is depicted with a range from 0 to 360, the ASPs are depicted with a range from −470 to 0 and the SED is depicted with a range from 0 to 110. The other parameters are the same as in the basic case. From the figures, we see that the social dilemma

appears just after R_0 crosses 1 and decreases for a while and then again monotonically increasing with the increase in both waning immunity rate and basic reproduction number. The dilemma will be maximum if both R_0 and ω is maximum.

The top row of Figure 9 provides a comprehensive overview of crucial metrics for the NE state, including the total number of vaccinated individuals, the total number of infected individuals, and the Average Social Payoff (ASP). The second row focuses on the SO state, featuring the total number of vaccinated individuals, the total number of infected individuals, the ASP, and the SED. Each panel is delineated by the cost of vaccine 1 (c_{v1}) along the $y-$axis (ranging from 0 to 1) and the cost of vaccine 2 (c_{v2}) along the $x-$axis (ranging from 0 to c_{v1}).

In panel (a), the total number of vaccinated individuals reaches a minimum when both vaccine costs are maximized, a scenario that aligns with expectations. As the cost of vaccine 1 increases significantly, panel (b) illustrates a corresponding increase in the total number of infected individuals.

Panel (c) depicts the ASP, considering the total number of infected and vaccinated individuals multiplied by their associated costs. Notably, an increase in vaccination costs leads to a rise in the total average social payoff.

In the social optimum (SO) panels (d)−(f), the suggested strategy is to maximize the number of vaccinated individuals, minimize the number of infected individuals, and consequently, minimize the ASP respectively. The difference between panel (f) and panel (c) is represented in panel (g), illustrating the SED. In the SED panel, it is evident that an increase in both vaccine costs exacerbates the social dilemma, reaching its maximum when both costs are at their highest levels.

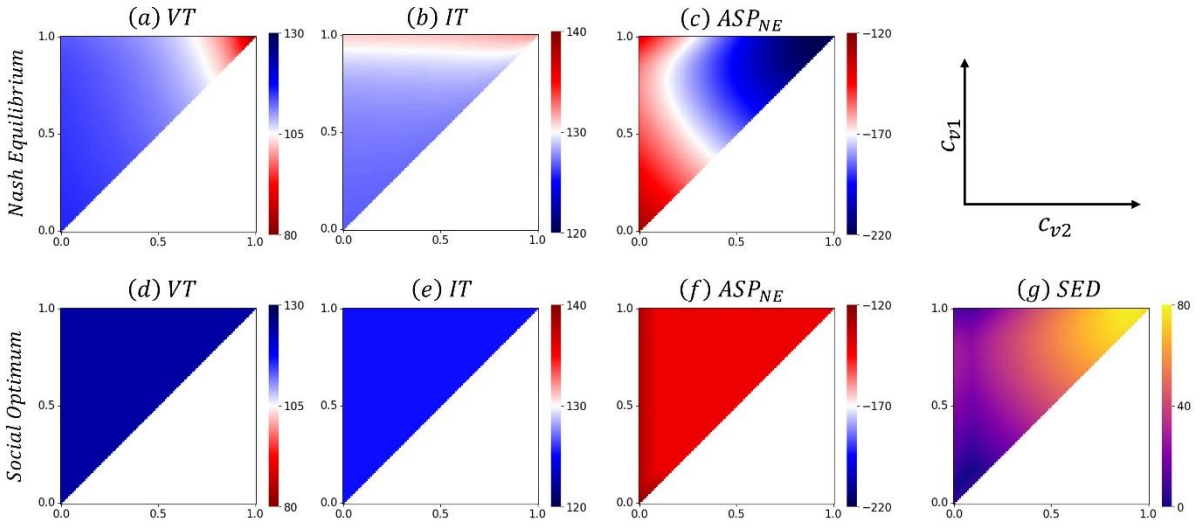

Figure 9: The total number of vaccinated people, the total number of infected people, ASP, and SED. Panels (a) − (c) are for the NE case and panels (d) − (f) are for the SO case. Panel (g) represents the SED, which is the difference between panels (f) and (c). All the panels are drawn in terms of the cost

of vaccine 1 (c_{v1}) along the $y-$axis ranging from 0 to 1 and the cost of vaccine 2 (c_{v2}) along the $x-$axis both ranging from 0 to c_{v1}. The total number of vaccinated people is depicted with a range from 0 to 130, the total number of infected people is depicted with a range from 0 to 140, the ASPs are depicted with a range from -220 to -120 and the SED is depicted with a range from 0 to 80. The other parameters are the same as in the basic case. From the figures, we see that the social dilemma is maximum when both the cost is maximum.

A detailed analysis of the most important metrics for the NE state is shown in the upper row of Figure 10. These metrics include the total number of vaccinated persons, the total number of infected individuals, and the Average Social Payoff (ASP). The second row focuses on the SO state, featuring the total number of vaccinated individuals, the total number of infected individuals, the ASP, and the SED. Each panel is delineated by the inertial effect of vaccination (m) along the $y-$axis (ranging from 0 to 1) and the sensitivity parameter (k) along the $x-$axis (ranging from 0 to 1).

In panels (a)$-$(b), an observable trend emerges, indicating that an increase in the inertial effect (m) and a decrease in the sensitivity parameter (k) correspond to an increase in vaccination uptake and a decrease in the number of infected individuals. This alignment is plausible, as a higher inertial effect tends to boost vaccination uptake, while lower sensitivity to cost reduces vaccination uptake. The impact on infected individuals follows a similar pattern.

Panel (c) presents the Average Social Payoff (ASP), combining the outcomes from panels (a) and (b) with their associated costs. The ASP is depicted as not being particularly sensitive to the parameters m and k.

In the social optimum panels (d)$-$(e), vaccination remains at a maximum level, and infection remains at a minimum level. Given that the parameters m and k are not present in the equations for vaccination flow, the social optimum suggests that both vaccination and infection should incur minimum costs. Panel (f), representing the average social payoff, also exhibits low sensitivity to the parameters m and k.

The difference between panel (f) and panel (c) is represented in panel (g), depicting the Social SED. In the SED panel, a monotonic increase in the dilemma is observed with an increase in the inertial effect (m) and a decrease in the sensitivity parameter (k). This illustrates that a higher inertial effect and lower sensitivity lead to an escalation of the social dilemma.

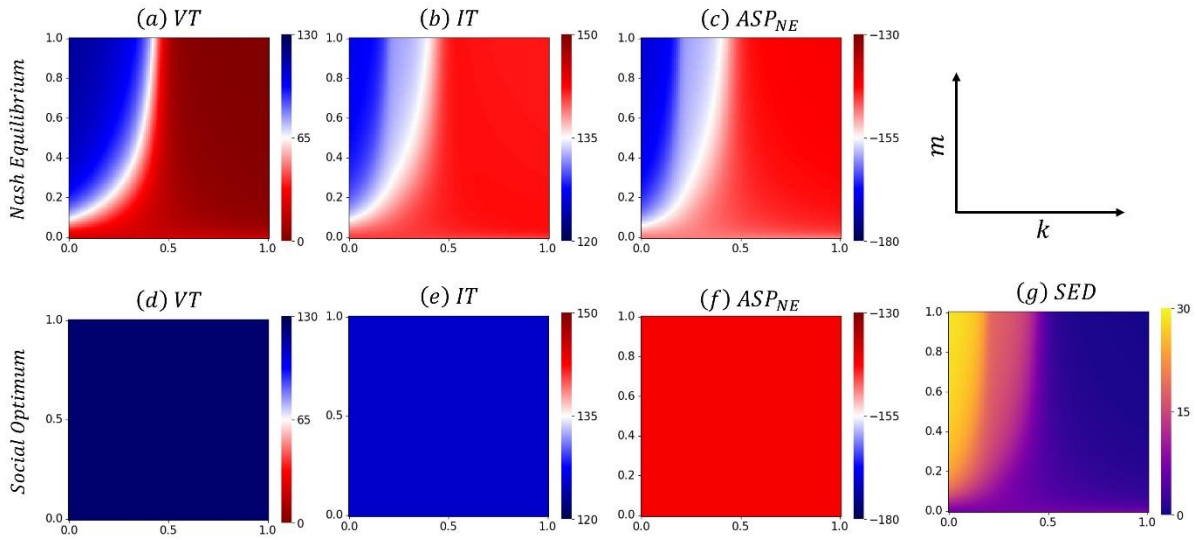

Figure 10: The total number of vaccinated people, the total number of infected people, ASP, and SED. Panels (a) − (c) are for the NE case and panels (d) − (f) are for the SO case. Panel (g) represents the SED, which is the difference between panels (f) and (c). All the panels are drawn in terms of the relative sensitivity due to vaccination cost (k) along the $x-$axis ranging from 0 to 1 and the inertial effect of vaccination rate (m) along the $y-$ axis both ranging from 0 to 1. The total number of vaccinated people is depicted with a range from 0 to 130, the total number of infected people is depicted with a range from 0 to 150, the ASPs are depicted with a range from -180 to -130 and the SED is depicted with a range from 0 to 30. The other parameters are the same as in the basic case. From the figures, we see that the social dilemma is monotonically increasing with the increase of m and decrease of k.

5.4 Conclusion

The dynamics of infectious diseases and the vaccination process are invariably shaped by individual behaviors. In the context of multistrain infectious diseases such as seasonal influenza and COVID-19, the decision-making process is predominantly contingent upon factors such as the cost and efficacy of available vaccinations. Furthermore, the rate of waning immunity constitutes a crucial determinant in the selection of vaccinations.

In the context of epidemic models, each individual is initially regarded as susceptible and possesses the freedom to opt for any available vaccination. The initial selection is contingent upon factors such as the overall count of infected individuals, as well as the cost and efficacy of the vaccinations. Typically, individuals tend to opt for vaccinations with lower costs. Given the inherent imperfections in vaccinations, individuals experience a gradual decline in immunity over time. Consequently, the phenomenon of waning immunity also exerts a notable influence on the selection of vaccinations, particularly in consideration of their long-term efficacy.

Some previous studies also studied these kinds of models. Epidemic models with multiple vaccination options considering cost and efficacy were mentioned in [5]. The vaccination behavior of humans and the waning immunity effect in epidemic models were also analyzed in [1–4,12,16,49]. Some analytic and numerical simulations concerning the multistrain epidemic model were presented in [3–5]. Human behavior towards vaccination involving cost and efficacy was studied in [3,5,6,8]. However, no other studies were conducted concerning a multi-strain epidemic model considering two vaccination options in the presence of waning immunity and the cost-effectiveness of vaccinations.

In our current study, we employed behavior equations to scrutinize vaccination choices, considering the presence of multistrain dynamics. Through numerical simulations, we observed an initial preference among individuals for vaccines with lower costs and reduced efficacy. However, as the waning rate increased, there was a shift towards favoring vaccines with higher costs and efficacy. Notably, the presence of multistrain dynamics led to an earlier attainment of vaccine equilibrium.

Our subsequent investigation focused on vaccine dominance, revealing scenarios where both vaccines could dominate within specific parameter ranges. Additionally, we identified instances of co-existence, where both vaccines were chosen equally. The analysis of equilibrium highlighted that increasing the efficacy ratio between two vaccines diminished certain dominance patterns.

Furthermore, our examination delved into the social dilemma inherent in the model. We computed average social payoffs at equilibrium, encompassing costs associated with infection and vaccination. A comparison was made with socially optimum average social payoffs, determined by considering a time-constant vaccination rate for both vaccines. Discrepancies between these two payoffs elucidated the social efficiency deficit, explaining the social dilemma inherent in the model. Our findings indicated that escalating waning immunity rates and transmission rates heightened the social dilemma. Regarding vaccination costs, the dilemma reached its maximum when both vaccination costs were at their peak. Moreover, the social dilemma was exacerbated when the sensitivity constant related to vaccination cost was minimized, and the inertial effect of vaccination rate was maximized.

Our exploration of vaccination behavior, vaccine dominance, and the social dilemma was conducted using a simple ordinary differential equation model (mean-field approximation). The inclusion of a social context in our data lends credibility to our results. In future investigations, we plan to employ a multiagent simulation approach to further analyze and validate these findings.

References

[1] B. Buonomo, Effects of information-dependent vaccination behavior on coronavirus outbreak : insights from a SIRI model, Ric. Di Mat. 69 (2020) 483–499. https://doi.org/10.1007/s11587-020-00506-8.

[2] C. Zuo, F. Zhu, Y. Ling, Analyzing COVID-19 Vaccination Behavior Using an SEIRM/V

Epidemic Model With Awareness Decay, Front. Public Heal. 10 (2022) 1–12. https://doi.org/10.3389/fpubh.2022.817749.

[3] M.M.-U.-R. Khan, M.R. Arefin, J. Tanimoto, Time delay of the appearance of a new strain can affect vaccination behavior and disease dynamics: An evolutionary explanation, Infect. Dis. Model. 8 (2023) 656–671. https://doi.org/https://doi.org/10.1016/j.idm.2023.06.001.

[4] M.M.U.R. Khan, M.R. Arefin, J. Tanimoto, Investigating vaccination behavior and disease dynamics of a time-delayed two-strain epidemic model: An evolutionary approach, Int. Exch. Innov. Conf. Eng. Sci. (2022) 147–154. https://doi.org/10.5109/5909084.

[5] M. Rajib Arefin, T. Masaki, K.M. Ariful Kabir, J. Tanimoto, Interplay between cost and effectiveness in influenza vaccine uptake: A vaccination game approach, Proc. R. Soc. A Math. Phys. Eng. Sci. 475 (2019). https://doi.org/10.1098/rspa.2019.0608.

[6] K.M.A. Kabir, J. Tanimoto, Cost-efficiency analysis of voluntary vaccination against n -serovar diseases using antibody-dependent enhancement : A game approach, J. Theor. Biol. 503 (2020) 110379. https://doi.org/10.1016/j.jtbi.2020.110379.

[7] K.M.A. Kabir, T. Risa, J. Tanimoto, Prosocial behavior of wearing a mask during an epidemic: an evolutionary explanation, Sci. Rep. 11 (2021) 1–14. https://doi.org/10.1038/s41598-021-92094-2.

[8] K.M. Ariful Kabir, M. Jusup, J. Tanimoto, Behavioral incentives in a vaccination-dilemma setting with optional treatment, Phys. Rev. E. 100 (2019) 1–13. https://doi.org/10.1103/PhysRevE.100.062402.

[9] R. Tori, J. Tanimoto, A study on prosocial behavior of wearing a mask and self-quarantining to prevent the spread of diseases underpinned by evolutionary game theory, Chaos, Solitons and Fractals. 158 (2022) 112030. https://doi.org/10.1016/j.chaos.2022.112030.

[10] E.P. Fenichela, C. Castillo-Chavezb, M.G. Ceddiac, G. Chowellb, P.A. Gonzalez Parrae, G.J. Hickling, G. Holloway, R. Horan, B. Morin, C. Perrings, M. Springborn, L. Velazquez, C. Villalobos, Adaptive human behavior in epidemiological models, Proc. Natl. Acad. Sci. U. S. A. 108 (2011) 6306–6311. https://doi.org/10.1073/pnas.1011250108.

[11] A.C.S. Chun-Miin Chen, Simulating influenza epidemics with waning vaccine immunity, Medicine (Baltimore). (2021). https://doi.org/http://dx.doi.org/10.1097/MD.0000000000027169.

[12] K.M.A. Kabir, How evolutionary game could solve the human vaccine dilemma, Chaos, Solitons and Fractals. 152 (2021) 111459. https://doi.org/10.1016/j.chaos.2021.111459.

[13] G. Webb, A COVID-19 epidemic model predicting the effectiveness of vaccination in the US, Infect. Dis. Rep. 13 (2021) 654–667. https://doi.org/10.3390/IDR13030062.

[14] R. Markovič, M. Šterk, M. Marhl, M. Perc, M. Gosak, Socio-demographic and health factors drive the epidemic progression and should guide vaccination strategies for best COVID-19 containment, Results Phys. 26 (2021). https://doi.org/10.1016/j.rinp.2021.104433.

[15] S. Nana-kyere, F.A. Boateng, P. Jonathan, A. Donkor, G.K. Hoggar, B.D. Titus, D. Kwarteng, I.K. Adu, Global Analysis and Optimal Control Model of COVID-19, Comput. Math. Methods Med. 2022 (2022). https://doi.org/https://doi.org/10.1155/2022/9491847.

[16] C. Zuo, F. Zhu, Z. Meng, Y. Ling, Y. Zheng, X. Zhao, Analyzing the COVID-19 vaccination behavior based on epidemic model with awareness-information, Infect. Genet. Evol. 98 (2022) 105218. https://doi.org/10.1016/j.meegid.2022.105218.

[17] Z. Wu, Social distancing is a social dilemma game played by every individual against his/her population, PLoS One. 16 (2021) 1–26. https://doi.org/10.1371/journal.pone.0255543.

[18] W.O. Kermack, A.G. McKendrick, A contribution to the mathematical theory of epidemics, Proc. R. Soc. A Math. Phys. Eng. Sci. 115 (1927) 700–721. https://doi.org/10.1098/rspa.1927.0118.

[19] M. Turkyilmazoglu, A restricted epidemic SIR model with elementary solutions, Phys. A Stat. Mech. Its Appl. 600 (2022) 127570. https://doi.org/10.1016/j.physa.2022.127570.

[20] F. Wang, M. Liu, L. Zhang, B. Xie, Bifurcation analysis and optimal control of a network- based SIR model with the impact of medical resources, Nonlinear Anal. Model. Control. 28 (2023) 209–227. https://doi.org/https://doi.org/10.15388/namc.2023.28.30770.

[21] M. Turkyilmazoglu, Explicit formulae for the peak time of an epidemic from the SIR model, Phys. D Nonlinear Phenom. 422 (2021) 132902. https://doi.org/10.1016/j.physd.2021.132902.

[22] M. Cabrera, F. Córdova-Lepe, J.P. Gutiérrez-Jara, K. Vogt-Geisse, An SIR-type epidemiological model that integrates social distancing as a dynamic law based on point prevalence and socio-behavioral factors, Sci. Rep. 11 (2021) 1–16. https://doi.org/10.1038/s41598-021-89492-x.

[23] S.L. Khalaf, H.S. Flayyih, Analysis , predicting , and controlling the COVID-19 pandemic in Iraq through SIR model, Results Control Optim. 10 (2023) 100214. https://doi.org/10.1016/j.rico.2023.100214.

[24] K.M.A. Kabir, K. Kuga, J. Tanimoto, Analysis of SIR epidemic model with information spreading of awareness, Chaos, Solitons and Fractals. 119 (2019) 118–125. https://doi.org/10.1016/j.chaos.2018.12.017.

[25] M. Kumar, S. Abbas, Age-Structured SIR Model for the Spread of Infectious Diseases Through Indirect Contacts, Mediterr. J. Math. 19 (2022) 1–18. https://doi.org/10.1007/s00009-021-01925-z.

[26] S. Dong, L. Xu, Z.L. Ding, X. Bo, Application of a time-delay SIR model with vaccination in COVID-19 prediction and its optimal control strategy, Nonlinear Dyn. 111 (2023) 10677–10692. https://doi.org/10.1007/s11071-023-08308-x.

[27] M. Turkyilmazoglu, An extended epidemic model with vaccination: Weak-immune SIRVI, Phys. A Stat. Mech. Its Appl. 598 (2022) 127429. https://doi.org/10.1016/j.physa.2022.127429.

[28] S. Utsumi, M.R. Arefin, Y. Tatsukawa, J. Tanimoto, How and to what extent does the anti-social behavior of violating self-quarantine measures increase the spread of disease?, Chaos, Solitons and Fractals. 159 (2022). https://doi.org/10.1016/j.chaos.2022.112178.

[29] R.C. Tyson, S.D. Hamilton, A.S. Lo, B.O. Baumgaertner, S.M. Krone, The Timing and Nature of Behavioural Responses Affect the Course of an Epidemic, Bull. Math. Biol. 82 (2020) 1–28. https://doi.org/10.1007/s11538-019-00684-z.

[30] K.M.A. Kabir, K. Kuga, J. Tanimoto, Effect of information spreading to suppress the disease contagion on the epidemic vaccination game, Chaos, Solitons and Fractals. 119 (2019) 180–187. https://doi.org/10.1016/j.chaos.2018.12.023.

[31] K.A. Kabir, K. Kuga, J. Tanimoto, The impact of information spreading on epidemic vaccination game dynamics in a heterogeneous complex network- A theoretical approach, Chaos, Solitons and Fractals. 132 (2020) 109548. https://doi.org/10.1016/j.chaos.2019.109548.

[32] M.M.-U.-R. Khan, J. Tanimoto, Investigating the social dilemma of an epidemic model with provaccination and antivaccination groups : An evolutionary approach, Alexandria Eng. J. 75 (2023) 341–349. https://doi.org/10.1016/j.aej.2023.05.091.

[33] M.M.-U.-R. Khan, M.R. Arefin, J. Tanimoto, Investigating the trade-off between self-quarantine and forced quarantine provisions to control an epidemic: An evolutionary approach, Appl. Math. Comput. 432 (2022) 127365. https://doi.org/https://doi.org/10.1016/j.amc.2022.127365.

[34] J. Tanimoto, Sociophysics approach to epidemics, Springer (Tokyo), 2021.

[35] J. Tanimoto, Fundamentals of evolutionary game theory and its applications, Springer (Tokyo), 2015.

[36] C.T. Bauch, Imitation dynamics predict vaccinating behaviour, Proc. R. Soc. B Biol. Sci. 272 (2005) 1669–1675. https://doi.org/10.1098/rspb.2005.3153.

[37] I. Nishimura, R. Arefin, Y. Tatsukawa, S. Utsumi, Social dilemma analysis on vaccination game

accounting for the effect of immunity waning, Chaos, Solitons and Fractals. 171 (2023) 113426. https://doi.org/10.1016/j.chaos.2023.113426.

[38] K.M.A. Kabir, M.A. Ovi, S. Murtyas, A. Hagishima, J. Tanimoto, Acceptance and Willingness-to-Pay of Vaccine for COVID-19 in Asian Countries: A Hypothetical Assessment Survey, Evergreen. 10 (2023) 617–625. https://doi.org/10.5109/6792807.

[39] M. Van Boven, H.E. De Melker, J.F.P. Schellekens, M. Kretzschmar, Waning immunity and sub-clinical infection in an epidemic model: Implications for pertussis in The Netherlands, Math. Biosci. 164 (2000) 161–182. https://doi.org/10.1016/S0025-5564(00)00009-2.

[40] C. Fahdilla, A.R. Putri, H. Haripamyu, Bifurcation analysis of epidemic model waning immunity, J. Phys. Conf. Ser. 1940 (2021) 012014. https://doi.org/10.1088/1742-6596/1940/1/012014.

[41] D. Hamami, R. Cameron, K.G. Pollock, C. Shankland, Waning immunity is associated with periodic large outbreaks of mumps: A mathematical modeling study of scottish data, Front. Physiol. 8 (2017) 1–11. https://doi.org/10.3389/fphys.2017.00233.

[42] Y. Nakata, R. Omori, Delay equation formulation for an epidemic model with waning immunity: An application to mycoplasma pneumoniae, IFAC-PapersOnLine. 28 (2015) 132–135. https://doi.org/10.1016/j.ifacol.2015.11.024.

[43] Y. Wei, Y. Lin, B. Wu, Vaccination dilemma on an evolving social network, J. Theor. Biol. 483 (2019). https://doi.org/10.1016/j.jtbi.2019.08.009.

[44] M.R. Arefin, K.M.A. Kabir, M. Jusup, H. Ito, J. Tanimoto, Social efficiency deficit deciphers social dilemmas, Sci. Rep. 10 (2020) 1–9. https://doi.org/10.1038/s41598-020-72971-y.

[45] K.M.A. Kabir, J. Tanimoto, Analysis of epidemic outbreaks in two-layer networks with different structures for information spreading and disease diffusion, Commun. Nonlinear Sci. Numer. Simul. 72 (2019) 565–574. https://doi.org/10.1016/j.cnsns.2019.01.020.

[46] K. Kuga, J. Tanimoto, Which is more effective for suppressing an infectious disease: imperfect vaccination or defense against contagion?, J. Stat. Mech. Theory Exp. 2018 (2018) 23407. https://doi.org/10.1088/1742-5468/aaac3c.

[47] Y. Tatsukawa, M.R. Arefin, S. Utsumi, J. Tanimoto, Investigating the efficiency of dynamic vaccination by consolidating detecting errors and vaccine efficacy, Sci. Rep. 12 (2022) 1–12. https://doi.org/10.1038/s41598-022-12039-1.

[48] Y. Tatsukawa, R. Arefin, M. Tanaka, J. Tanimoto, Free ticket , discount ticket or intermediate of the best of two worlds – Which subsidy policy is socially optimal to suppress the disease

spreading ?, J. Theor. Biol. 520 (2021) 110682. https://doi.org/10.1016/j.jtbi.2021.110682.

[49] Y. Wu, Z. Zhang, L. Song, C. Xia, Global stability analysis of two strains epidemic model with imperfect vaccination and immunity waning in a complex network, Chaos, Solitons and Fractals. 179 (2024) 114414. https://doi.org/10.1016/j.chaos.2023.114414.

Chapter 6

A New Concept of optimal control for epidemic spreading by Vaccination: Technique for Assessing social optimum employing Pontryagin's Maximum Principle

Abstract

This research introduces a new approach utilizing optimal control theory (OCT) to assess the Social Optimum (SO) of a vaccination game, navigating the intricate considerations of cost, availability, and distribution policies. By integrating an SIRS/V epidemic model with a behavior model, the study analyzes individual vaccination strategies. A unique optimal control framework, centered on vaccination costs, is proposed, diverging significantly from previous methods. Our findings confirm the effectiveness and feasibility of this approach in managing vaccination strategies. Moreover, we examine the underlying social dilemma of the vaccination game, investigating key parameters. By calculating the Nash equilibrium (NE) through the behavior model and determining the SO using our approach, we measure the Social Efficiency Deficit (SED), quantifying the overall cost gap between the NE and SO. Results indicate that an increased waning immunity rate exacerbates the social dilemma, although higher vaccination costs partially mitigate it. This research provides valuable insights into optimizing vaccination strategies amidst complex societal dynamics.

6.1 Introduction

Vaccination is key in managing infectious diseases, yet initial shortages occur in pandemics like COVID-19. The availability of vaccines becomes vital once developed. However, during COVID-19, only wealthier nations could offer widespread vaccination, leaving low-income countries grappling with distribution challenges. Cost also impacts coverage significantly; lower costs allow authorities to provide subsidies or free distribution [1–3]. High costs present obstacles in widespread vaccine distribution, impacting individuals' decisions to participate in vaccination programs, influenced by factors like infection rates, vaccine effectiveness, and cost. Meanwhile, authorities tasked with vaccine provision aim to develop cost-efficient distribution strategies [3–6].

To implement any intervention, such as vaccination, treatment, quarantine, or isolation, in an epidemic model, it is essential to examine the model from two perspectives: the situation without the intervention and the changes that occur when the intervention is introduced [7–11]. Numerous studies have been conducted during the COVID-19 pandemic, employing various interventions in epidemic models. Many of these studies utilized an epidemic model based on the Susceptible, Infected, Recovered (SIR) framework, augmented with additional compartments such as Exposed (E), Hospitalized (H), Aware

(A), Unaware (U), Treatment (T), Quarantine (Q), Protected (P), Death (D), and others [5–9,11–37]. These investigations aimed to analyze the impact of interventions on disease spread. Many studies utilized Pontryagin's Maximum Principle, an optimal control theory approach, to minimize an objective function. However, they overlooked vaccination costs, assuming the objective function only comprised infection prevalence and intervention rates squared, which doesn't reflect total social costs. To truly minimize social costs, including disease and intervention costs, a new framework must be established. This study aims to address this gap.

Furthermore, when analyzing the social dilemma within an epidemic model, it is essential to consider the costs associated with infection and vaccination [38]. Calculating the social optimum is another significant aspect of such analysis [4,38–46]. Some previous studies have employed time-constant vaccination rates to determine the social optimum, which can sometimes be impractical for authorities as it may suggest vaccinating 100% of individuals at the outset, which is nearly impossible in real-world scenarios [2–4,39,40,47–56]. Furthermore, the waning rate of immunity added more urgency to the situation. In this regard, optimal control theory provides a more suitable and mathematically acceptable approach to calculating the socially optimal vaccination level at any given time.

Our study focuses on a simplified SIRS/V epidemic model, examining how individuals respond to vaccination costs. We determine the optimal vaccination level using optimal control theory, integrating vaccination costs. Our novel objective function, aligning with Pontryagin's maximum principle, combines vaccination and infection costs. Individuals decide on vaccination based on observed infection rates and vaccination costs. Social optimum is chosen to minimize the total social cost, including infection and vaccination costs. We compare the payoff disparities between models to illustrate the Social Efficiency Deficit (SED), revealing the social dilemma within our proposed model [3,39,47,50,52].

6.2 Model Depiction

6.2.1 Epidemic model with behavior dynamics

This addresses the novelty of our concept for building the objective function for an optimal control problem; we presume a relatively simple vaccination game where a simple compartment model is coupled with a behavior model.

Our research utilized an epidemic model with four compartments based on the dynamics of SIRS/V populations. The total population is initially categorized as the susceptible group (S), consisting of individuals who are susceptible to the infection. These individuals can contract the infection disease determined by the transmission rate (β) and transition to the infected compartment (I). Subsequently, infected individuals recover from the infection at a rate of (γ) and move to the recovered compartment. To incorporate vaccination into the model, we introduced a separate compartment for vaccinated

individuals (V). This compartment represents individuals who have received the vaccine. The individuals' transition from the susceptible compartment to the vaccination compartment is denoted as $x(t)$. This rate is determined using the behavior model [57−61], which considers factors such as the number of infected individuals in different states and the cost associated with vaccination. It is worth noting that we consider vaccination to be regarded, where we represent the vaccine's efficacy as η. Therefore, individuals in the vaccination compartment can still contract the infection at a rate of $(1-\eta)\beta$. Additionally, we accounted for the waning rate of immunity, represented by ω, which captures the gradual decrease in immunity over time. The flow diagram and formulation of the proposed model are as follows:

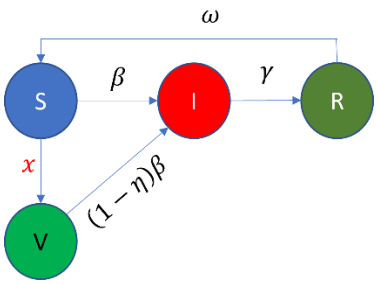

Figure 1: Model Flowchart (including behavioral dynamics). In this diagram, susceptible individuals may become infected at a transmission rate, β, transitioning from compartment S to compartment I. Infected individuals can recover at a rate of γ, moving to the recovered compartment R. Susceptible individuals can transition to the vaccinated compartment V at a rate determined by behavior dynamics, denoted by x. Vaccinated individuals can be infected with a discounted transmission rate $(1-\eta)\beta$ and move to the infected compartment. Recovered individuals may become susceptible again at a rate of waning immunity, represented by ω.

$$\dot{S} = -\beta SI - xS + \omega R, \tag{1}$$

$$\dot{V} = xS - (1-\eta)\beta VI, \tag{2}$$

$$\dot{I} = \beta SI + (1-\eta)\beta VI - \gamma I, \tag{3}$$

$$\dot{R} = \gamma I - \omega R, \tag{4}$$

$$S(t) + V(t) + I(t) + R(t) = 1, \tag{5}$$

$$\dot{x} = mx(1-x)(cI - kc_V), \tag{6}$$

where m is the inertial effect of the vaccination, c is the disease cost due to infection, c_v is the vaccination cost, and k is the relative sensitivity due to the cost of vaccination.

6.2.2 Epidemic model with optimal control

In this section, we extend the epidemic model discussed earlier by introducing a control variable (u) that represents the flux of vaccination from the susceptible compartment to the vaccination compartment. We utilize optimal control theory to find the optimal value u, specifically applying Pontryagin's maximum principle. This principle helps us determine the optimal control strategy that minimizes the objective function, considering the dynamics of the epidemic model and the constraints imposed by the system. By employing this approach, we can identify the most effective vaccination strategy to combat the spread of the disease and maximize the desired outcomes. All the model parameters and their description are shown in Table 1. The schematic diagram and formulation of the model can be summarized as follows:

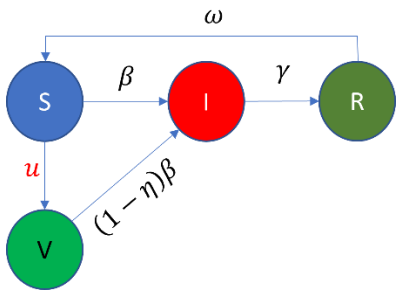

Figure 2: Model Flowchart (incorporating optimal control). This diagram illustrates the progression of individuals within the model. Susceptible individuals may contract the infection at a transmission rate, β, moving from compartment S to compartment I. Infected individuals can recover at a rate of γ, transitioning to the recovered compartment R. Susceptible individuals may opt for vaccination, transitioning to compartment V at a rate determined by optimal control, denoted by u. Vaccinated individuals may still become infected at a discounted transmission rate $(1-\eta)\beta$, moving to the infected compartment. Recovered individuals may lose immunity over time, potentially becoming susceptible again at a rate of waning immunity represented by ω.

Table 1: Description of the model parameters

Parameter symbol	Parameter Description
β	Disease Transmission rate
γ	The recovery rate
m	Effect of inertia when switching from S to V
c	Cost of infection
k	Relative sensitivity due to vaccine's cost
c_v	Cost of vaccination
ω	Waning rate against immunity

$$\dot{S} = -\beta SI - uS + \omega R, \tag{7}$$

$$\dot{V} = uS - (1-\eta)\beta VI, \tag{8}$$

$$\dot{I} = \beta SI + (1-\eta)\beta VI - \gamma I, \tag{9}$$

$$\dot{R} = \gamma I - \omega R, \tag{10}$$

$$S(t) + V(t) + I(t) + R(t) = 1, \tag{11}$$

where $u(t)$ is the vaccination control that needs to be optimized at any time t.

According to Pontryagin's maximum principle, we define the objective function for the above model as

$$J = \min \int_0^T (cI + c_v uS)^2 dt, \tag{12}$$

where c and c_v are the disease cost due to infection and the vaccination cost respectively. Note that $c \cdot I(t)$ indicates the disease cost, socially accumulated, at time t and $c_v \cdot u(t) \cdot S(t)$ means the socially accumulated vaccination cost at time t. To make sure the following mathematical process obeys Pontryagin's maximum principle heathy, we impose a square operator to this instead of the simple accumulated cost, which is quite analogous to the concept of the Least Square Method (LSM). The square ensures the convexity of the function defined in the objective function according to Pontryagin's maximum principle.

Next, we define the Hamiltonian as follows:

$$H = (cI + c_v uS)^2 + \lambda_1 \dot{S} + \lambda_2 \dot{V} + \lambda_3 \dot{I} + \lambda_4 (\gamma I - wrR), \tag{13}$$

where

$$\dot{\lambda_1} = -\frac{\partial H}{\partial S} = 2(cI + c_v uS)c_v u + \lambda_1(-\beta I - u) + \lambda_2 \beta I + \lambda_3 u, \tag{14}$$

$$\dot{\lambda_2} = -\frac{\partial H}{\partial I} = 2(cI + c_v uS)c + \lambda_2(\beta S - \gamma + (1-\eta)\beta V) + \lambda_3(1-\eta)\beta V, \tag{15}$$

$$\dot{\lambda_3} = -\frac{\partial H}{\partial V} = \lambda_2(1-\eta)\beta I - \lambda_3(-(1-\eta)\beta I), \tag{16}$$

$$\dot{\lambda_4} = -\frac{\partial H}{\partial R} = \lambda_1 \omega - \lambda_4 \omega, \tag{17}$$

$\lambda_i(T) = 0$, (Transversality condition) (18)

Thus the optimality condition is,

$$\frac{\partial H}{\partial u} = 2(cI + c_v uS)c_v u - \lambda_1 S + \lambda_3 S = 0, \text{ at } u^* \tag{19}$$

which implies, $u^* = \frac{1}{c_v S}\left(\frac{\lambda_1 - \lambda_3}{2} - cI\right)$, given that $\lambda_1 - \lambda_3 \geq 2cI$, and $c_v \neq 0$. (20)

Thus, the optimal control will be

$$u^* = \min\left\{\max\left\{0, \frac{1}{C_v S}\left(\frac{\lambda_1 - \lambda_3}{2c_v} - cI\right)\right\}, u^{max}\right\}, \quad (21)$$

u^{max} is the maximum rate of control that can be applied.

6.2.3 Primary Reproduction Number, Cumulative infection, Cumulative vaccination, Average Social payoff (ASP), Social efficiency deficit (SED)

In this study, we considered the primary reproduction number, $R_0 = \frac{\beta}{\gamma} = 2.5$ [4,47,48,58].

The cumulative number of infected individuals is:

$$IT = \int_0^\infty (\beta SI + (1-\eta)\beta VI)\, dt, \quad (22)$$

The cumulative number of vaccinated individuals is:

$$VT = \int_0^\infty xS\, dt, \ [\int_0^\infty uS\, dt \text{ for the optimal control}] \quad (23)$$

Where $t = \infty$ indicates a state of equilibrium (we say it, Nash equilibrium, NE).

The Average social payoff (ASP) at NE is described as follows.:

$$ASP_{NE} = -IT * C - VT * c_v, \quad [x \text{ is the vaccination rate}] \quad (24)$$

The first and second terms on the right show the total rewards for the infected and immunized individuals, respectively.

The ASP at Social Optimum is defined as follows:

$$ASP_{SO} = -IT * C - VT * c_v, \quad [u \text{ is the vaccination rate}] \quad (25)$$

In the model, the first expression on the right-hand side represents the sum of people's payoff who become infected. In contrast, the second term represents the total payoffs of vaccinated individuals. The SED is defined as follows:

$$SED = ASP_{SO} - ASP_{NE}. \quad (26)$$

6.3 The Findings and Discussion

6.3.1 Illustration from timeseries (with typical values):

In this section, we provide the time series data for the compartments and vaccination rates in the behavior and optimal control models using values of the common parameters. The initial values for the compartments and rates are shown in Table 3, whereas the standard parameter values are shown in Table 2. To solve equations (1)−(6) in the behavior model, we employed the explicit finite difference method

with a time step size of $dt = 0.1$. We solved equations (7)−(21) for the optimal control model using the forward-backward sweep method and fourth-order Runge-Kutta method, with a time step size of 0.1. In the behavior model, we set the initial vaccination rate to 0.1, while in the optimal control model, we assumed that a maximum control rate of vaccination, u^{max}, could be applied up to 0.1. This value is considered reasonable and feasible by any authority.

Figure 3(a) presents the compartments' time series using the behavior model's dynamics with standard parameter values. The susceptible (S), infected (I), recovered (R), and vaccinated (V) compartments are depicted over time. Similarly, in Figure 3(b), we display the corresponding vaccination rate using the same parameter settings. Moving on to Figures 3(c) and 3(d), we showcase the time series of the model compartments and the optimal control vaccine flow, respectively, using the suggested optimal control concept. The optimal control approach notably leads to a more stabilized vaccination rate than the behavior model dynamics. Even though the susceptible population continues to increase, the vaccination rate reaches a steady 400 days. Contrastingly, Figures 3(a) and 3(b) demonstrate that without the optimal control approach, the number of vaccinated and susceptible individuals gradually increases, necessitating a prolonged vaccination campaign. Furthermore, the peak of the vaccination flow approaches 12%. Therefore, based on the same parameter combination, utilizing the optimal control idea proves more advantageous to society in regulating vaccination strategies and achieving desired outcomes.

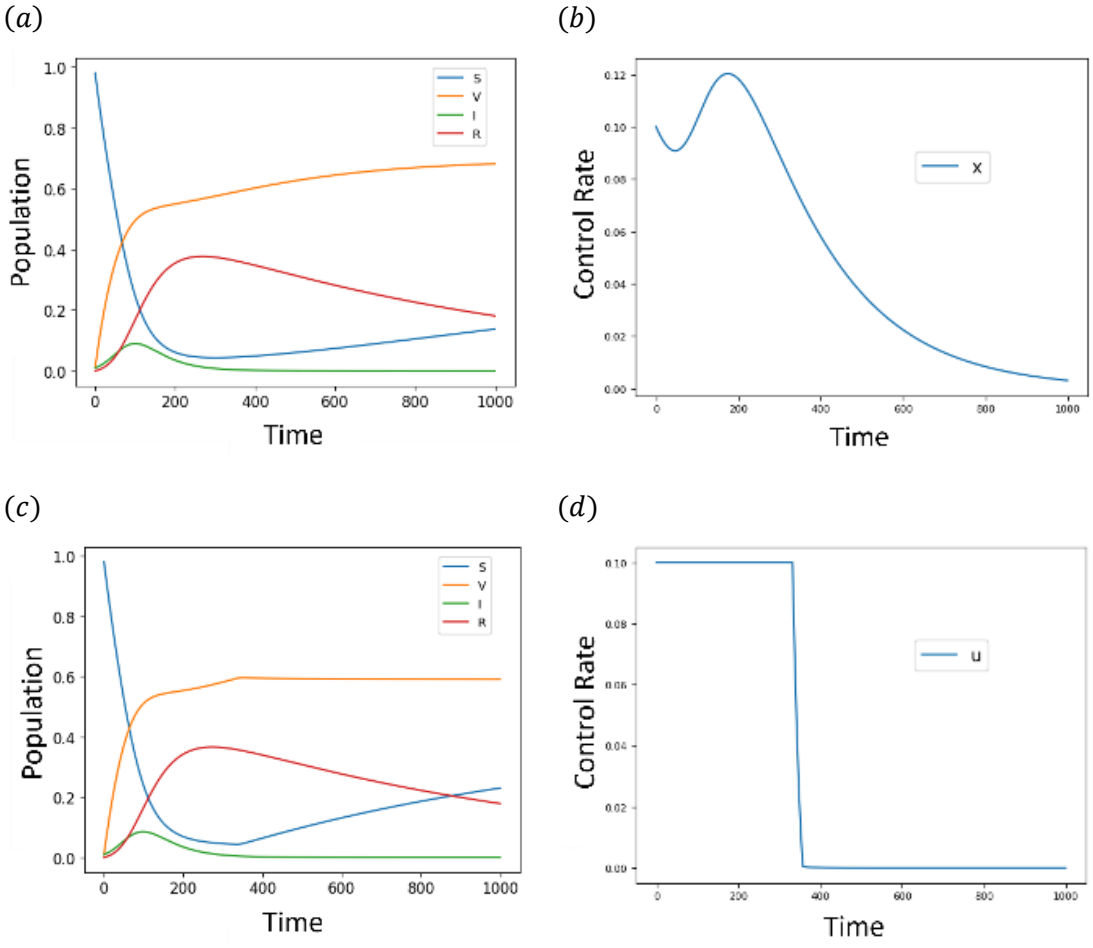

Figure 3: In panels (a) and (b) of the figure, the time series representation of the compartments and vaccination rate is provided for the behavior model. The blue line corresponds to the susceptible individuals, the green line represents the infected individuals, the orange line represents the immunized individuals, and the red line corresponds to the recovered individuals. In panel (b), the line depicts the vaccination rate. Similarly, panels (c) and (d) illustrate the compartments and vaccination rate for the optimal control model. The blue, green, orange, and red lines in panel (c) represent the susceptible, infected, vaccinated, and recovered individuals, respectively. Panel (d) shows the vaccination rate. By comparing the behavior model with the optimal control model, using the same parameter settings, we observe that the vaccination equilibrium reaches sooner in the optimal control model. So the optimal control strategy facilitates the achievement of a stable vaccination rate in a shorter duration compared to the behavior model.

Table 2: Standard values of the parameters [38,47,50,52]

Parameter	Value	Parameter	Value
β	0.833	ω	1/90
γ	0.333	k	0.1
m	1.0	c_v	0.5
c	1.0	u^{max}	0.1

Table 3: Initial values for the compartments and vaccination rates

State	At $t = 0$	State/Rate	At $t = 0$
S	0.98	R	0.00
V, I	0.01	x	0.1

6.3.2 Timeseries comparison based on wanning immunity, ω:

In this section, we will examine the impact of the immunity-waning rate on both the behavior model and the optimal control model. Figure 4 displays the time series of the compartments to observe the effect. We consider four different values for the waning rate of immunity ($\omega = 0.0, \frac{1}{90}, \frac{1}{60}, \text{and} \frac{1}{30}$ day^{-1}). In panels (a) to (d), the time series of the susceptible, vaccinated, infected, and vaccination rates are shown for the behavior model with varying values of the immunity-waning rate. Correspondingly, panels (e) to (h) illustrate the identical diagrams for the optimal control model. When we observe panels (a) and (e), we notice that the behavior of the susceptible cases remains almost the same across different values of ω. The patterns in the susceptible compartment are similar irrespective of the waning rate of immunity. Some significant characteristics are evident in panels (b) and (f), which represent the vaccinated individuals. In the case of the behavior model, the vaccination peak is significantly higher than the optimal control model. Additionally, the optimal control model's equilibrium point occurs earlier than the behavior model's. This trend holds for all values of ω. Panels (c) and (d), representing the infected individuals, exhibit essentially the same patterns in both models. Despite variations in the level of immunity, the peaks of infection remain unchanged in both the behavior and optimal control models. Finally, panels (d) and (h) depict the vaccination rates. Between the two models, noticeable differences were observed. The optimal control model ensures that vaccination is not continued until close to the end of the season, resulting in greater cost-effectiveness for the authorities and better overall outcomes. Considering all these observations, we can conclude that increasing the waning immunity rate encourages more individuals to get vaccinated, which aligns with our expectations.

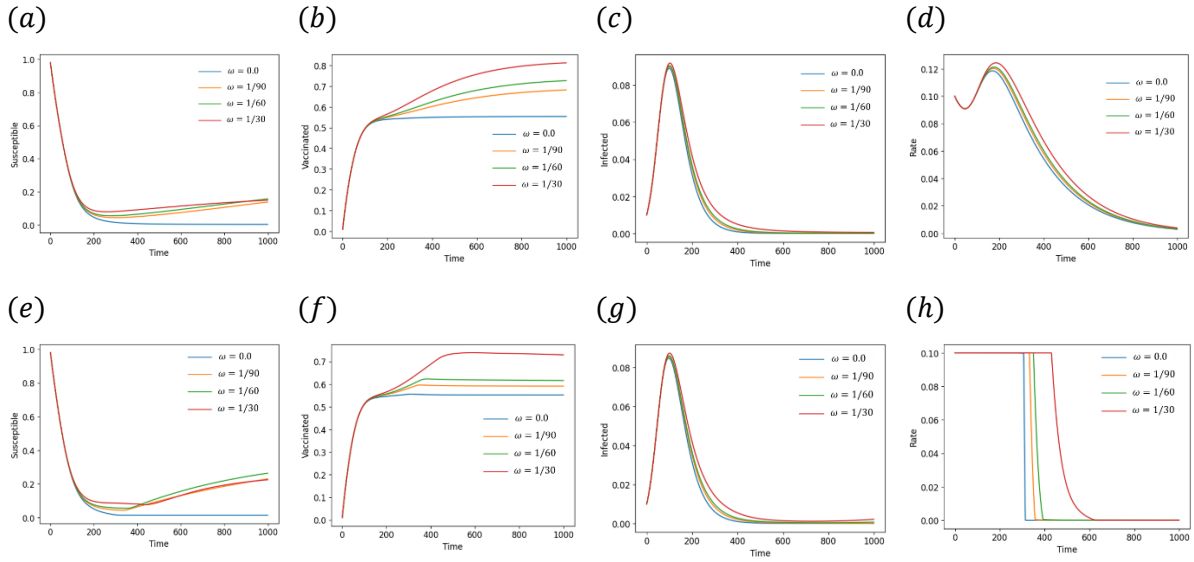

Figure 4: In panels (a) to (c), the time series of the susceptible, vaccinated, and infected compartments are displayed. The curves in blue, orange, green, and red correspond to the waning rates of $0.0, \frac{1}{90}, \frac{1}{60}, and \frac{1}{30}\ day^{-1}$, respectively. These panels provide insights into the behavior model. Similarly, panels (e) to (g) show the time series of the susceptible, vaccinated, and infected compartments for the optimal control model. The same color scheme (blue, orange, green, and red) represents the waning rates. Panel (d) shows the vaccination rate for the behavior model, while panel (h) shows the vaccination rate for the optimal control model. The panels mentioned above show that increasing the waning immunity rate leads to more vaccinations. Additionally, we can see that the optimal control model achieves equilibrium more quickly than the behavior model. So the optimal control model effectively regulates the vaccination strategy and stabilizes the system at a faster pace. In summary, raising the waning rate of immunity encourages more individuals to get vaccinated, and the optimal control model outperforms the behavior model by achieving equilibrium more rapidly.

6.3.3 Time series comparison based on vaccination cost, c_v:

In this section, we will examine how the cost of vaccination impacts both the behavior and optimal control models. Figure 5 provides the time series of the compartments for both models to observe the effect. We consider three different values for the vaccination cost ($c_v = 0.2, 0.5, \text{and } 0.9$). In panels (a) to (d), the time series of the susceptible, vaccinated, infected, and vaccination rates are displayed for the behavior model with varying vaccination costs. Similarly, panels (e) to (h) illustrate the same diagrams for the optimal control model. Examining panels (a) and (e) for the susceptible cases, we observe that in the behavior model, higher vaccination costs result in a larger portion of the population remaining susceptible for a longer period. In contrast, the optimal control model shows minimal impact on the susceptible individuals as vaccination costs increase. We observe similar trends in panels (b) and (f), which represent the vaccinated individuals. Lower vaccination costs lead to higher vaccination rates in both the behavior and optimal control models. However, the optimal control model achieves

equilibrium sooner than the behavior model. Panels (c) and (g) depict the infection level. In the behavior model, when the cost of vaccination increases, it leads to a rise in the infection peak. On the other hand, the optimal control model maintains a relatively steady level of infection despite variations in vaccination costs. Finally, panels (d) and (h) display the vaccination rates. Significantly different patterns emerge between the behavior model and the optimal control model. In the optimal control model, an increase in vaccination cost allows for a shorter duration of control, which is more favorable for the healthcare authority. Conversely, the behavior model exhibits a significant increase in vaccination with a decrease in vaccination cost, but this process continues until the end of the season, which can burden the healthcare authority. Considering all aspects, we can conclude that the optimal control model is more suitable for limiting the threat of the epidemic. Higher vaccination costs tend to decrease the vaccination rate, while lower costs increase the vaccination rate.

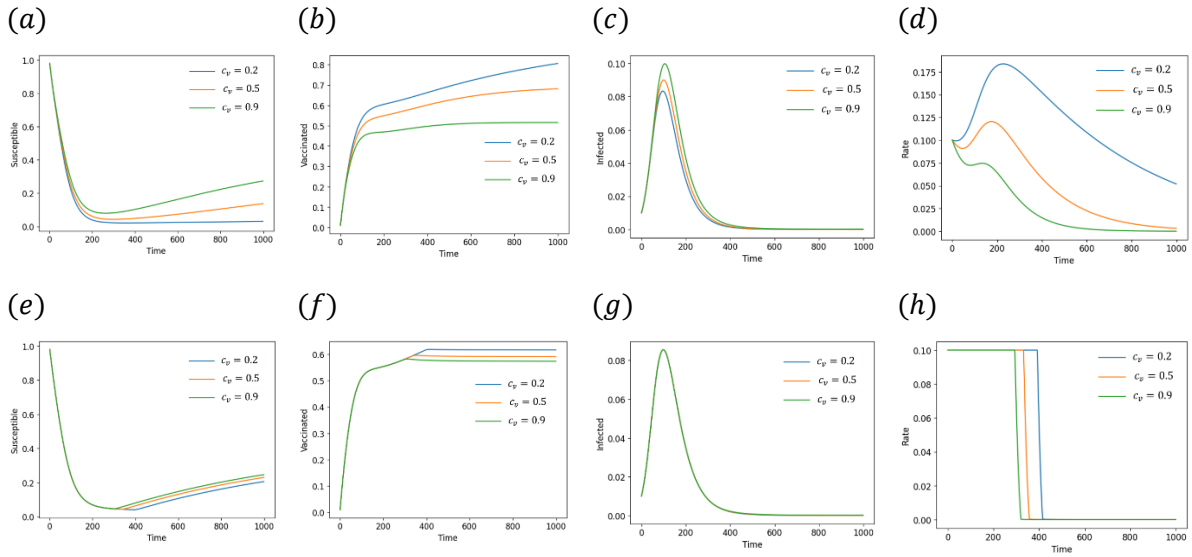

Figure 5: The time series of the susceptible, vaccinated, and infected compartments are depicted in panels (a) to (c) in the behavior model, respectively. Panel (d) displays the vaccination rate in the behavior models, with the blue, orange, and green curves representing vaccine costs of 0.2, 0.5, and 0.9, respectively. In panels (e) to (g), the time series of the susceptible, vaccinated, and infected compartments are presented for the optimal control model, while panel (h) shows the vaccination rate. We use the same color scheme to represent the vaccine costs. Considering the overall situation, we can conclude that optimal control is more suitable for reducing the threat of the epidemic. Higher vaccine costs lead to reduced vaccination rates, while lower costs result in increased vaccination rates. This conclusion is highly plausible and aligns with our understanding.

6.3.4 Timeseries comparison based on vaccine efficiency, η:

In Figure 6, we examine how the effectiveness of vaccination impacts the models. The time series of the compartments for the behavior model and the optimal control model is displayed to observe the effect. We consider three vaccination efficiency values: $\eta = 0.4, 0.7,$ and 0.9. Panels (a) to (d) illustrate

the time series of the susceptible, vaccinated, infected, and vaccination rates, respectively, with variations in vaccine effectiveness and the behavior model. Panels (f) to (h) present the same diagrams for the optimal control problem. Comparing panels (a) and (e) for the susceptible cases, we observe similar trends in both models, indicating a decrease in the number of susceptible individuals over time as vaccine effectiveness increases. The panels for vaccinated individuals (b) and (f) also exhibit similar patterns. Lower vaccine effectiveness leads to lower vaccination rates, but the optimal control model reaches equilibrium faster than the behavior model. The infection peak patterns are identical for both the behavior and optimal control models, as shown in panels (c) and (g). The vaccination rate panels (d) and (h) demonstrate noteworthy differences. With improved vaccine effectiveness, the optimal control model can apply control for a shorter duration, which is generally advantageous for the healthcare authority. In contrast, according to the behavior model, vaccination rates increase significantly as vaccine efficacy declines, and this process continues until the end of the season, placing a burden on the healthcare authority. Considering the complete picture, we can conclude that optimal control is more effective in reducing the threat, and higher vaccine efficiency results in fewer overall vaccinations, while lower efficiency leads to more overall vaccinations.

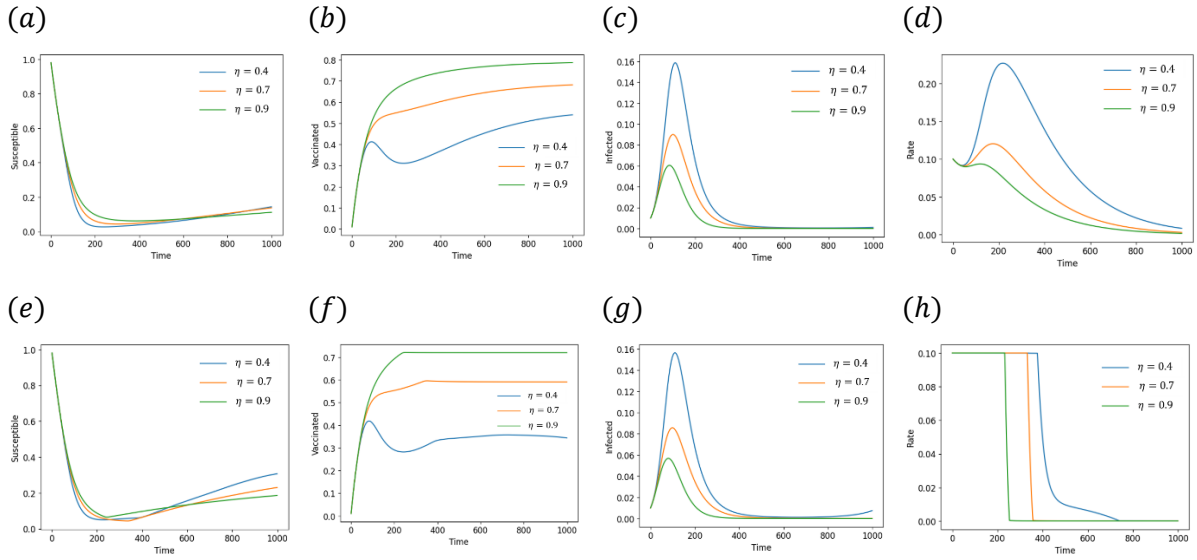

Figure 6: In panels (a)−(c) of the behavior model, the blue, orange, and green curves represent the time series of the susceptible, vaccinated, and infected compartments, respectively, for different values of vaccine efficacy ($\eta = 0.4, 0.7, \text{and } 0.9$). We can observe that as the vaccine efficacy increases, the number of susceptible individuals decreases over time. Similarly, in panels (e)−(g) of the optimal control model, the blue, orange, and green curves represent the time series of the susceptible, vaccinated, and infected compartments, respectively, with different values of vaccine efficacy. The trends are consistent with the behavior model, indicating that higher vaccine efficacy leads to fewer susceptible individuals. Panel (d) of the behavior model shows the rate of vaccination. We can see that as the vaccine efficacy increases, the vaccination rate decreases. This suggests that higher vaccine efficacy leads to a decreased requirement for vaccination. Panel (h) of the optimal control model

displays the vaccination rate. Similar to the behavior model, the vaccination rate decreases as the vaccine efficacy increases. This implies that higher vaccine efficacy leads to a decrease in the optimal control's recommendation for vaccination. Considering the overall situation, We can conclude that optimal control is more appropriate for mitigating the threat of the epidemic. Additionally, higher vaccine efficacy is associated with a decrease in overall vaccination rates, while lower efficacy promotes vaccination. This conclusion aligns with the expected behavior, as higher-efficacy vaccines would provide better protection and reduce the need for vaccination.

6.3.5 ASP and SED:

In Figure 7.1, the first row of panels (a) through (c) represents the total number of infected, vaccinated, and asymptomatic individuals at the equilibrium state using the behavior model (Nash equilibrium, NE). The second row of panels (d) through (f) represents the same quantities using the optimal control problem (Social optimum, SO). Panel (g) depicts the SED, which distinguishes the two total social payoffs in panels (f) and (c). In panel (a), which corresponds to the behavior model, the total number of infected individuals shows a monotonic increase as the transmission rate (β) increases. This indicates that higher transmission rates lead to higher infection rates in the behavior model.

Similarly, panel (d) shows that high infection rates can result from high transmission rates and low vaccine efficiency in the optimal control model. Panel (b) demonstrates that the behavior model consistently recommends vaccination throughout the season, regardless of the transmission rate. On the other hand, panel (e) shows that the optimal control model advises more vaccination as the transmission rate increases. This suggests that the optimal control model acknowledges the necessity of increasing vaccination rates in response to higher transmission rates. In panels (c) and (f), the ASPs are depicted for the behavior and optimal control models, respectively. The behavior model maintains a high level of social payoff across the entire parameter space, indicating that it is less sensitive to changes in vaccine efficiency compared to the optimal control model. The optimal control model, on the other hand, achieves higher social payoffs by balancing the trade-off between vaccination and infection. Panel (g) displays the SED, representing the difference between the optimal control model's social payoff and the behavior model's. Three regions are observed in the SED panel. The lower blue zone represents a low dilemma, where the transmission rate remains low, and both models achieve relatively high social payoffs. The dark blue area in the middle indicates almost no dilemma, as the optimal control model maintains higher vaccination rates and lower infection rates than the behavior model. However, as the transmission rate and vaccine efficiency increase, the light blue zone emerges, representing the most challenging region. In this region, the behavior model's social payoff is significantly higher than that of the optimal control model, as the behavior model is less sensitive to vaccine efficiency.

In conclusion, the optimal control model demonstrates a better balance between vaccination and infection rates, leading to higher social payoffs. While consistently recommending vaccination, the

behavior model may result in higher infection costs compared to the optimal control model. The SED analysis highlights the regions where challenges and dilemmas arise, with the behavior model showing higher costs and the optimal control model achieving a better balance.

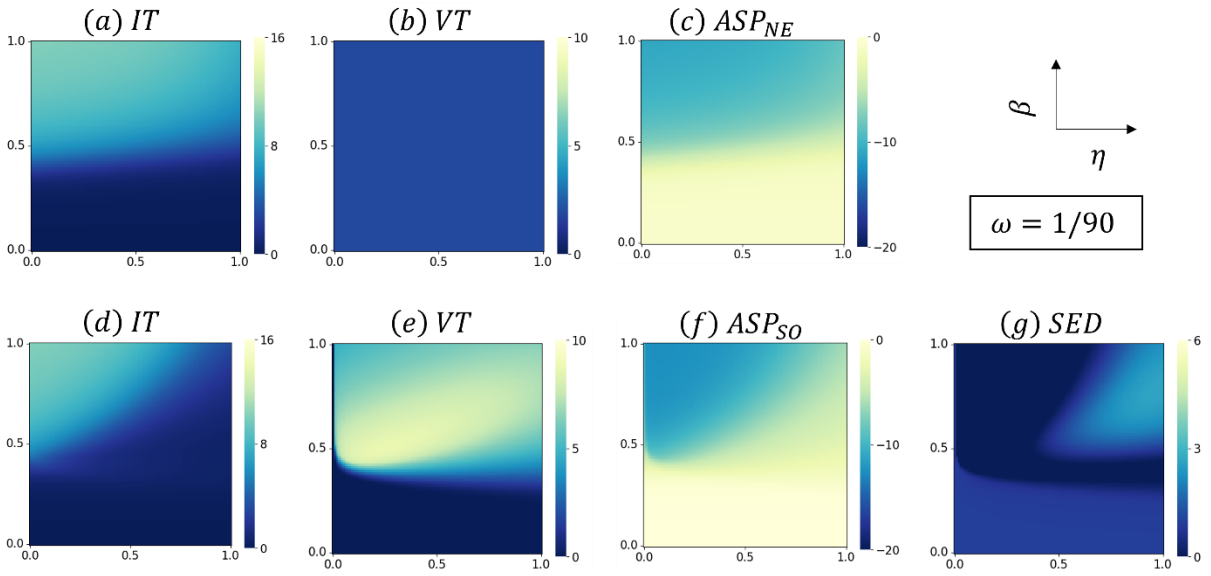

Figure 7.1: In the given Figure, panels (a) through (c) represent the overall prevalence of infection, vaccination, and ASP (Average Social Payoff) in the Nash equilibrium (NE) situation using the behavior model. Panels (d) through (f) represent the same quantities in the social optimum (SO) situation using the optimal control model. Panel (g) displays the SED, which distinguishes the two ASPs in panels (f) and (c). The y-axis represents the transmission rate, ranging from 0.0 to 1.0, and the x-axis represents the vaccine effectiveness, from 0.0 to 1.0. The color scale indicates the values of the respective variables, with the cumulative number of infected individuals ranging from 0 to 16, the total number of vaccinated individuals ranging from 0 to 10, and the SED ranging from 0 to 6. The ASPs ranges are -20 to 0. By examining the figure, we can observe that as both the transmission rate and vaccine effectiveness increase, the social problem becomes more significant. This implies that higher transmission rates and more effective vaccines lead to more significant challenges in achieving a desirable social outcome. The SED panel (g) visually represents the differences between the optimal control model and the behavior model in terms of social payoffs. The figure demonstrates that addressing the social problem becomes more challenging as the transmission rate and vaccine effectiveness increase. This emphasizes the significance of identifying optimal control strategies to effectively manage vaccination efforts and prevent infections, ultimately leading to the attainment of optimal social outcomes.

In Figures 7.2 and 7.3, the panels from Figure 7.1 are replicated with changes in the waning immunity rate. Figure 7.2 uses a waning immunity rate of $\omega = \frac{1}{60}\ day^{-1}$, while Figure 7.3 uses a waning immunity rate of $\omega = \frac{1}{30}\ day^{-1}$. The purpose is to examine the impact of waning immunity on the

social dilemma scenario while maintaining an identical range for the panels. Upon comparing the relevant panels in Figures 7.1, 7.2, and 7.3, we can observe that more individuals are vaccinated as the waning immunity rate increases. This decreases the average social payoff towards the socially ideal level in the context of optimal control. The SED panels allow us to identify regions similar to those in Figure 7.1 but with higher positive SED values. From these observations, we can conclude that increasing the rate of waning immunity amplifies the social dilemma, which aligns with expectations. This indicates that when waning immunity occurs faster, balancing vaccination efforts and achieving the desired social outcomes becomes more challenging.

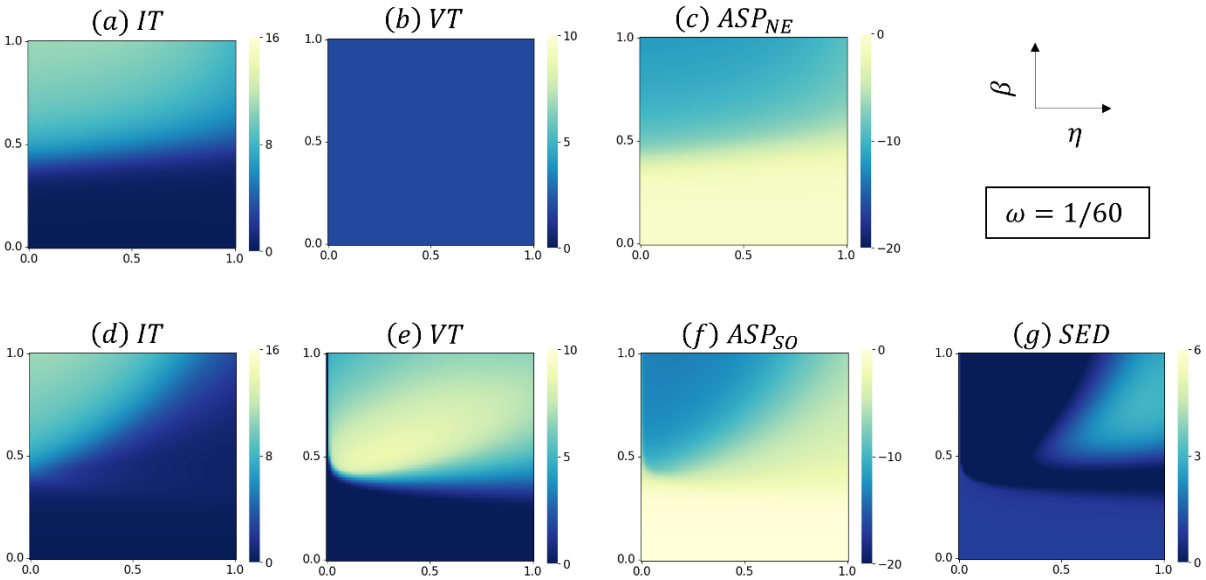

Figure 7.2: The Figure shows the overall prevalence of infection, vaccination, and ASP from the behavior model and optimal control model, as well as SED. All the ranges are the same as in Figure 7.1, with standard values of parameters as well, except the wanning immunity rate (ω).

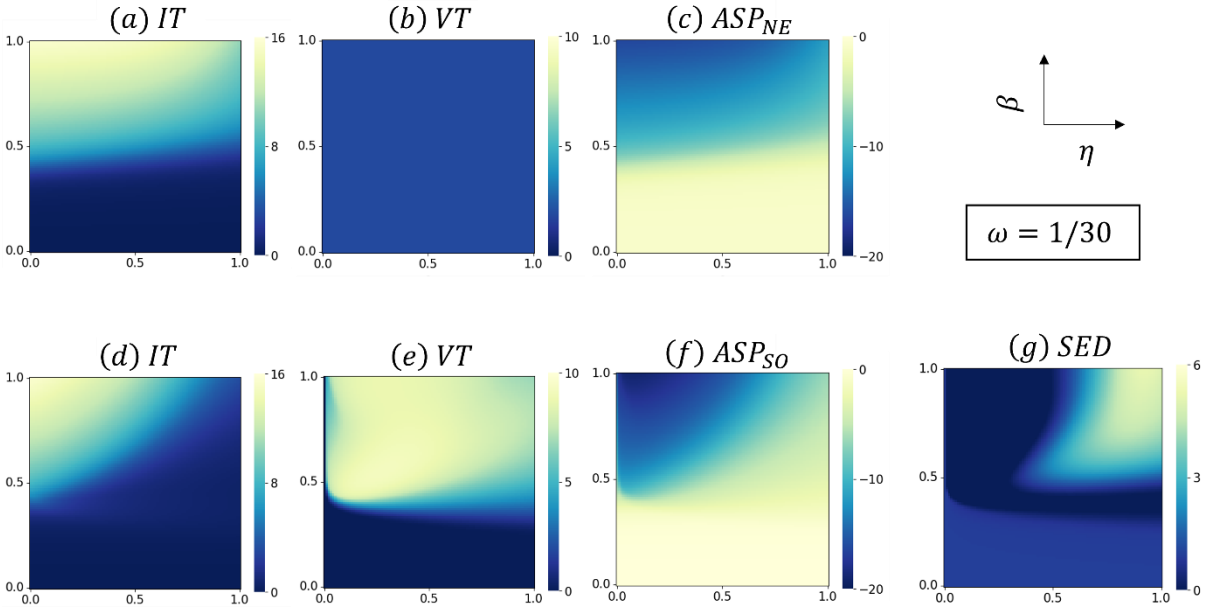

Figure 7.3: This Figure displays the overall prevalence of infection, vaccination, and ASP from the behavior model and optimal control model, as well as SED. Except for the wanning immunity rate (ω), all ranges and standard parameter values are identical to Figure 7.1.

Figure 7.4 focuses on the impact of the cost of the disease (c) and the cost of vaccination (c_v) on the social dilemma scenario, as well as the total number of infected individuals, vaccinated individuals, and the ASPs for both the behavior and optimal control models. The figure considers a range of values for the disease cost (c) from 0.01 to 1.01 and the vaccination cost (c_v) from 0.01 to c, with all other parameters set to their default values. From the panels representing the behavior model in the first row, we can observe that as the cost of vaccination increases, fewer individuals choose to get vaccinated, resulting in a higher overall number of people becoming infected. However, when comparing the behavior model to the optimal control model, it is evident that vaccination rates remain high and regional infection rates remain low in the latter. The panels depicting the average social payoff show a similar trend. When the costs of disease and vaccination are combined, the average social payoff increases as the cost of vaccination rises. This suggests higher vaccination costs incentivize individuals to prioritize vaccination, improving overall social outcomes. One interesting observation can be made from the SED panel. The SED is largest when the disease cost is high, and the cost of vaccination is around 0.4. This indicates that when the cost of the disease is high, but the cost of vaccination is moderately high, people hesitate to get vaccinated. As a result, the decision to get vaccinated becomes more dependent on the expense of the vaccination itself. Similar patterns have been observed in previous figures, such as Figures 7.1-7.3, where increasing the immunity rate resulted in higher values of SED, indicating an intensified social dilemma. This behavior aligns with human behavior and decision-making processes.

In summary, Figure 7.4 demonstrates how the costs of disease and vaccination impact vaccination rates, infection rates, average social payoffs, and the intensity of the social dilemma. Higher vaccination costs lead to lower and higher infection rates, while the combined costs of disease and vaccination influence the average social payoff. The SED panel reveals the regions where the social dilemma is most pronounced, highlighting the interplay between vaccination costs and disease in shaping individual behavior and overall social outcomes.

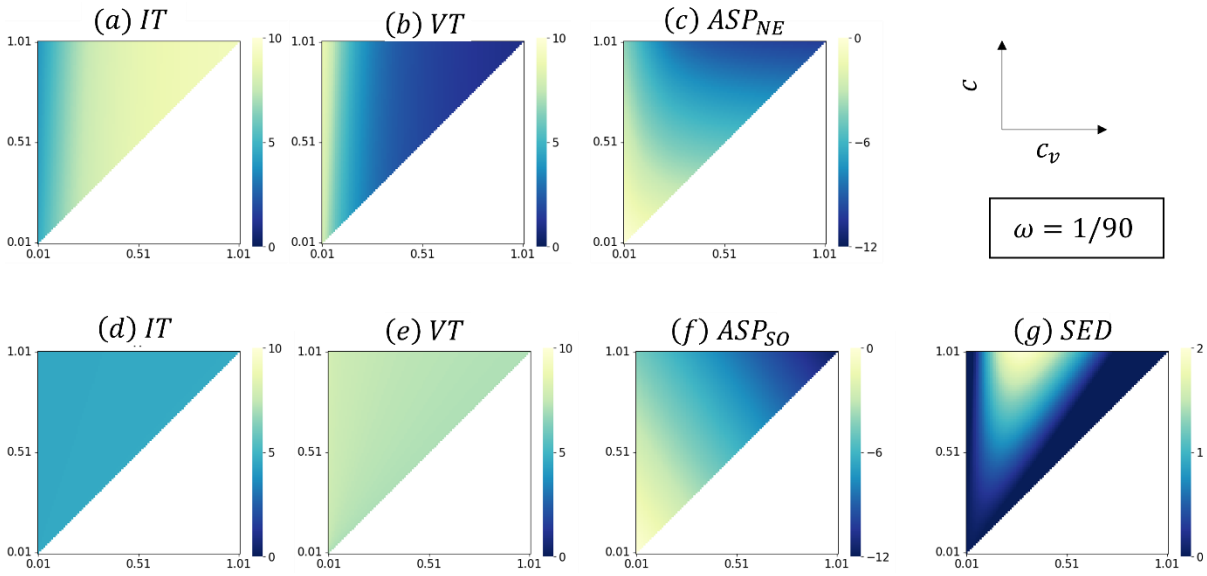

Figure 7.4: This Figure illustrates the prevalence of infection, vaccination, and the ASPs from both the behavior model (NE) and the optimal control model (SO), along with the SED panel. Panels (a) through (c) represent the NE condition, while panels (d) through (f) depict the SO case. Panel (g) specifically shows the SED, distinguishing it from panels (f) and (c). The figure uses the cost of disease (c) on the y-axis and the cost of vaccination (c_v) on the x-axis, with ranges of 0.01 to 1.01 for the disease cost and 0.01 to c for the vaccination cost. The cumulative number of infected and vaccinated people ranges from 0 to 10, while the ASP ranges from -12 to 0. The SED ranges from 0 to 2, and the remaining variables follow the base case. As the cost of disease increases, it is evident that the social dilemma worsens. However, the most significant social dilemma occurs when the cost of vaccination is approximately 0.4, and it diminishes as the vaccination cost increases. This implies that when the cost of vaccination is moderate, people are more hesitant to get vaccinated despite the higher cost of the disease. This behavior highlights the delicate balance between vaccination costs and disease in influencing individual decisions and social outcomes.

In summary, Figure 7.4 demonstrates the relationship between disease costs and vaccination and their impact on the social dilemma. Higher costs of disease exacerbate the social dilemma, but the intensity of the dilemma is greatest when the cost of vaccination is around 0.4. As the cost of vaccination increases, the social dilemma becomes less pronounced. The SED panel visually represents the regions where the social dilemma is most significant, shedding light on the interplay between the costs of vaccination and disease in shaping individual choices and the overall social dynamics.

6.4 Conclusion

When exploring an epidemic model and its associated social dilemma, particularly concerning vaccination, the primary focus is on implementing effective vaccination strategies. For individuals, the priority lies in vaccination uptake, taking into account factors like the eventual epidemic size, its peak,

and the cost of vaccination. Conversely, authorities aim to minimize disease spread while keeping costs low. The rate of immunity waning significantly affects strategy implementation for both individuals and authorities. Thus, integrating the epidemic model with optimal control theory becomes a valuable tool for healthcare professionals and management authorities in crafting and sustaining effective vaccination strategies. Previous studies have offered various analytical and numerical insights into optimal vaccination control strategies, often utilizing Pontryagin's maximum principle [7,8,11,15,23,24,26,37,56]. However, these studies frequently overlooked vaccination costs in their models and analyses. Moreover, some explored constant-rate vaccination or interventions, posing challenges for real-world implementation [4,38,47,52,58,59,62].

This research takes a direct approach by incorporating vaccination costs into the analysis to derive an optimal vaccination control strategy while upholding Pontryagin's maximum principle. Unlike prior works, we introduce a novel objective function that rigorously reflects the socially accumulated total cost. We compare a conventional cost-based behavior model, which considers human responses to vaccination based on epidemic conditions and costs, with our proposed optimal control model integrating vaccination and infection costs under the same parameters. Both models undergo thorough analysis and comparison, revealing the practicality and quicker stabilization of vaccination with the optimal control model. Regarding the social dilemma, numerical results illustrate how increasing rates of immunity waning amplify the Social Efficiency Deficit (SED), while higher vaccination costs somewhat mitigate it. Furthermore, the method used to calculate social dilemmas in this research is deemed more reliable for understanding social scenarios.

While this study focuses on a simple model incorporating a single control—vaccination—it's crucial to note that managing pandemics involves considering various interventions like isolation, quarantine, treatment, and testing policies. Future work will extend our model to include multiple interventions to enhance the effectiveness of analyzing epidemic models and optimal control strategies for preventive measures. This broader perspective aims to provide a comprehensive understanding of how different interventions interact to manage and control pandemics.

References

[1] K.M.A. Kabir, J. Tanimoto, Cost-efficiency analysis of voluntary vaccination against n -serovar diseases using antibody-dependent enhancement : A game approach, J. Theor. Biol. 503 (2020) 110379. https://doi.org/10.1016/j.jtbi.2020.110379.

[2] Y. Tatsukawa, R. Arefin, M. Tanaka, J. Tanimoto, Free ticket, discount ticket or intermediate of the best of two worlds – Which subsidy policy is socially optimal to suppress the disease spreading ?, J. Theor. Biol. 520 (2021) 110682. https://doi.org/10.1016/j.jtbi.2021.110682.

[3] M. Rajib Arefin, T. Masaki, K.M. Ariful Kabir, J. Tanimoto, Interplay between cost and

effectiveness in influenza vaccine uptake: A vaccination game approach, Proc. R. Soc. A Math. Phys. Eng. Sci. 475 (2019). https://doi.org/10.1098/rspa.2019.0608.

[4] K.M.A. Kabir, T. Risa, J. Tanimoto, Prosocial behavior of wearing a mask during an epidemic: an evolutionary explanation, Sci. Rep. 11 (2021) 1–14. https://doi.org/10.1038/s41598-021-92094-2.

[5] T.T. Yusuf, A. Abidemi, Effective strategies towards eradicating the tuberculosis epidemic: An optimal control theory alternative, Healthc. Anal. 3 (2023) 100131. https://doi.org/10.1016/j.health.2022.100131.

[6] R. Amin, Optimal control analysis of COVID-19 vaccine epidemic model : a case study, Eur. Phys. J. Plus. 123 (2022). https://doi.org/10.1140/epjp/s13360-022-02365-8.

[7] A. Olivares, E. Staffetti, Optimal control-based vaccination and testing strategies for COVID-19, Comput. Methods Programs Biomed. 211 (2021) 106411. https://doi.org/10.1016/j.cmpb.2021.106411.

[8] A. Ayalew, Y. Molla, T. Tilahun, T. Tesfa, Mathematical Model and Analysis on the Impacts of Vaccination and Treatment in the Control of the COVID-19 Pandemic with Optimal Control, J. Appl. Math. Vol. 2023 (2023). https://doi.org/https://doi.org/10.1155/2023/8570311.

[9] A. Rajput, M. Sajid, C. Shekhar, R. Aggarwal, Optimal control strategies on COVID-19 infection to bolster the efficacy of vaccination in India, Sci. Rep. (2021) 1–18. https://doi.org/10.1038/s41598-021-99088-0.

[10] B. Buonomo, Effects of information-dependent vaccination behavior on coronavirus outbreak : insights from a SIRI model, Ric. Di Mat. 69 (2020) 483–499. https://doi.org/10.1007/s11587-020-00506-8.

[11] A. Olivares, E. Staffetti, Optimal Control Applied to Vaccination and Testing Policies for COVID-19, Mathematics. 9 (2021). https://doi.org/https://www.mdpi.com/2227-7390/9/23/3100.

[12] C.J. Silva, C. Cruz, D.F.M. Torres, A.P. Muñuzuri, A. Carballosa, I. Area, J.J. Nieto, R.F. Pinto, R. Passadouro, E. Soares, W. Abreu, J. Mira, Optimal control of the COVID - 19 pandemic : controlled sanitary deconfinement in Portugal, Sci. Rep. (2021) 1–15. https://doi.org/10.1038/s41598-021-83075-6.

[13] N. Chen, H. Fan, Credit risk contagion and optimal dual control — An SIS / R model, Math. Comput. Simul. 210 (2023) 448–472. https://doi.org/10.1016/j.matcom.2023.03.031.

[14] Z. Abbasi, I. Zamani, A. Hossein, A. Mehra, M. Shafieirad, Optimal Control Design of Impulsive

SQEIAR Epidemic Models with Application to COVID-19, Chaos, Solitons Fractals Interdiscip. J. Nonlinear Sci. Nonequilibrium Complex Phenom. 139 (2020). https://doi.org/10.1016/j.chaos.2020.110054.

[15] H. Gaff, E. Schaefer, Optimal Control Applied To Vaccination And Treatment Strategies For Various Epidemiological Models, Math. Biosci. Eng. 6 (2009) 469–492. https://doi.org/10.3934/mbe.2009.6.469.

[16] S. Seddighi, S. Seddighi, J. Hassanzadeh, P. See, Controlling of pandemic COVID-19 using optimal control theory, Results Phys. 26 (2021) 104311. https://doi.org/10.1016/j.rinp.2021.104311.

[17] I.M. Hezam, A. Foul, A. Alrasheedi, A dynamic optimal control model for COVID-19 and cholera co-infection in Yemen, Adv Differ Equ. 6 (2021). https://doi.org/10.1186/s13662-021-03271-6.

[18] S.Y. Tchoumi, C.W.C.M.L. Diagne, H.R.M.L. Juga, Optimal control of a two-group malaria transmission model with vaccination, Netw. Model. Anal. Heal. Informatics Bioinforma. 0 (2023) 1–19. https://doi.org/10.1007/s13721-022-00403-0.

[19] S. Nana-kyere, F.A. Boateng, P. Jonathan, A. Donkor, G.K. Hoggar, B.D. Titus, D. Kwarteng, I.K. Adu, Global Analysis and Optimal Control Model of COVID-19, Comput. Math. Methods Med. 2022 (2022). https://doi.org/https://doi.org/10.1155/2022/9491847.

[20] F. Wang, M. Liu, L. Zhang, B. Xie, Bifurcation analysis and optimal control of a network-based SIR model with the impact of medical resources, Nonlinear Anal. Model. Control. 28 (2023) 209–227. https://doi.org/https://doi.org/10.15388/namc.2023.28.30770.

[21] A. Khan, R. Zarin, A. Akgül, A. Saeed, T. Gul, Fractional optimal control of COVID-19 pandemic model with generalized Mittag-Leffler function, Adv Differ Equ. (2021). https://doi.org/10.1186/s13662-021-03546-y.

[22] P. Yang, J. Jia, W. Shi, J. Feng, X. Fu, Stability analysis and optimal control in an epidemic model on directed complex networks with nonlinear incidence, Commun. Nonlinear Sci. Numer. Simul. 121 (2023) 107206. https://doi.org/10.1016/j.cnsns.2023.107206.

[23] G. Barbosa, F. Sérgio, G. Mendes, A.J. Silva, Determination of an optimal control strategy for vaccine administration in COVID-19 pandemic treatment, Comput. Methods Programs Biomed. 196 (2020) 105664. https://doi.org/10.1016/j.cmpb.2020.105664.

[24] Y. Tu, T. Hayat, A. Hobiny, X. Meng, Modeling and multi-objective optimal control of reaction-diffusion COVID-19 system due to vaccination and patient isolation, Appl. Math. Model. 118

(2023) 556–591. https://doi.org/10.1016/j.apm.2023.02.002.

[25] T. Li, Y. Xiao, Optimal strategies for coordinating infection control and socio-economic activities, Math. Comput. Simul. 207 (2023) 533–555. https://doi.org/10.1016/j.matcom.2023.01.017.

[26] S. Dong, L. Xu, Z.L. Ding, X. Bo, Application of a time-delay SIR model with vaccination in COVID-19 prediction and its optimal control strategy, Nonlinear Dyn. 111 (2023) 10677–10692. https://doi.org/10.1007/s11071-023-08308-x.

[27] A. Kouidere, L. El, H. Ferjouchia, O. Balatif, M. Rachik, Optimal Control of Mathematical modeling of the spread of the COVID-19 pandemic with highlighting the negative impact of quarantine on diabetics people with Cost-effectiveness, Chaos, Solitons and Fractals. 145 (2021) 110777. https://doi.org/10.1016/j.chaos.2021.110777.

[28] T. Li, Y. Guo, Optimal control and cost-effectiveness analysis of a new COVID-19 model for Omicron strain, Physica A. 606 (2022) 128134. https://doi.org/10.1016/j.physa.2022.128134.

[29] S. Lee, G. Chowell, Exploring optimal control strategies in seasonally varying flu-like epidemics, J. Theor. Biol. 412 (2017) 36–47. https://doi.org/10.1016/j.jtbi.2016.09.023.

[30] S.L. Khalaf, H.S. Flayyih, Analysis, predicting, and controlling the COVID-19 pandemic in Iraq through SIR model, Results Control Optim. 10 (2023) 100214. https://doi.org/10.1016/j.rico.2023.100214.

[31] E.F. Arruda, S.S. Das, C.M. Dias, D.H. Pastore, Modelling and optimal control of multi strain epidemics, with application to COVID-19, PLoS One. 16 (2021) 1–18. https://doi.org/10.1371/journal.pone.0257512.

[32] M. Zamir, T. Abdeljawad, F. Nadeem, A. Wahid, A. Yousef, An optimal control analysis of a COVID-19 model, Alexandria Eng. J. 60 (2021) 2875–2884. https://doi.org/10.1016/j.aej.2021.01.022.

[33] E.I. Abouelmagd, M.E. Awad, E.M.A. Elzayat, I.A. Abbas, Reduction the secular solution to periodic solution in the generalized restricted three-body problem, Astrophys. Space Sci. 350 (2014) 495–505. https://doi.org/10.1007/s10509-013-1756-z.

[34] Y. Liu, W. Liu, M.A. Obaid, I.A. Abbas, Exponential stability of Markovian jumping Cohen–Grossberg neural networks with mixed mode-dependent time-delays, Neurocomputing. 177 (2016) 409–415. https://doi.org/https://doi.org/10.1016/j.neucom.2015.11.046.

[35] B. Du, Y. Liu, I. Atiatallah Abbas, Existence and asymptotic behavior results of periodic solution for discrete-time neutral-type neural networks, J. Franklin Inst. 353 (2016) 448–461.

https://doi.org/https://doi.org/10.1016/j.jfranklin.2015.11.013.

[36] D. Lestari, F. Adi-kusumo, N.Y. Megawati, N. Susyanto, A minimum principle for stochastic control of hepatitis C epidemic model, BoundaryValue Probl. 3 (2023). https://doi.org/10.1186/s13661-023-01740-3.

[37] G. Angelov, R. Kovacevic, N.I. Stilianakis, V.M. Veliov, Optimal vaccination strategies using a distributed model applied to COVID-19, Cent. Eur. J. Oper. Res. 31 (2023) 499–521. https://doi.org/10.1007/s10100-022-00819-z.

[38] I. Nishimura, R. Arefin, Y. Tatsukawa, S. Utsumi, Social dilemma analysis on vaccination game accounting for the effect of immunity waning, Chaos, Solitons and Fractals. 171 (2023) 113426. https://doi.org/10.1016/j.chaos.2023.113426.

[39] M.R. Arefin, K.M.A. Kabir, M. Jusup, H. Ito, J. Tanimoto, Social efficiency deficit deciphers social dilemmas, Sci. Rep. 10 (2020) 1–9. https://doi.org/10.1038/s41598-020-72971-y.

[40] K.M.A. Kabir, K. Kuga, J. Tanimoto, Analysis of SIR epidemic model with information spreading of awareness, Chaos, Solitons and Fractals. 119 (2019) 118–125. https://doi.org/10.1016/j.chaos.2018.12.017.

[41] H.J. Li, W. Xu, S. Song, W.X. Wang, M. Perc, The dynamics of epidemic spreading on signed networks, Chaos, Solitons and Fractals. 151 (2021) 111294. https://doi.org/10.1016/j.chaos.2021.111294.

[42] R. Markovič, M. Šterk, M. Marhl, M. Perc, M. Gosak, Socio-demographic and health factors drive the epidemic progression and should guide vaccination strategies for best COVID-19 containment, Results Phys. 26 (2021). https://doi.org/10.1016/j.rinp.2021.104433.

[43] Q. Sun, Z. Wang, D. Zhao, C. Xia, M. Perc, Diffusion of resources and their impact on epidemic spreading in multilayer networks with simplicial complexes, Chaos, Solitons and Fractals. 164 (2022) 112734. https://doi.org/10.1016/j.chaos.2022.112734.

[44] J. Fan, Q. Yin, C. Xia, M. Perc, Epidemics on multilayer simplicial complexes, Proc. R. Soc. A Math. Phys. Eng. Sci. 478 (2022). https://doi.org/10.1098/rspa.2022.0059.

[45] M. Jusup, P. Holme, K. Kanazawa, M. Takayasu, I. Romić, Z. Wang, S. Geček, T. Lipić, B. Podobnik, L. Wang, W. Luo, T. Klanjšček, J. Fan, S. Boccaletti, M. Perc, Social physics, Phys. Rep. 948 (2022) 1–148. https://doi.org/10.1016/j.physrep.2021.10.005.

[46] D. Helbing, D. Brockmann, T. Chadefaux, K. Donnay, U. Blanke, O. Woolley-Meza, M. Moussaid, A. Johansson, J. Krause, S. Schutte, M. Perc, Saving Human Lives: What Complexity Science and Information Systems can Contribute, 2015. https://doi.org/10.1007/s10955-014-

1024-9.

[47] R. Tori, J. Tanimoto, A study on prosocial behavior of wearing a mask and self-quarantining to prevent the spread of diseases underpinned by evolutionary game theory, Chaos, Solitons and Fractals. 158 (2022) 112030. https://doi.org/10.1016/j.chaos.2022.112030.

[48] Y. Tatsukawa, M.R. Arefin, S. Utsumi, J. Tanimoto, Investigating the efficiency of dynamic vaccination by consolidating detecting errors and vaccine efficacy, Sci. Rep. 12 (2022) 1–12. https://doi.org/10.1038/s41598-022-12039-1.

[49] K.M. Ariful Kabir, J. Tanimoto, Impact of awareness in metapopulation epidemic model to suppress the infected individuals for different graphs, Eur. Phys. J. B. 92 (2019). https://doi.org/10.1140/epjb/e2019-90570-7.

[50] M.M.-U.-R. Khan, M.R. Arefin, J. Tanimoto, Investigating vaccination behavior and disease dynamics of a time-delayed two-strain epidemic model : An evolutionary approach, Proc. Int. Exch. Innov. Conf. Eng. Sci. 8 (2022) 147–154. https://doi.org/https://doi.org/10.5109/5909084.

[51] J. Tanimoto, Fundamentals of evolutionary game theory and its applications, Springer (Tokyo), 2015.

[52] M.M.-U.-R. Khan, M.R. Arefin, J. Tanimoto, Investigating the trade-off between self-quarantine and forced quarantine provisions to control an epidemic: An evolutionary approach, Appl. Math. Comput. 432 (2022) 127365. https://doi.org/https://doi.org/10.1016/j.amc.2022.127365.

[53] S. Lee, G. Chowell, C. Castillo-cha, Optimal control for pandemic influenza : The role of limited antiviral treatment and isolation, J. Theor. Biol. 265 (2010) 136–150. https://doi.org/10.1016/j.jtbi.2010.04.003.

[54] S.A. Nowak, P.N. De Lima, R. Vardavas, Optimal non-pharmaceutical pandemic response strategies depend critically on time horizons and costs, Sci. Rep. (2023) 1–9. https://doi.org/10.1038/s41598-023-28936-y.

[55] L.D. Valdez, L. Vassallo, L.A. Braunstein, Epidemic control in networks with cliques L., Phys. Rev. E. 107 (2023) 1–14. https://doi.org/10.1103/PhysRevE.107.054304.

[56] M. Piraveenan, S. Sawleshwarkar, M. Walsh, I. Zablotska, S. Bhattacharyya, H.H. Farooqui, T. Bhatnagar, A. Karan, M. Murhekar, S. Zodpey, K.S.M. Rao, P. Pattison, A. Zomaya, M. Perc, Optimal governance and implementation of vaccination programmes to contain the COVID-19 pandemic, R. Soc. Open Sci. 8 (2021). https://doi.org/10.1098/rsos.210429.

[57] C.T. Bauch, Imitation dynamics predict vaccinating behaviour, Proc. R. Soc. B Biol. Sci. 272 (2005) 1669–1675. https://doi.org/10.1098/rspb.2005.3153.

[58] M.M.-U.-R. Khan, J. Tanimoto, Investigating the social dilemma of an epidemic model with provaccination and antivaccination groups : An evolutionary approach, Alexandria Eng. J. 75 (2023) 341–349. https://doi.org/10.1016/j.aej.2023.05.091.

[59] M.M.-U.-R. Khan, M.R. Arefin, J. Tanimoto, Time delay of the appearance of a new strain can affect vaccination behavior and disease dynamics: An evolutionary explanation, Infect. Dis. Model. 8 (2023) 656 - 671. https://doi.org/https://doi.org/10.1016/j.idm.2023.06.001.

[60] B. Maayah, A. Moussaoui, S. Bushnaq, O. Abu Arqub, The multistep Laplace optimized decomposition method for solving fractional-order coronavirus disease model (COVID-19) via the Caputo fractional approach, Demonstr. Math. 55 (2022) 963–977. https://doi.org/10.1515/dema-2022-0183.

[61] B. Maayah, O. Abu Arqub, S. Alnabulsi, H. Alsulami, Numerical solutions and geometric attractors of a fractional model of the cancer-immune based on the Atangana-Baleanu-Caputo derivative and the reproducing kernel scheme, Chinese J. Phys. 80 (2022) 463–483. https://doi.org/10.1016/j.cjph.2022.10.002.

[62] M.M.U.R. Khan, J. Tanimoto, Influence of waning immunity on vaccination decision-making: A multi-strain epidemic model with an evolutionary approach analyzing cost and efficacy, Infect. Dis. Model. 9 (2024) 657–672. https://doi.org/10.1016/j.idm.2024.03.004.

Chapter 7
Summary and Conclusion

Throughout the journey of this thesis, we have embarked on a comprehensive exploration of epidemic models, behavior models, and optimal control theory, all aimed at unraveling the intricate dynamics of managing infectious diseases. While our investigation has traversed diverse epidemic scenarios, our overarching objective remained singular: to gain insights into how individuals respond to interventions and to uncover the social dilemmas inherent in epidemic situations. This pursuit has demanded a nuanced examination of individual behaviors across various circumstances, facilitated by an evolutionary approach grounded in mathematical modeling.

In Chapter 1, we introduced the study's background, outlined the thesis structure, and provided fundamental preliminary information essential for this research.

In Chapter 2, we immersed ourselves in an epidemiological model rooted in SEIR dynamics, where self-quarantine and forced quarantine interventions were entangled with human behavior dynamics. We discovered that the decision to self-quarantine was intricately linked to individual choices, driven by personal costs. Conversely, authorities could enforce quarantine through incentives, albeit constrained by budget limitations. These interventions, derived from behavioral modeling, emerged as pivotal strategies in curtailing infection peaks and addressing the social efficiency deficit, commonly referred to as the social dilemma.

With the emergence of multiple strains of infectious diseases, exemplified by the challenges posed by COVID-19, Chapter 3 unveiled a two-strain epidemic model featuring the delayed emergence of a new strain, while exploring pre-infection and post-infection vaccination strategies. Our exploration revealed that human behavior in committing to vaccination dynamically responded to prevailing circumstances, with a propensity to vaccinate intensifying as infection rates rose or highly transmissible variants emerged. Interestingly, our analysis illuminated that delaying the second strain not only reduced infection peaks but also alleviated the social dilemma associated with vaccination decisions.

Chapter 4 delved deeper into the intricacies of vaccination decision-making, casting light on the social dilemma by featuring both provaccination and antivaccination susceptible groups. We meticulously examined the impact of waning immunity on individuals' willingness to undergo revaccination, highlighting the influence of the current epidemic situation and the perceived outcomes of vaccination. Our findings underscored the significance of boosting vaccination rates to mitigate the social dilemma, notwithstanding the challenges posed by higher rates of waning immunity.

In the face of the complexity posed by multi-strain diseases and the availability of multiple vaccination options, individual decision-making emerged as a critical determinant, particularly in the context of

waning immunity. Chapter 5 addressed this complexity by introducing a comprehensive epidemiological model that embraced multiple disease strains and vaccination options. Our analysis uncovered a nuanced interplay between waning immunity, vaccine efficacy, and the presence of highly transmissible strains, emphasizing the importance of achieving equilibrium in vaccine adoption.

To fully comprehend the social dilemma inherent in epidemic models with interventions, it became imperative to scrutinize the flow of interventions and ascertain the social optimum. While previous studies predominantly relied on simplistic rate models, Chapter 6 pioneered a novel methodology leveraging optimal control theory to evaluate the Social Optimum of a vaccination game. By factoring in variables such as cost, availability, and distribution policies, our research yielded valuable insights into optimizing vaccination strategies within complex societal dynamics, underscoring the need to account for variables such as waning immunity and vaccination costs.

In conclusion, this thesis has provided a comprehensive understanding of epidemic dynamics, shedding light on the complexities of individual decision-making and the social dilemmas that underpin epidemic scenarios. Our findings have profound implications for policy-making and public health efforts, furnishing a roadmap for navigating the challenges posed by infectious diseases and optimizing intervention strategies in a dynamic and evolving landscape.

Limitations and Future Works

Acknowledging the various approaches researchers have employed to analyze epidemic scenarios alongside interventions, it is evident that understanding disease dynamics and human responses to preventive measures is paramount for effective decision-making by authorities. In this thesis, we present a range of epidemic models integrated with behavior models and optimal control strategies, addressing diverse epidemic scenarios. Our chosen approach, the mean field approximation (Simple Ordinary Differential Approach), offers a straightforward yet acceptable technique for analyzing disease dynamics and human behavior responses to interventions. However, a notable limitation of this study is the absence of real-life data, which could enrich our analysis. Additionally, while the multi-agent simulation (MAS) approach provides a more nuanced understanding of epidemic dynamics in structured populations, it was not utilized here. Stability analysis, another commonly employed method in concluding epidemic situations, was also not included in our work. Nevertheless, our extensive numerical simulations provide valuable insights into various epidemic scenarios, especially where stability analysis is challenging. Moving forward, our primary objective is to apply our proposed models to real-life data and validate our findings in structured populations, enhancing the realism and utility of our models for healthcare management authorities. Furthermore, we aim to expand our analysis beyond the simplest scenario presented in this thesis (vaccination only) to encompass more complex epidemic

models involving quarantine, treatment, etc. In addressing the social dilemma inherent in epidemic models, we have introduced a novel technique incorporating intervention costs, which promises greater efficiency. While our current focus is on vaccination, future endeavors will extend this approach to encompass a wider array of interventions. Through these efforts, we aspire to contribute to a deeper understanding of epidemic dynamics and provide actionable insights for effective epidemic management.